Micro and Nano Mechanics of Materials Response during Instrumented Frictional Sliding

by

Simon C Bellemare

B. Eng. and M.App.Sc., Materials Engineering
Ecole Polytechnique de Montreal (2002)

Submitted to the Department of Materials Science and Engineering
in partial fulfillment of the requirements for the degree of

Doctor of Philosophy in Materials Science and Engineering

at the

MASSACHUSETTS INSTITUTE OF TECHNOLOGY

JUNE 2006

Author .....
Department of Materials Science and Engineering
May 26, 2006

Certified by.....
Subra Suresh
Ford Professor of Engineering
Thesis Supervisor

Accepted by .....
Samuel M Allen
POSCO Professor of Physical Metallurgy
Chair, Departmental Committee on Graduate Students

Micro and Nano Mechanics of Materials Response during Instrumented Frictional Sliding

by

Simon C Bellemare

Submitted to the Department of Materials Science and Engineering
on May 26, 2006, in partial fulfillment of the requirements for the degree of
Doctor of Philosophy in Materials Science and Engineering

Abstract

Over the past decade, many computational studies have explored the mechanics of instrumented normal indentation. In contrast, very few studies have investigated quantitative aspects of frictional sliding contact in the elasto-plastic regime. In this thesis, a new framework was developed to establish relationships between the frictional sliding response, material properties and contact parameters. Dimensional analysis enabled to define scaling variables and dimensionless functions. Finite element methods were used to simulate the process of steady-state frictional sliding and evaluate the dimensionless functions. In frictional sliding, the representative plastic strain was found to be more than four times as large as in normal indentation. Further comparison with indentation indicated a three fold increase in the maximum pile-up height and an increased influence of the strain hardening on hardness.

Experimental studies were conducted with and without a liquid lubricant in selected material systems. Quantitative agreements with numerical predictions were observed in all cases. The strong influence of the strain hardening exponent on the pile-up height was illustrated from frictional sliding results obtained in copper and copper-zinc specimens of different grain sizes. Also, the influence of hardening characteristics was illustrated by preparing two microstructures of an aluminum alloy to have the same indentation hardness. These materials with same indentation hardness showed significantly different hardness and pile-up in frictional sliding. Experiments were also carried out on nanocrystalline nickel and alloys of different grain sizes. The addition of tungsten did not change significantly the strain hardening behavior of nanocrystalline nickel but it did stabilize significantly the microstructure in repeated pass experiments.

A reverse algorithm was developed to extract plastic flow properties from the frictional sliding response. This algorithm uses the scratch hardness and pile-up measurements to estimate yield strength and strain hardening exponent. Based on sensitivity analysis, the accuracy on these estimates is significantly improved as compared to reverse algorithms for instrumented indentation, especially for the strain hardening exponent. Frictional sliding is an alternative or complement to instrumented indentation. It can provide a different ranking of materials for their tribological resistance. It can also be used to estimate plastic flow properties.

Thesis Supervisor: Subra Suresh
Title: Ford Professor of Engineering

Acknowledgments

When you need help is when you realize how friendship is the most valuable asset to have. I could not have succeeded without the help from several people, and I would give a few special words to them. My first two years at MIT has been an enjoyable journey, but as the years passed by my desire to succeed and contribute really challenged my ability to keep up and to focus on the work. On the other hand, thanks to the individuals that I mention below, it has been a wonderful experience, and if I had to go back I would make the same choice.

I would like to first acknowledge Professor Subra Suresh for providing me with the opportunity and means to grow under his guidance. Professor Suresh has exceptional abilities as a scientist and advisor. His inspiration, his calmness and broad perceptions have contributed to my progress throughout my stay at MIT. His endless patience and encouragement have helped me pass through the ups and downs of the thesis experience.

Special thanks are also extended to Professor Christopher Schuh and Professor Raul Radovitzky for dedicating their valuable time to serve on my thesis committee. Their suggestions and support were greatly appreciated. Mr. Andrew Detor and Professor Chris Schuh are especially acknowledged for providing nanocrystalline alloys and for sharing their expertise in processing and characterization of the materials.

I am also extremely grateful to the Office of Naval Research and the Cambridge – MIT Institute for their financial support in the project presented herein and in a preliminary project that spanned the first two years of my studies. Special thanks to Professor Bill Clyne and Dr. Athina Markaki from Cambridge University for their support in the experimental characterization of the sandwich materials.

Professor J Ivan Dickson and Professor Martin N Bureau from École Polytechnique de Montréal also contributed indirectly to my PhD research, giving me the opportunity to develop skills for research throughout my Masters Degree thesis. They have been particularly helpful in developing my self-judgment and my English writing skills. I would like to thank them for their support all throughout my academic career. Also, Professor Thomas Eagar is greatly acknowledged for the numerous discussions and for the opportunity to add practical engineering to my MIT experience.

Dr. Demos Pafitis from Schlumberger-Doll Research is very much acknowledged for his advices and for the opportunity that he offered me to develop industrial experience when I was transitioning between thesis projects. Many thanks also to Dr. Alan Humphreys and his colleagues for sharing their experience and for giving me the opportunity to contribute to the research.

I want to acknowledge also the current and past members of Suresh Group for their direct and indirect contributions to my thesis work. I would give sincere appreciation to Mr. George LaBonte for his positive attitude and his leadership on organizing and maintaining the laboratory. George is

really a man to count on when you need help setting up an experiment or a new office. Many thanks also to Mr. Kenneth Greene for the numerous effective communications and his sense of humor.

Dr. Ming Dao and Mr. In-Suk Choi have been very helpful for setting up and analyzing the finite element results for this thesis. Ming is very experienced and knowledgeable and, in addition, he can cope with interacting with a scientific-engineer like me. Being particularly careful, patient and brilliant, In-Suk is a very good friend to have beside you when dealing with major and complicated technical issues.

Dr. Alan Schwartzman, Dr. Benedikt Moser, Dr. Ruth Schwaiger, Dr Nannaji Saka and Professor Upadrasta Ramamurty have been involved in different aspects of my experimental thesis work. Their intellectual contributions are greatly appreciated.

I would also give sincere appreciation to my current and past office mates Nuwong (Kob) Chollacoop, Timothy Hanlon, John Mills, Orian Regnier, Hidemi Kato, Dave Quinn, Anamika Prasad, Irene Chiang, Thibault Prevost and Alexandre Micoulet for their support and friendship. Many of them had to support my French slang when I was frustrated with simulation errors. Also, thank you Alexandre for all the little attentions and distractions. Finally, special thanks to Kob and Tim for their help with classes and their moral support.

Within the Materials Science Department, Kathleen Farrell, Gerald Hughes, and Stephen Malley have all helped in various ways to make my stay more enjoyable. I am specially thankful to Yin-Lin Xie for her help on specimen preparation and observation. I also express my gratitude to Peter Morley, Andrew Gallant, and all of the machinists at the MIT Central Machine Shop. Finally, special thanks to Dr. Bina Patel for her encouragements over the past few months.

A special thank to my friend Bruce Wu for his support in the periods when research was difficult. Bruce is especially skilled in communications and politics. And he is a very distinguished individual and a good listener. Our earlier appellation as our group M. was definitely not a complete appreciation of his personality and skills.

Special thanks also to my friends Taras Gorishnyy, Jorge Vieyra, Dr. Yuttanant Boonyongmaneerat, Dr. Dirk Mohr and Dr. Pierre-Yves Brisson for the good discussions and for making the MIT program more enjoyable and less technical, sometime. It is always good to share our opinions about these people and to make consensus about how life is hard.

I would now express my gratitude to my family. My parents Claire Tourigny and Alain Bellemare raised my sister Julie and I with good analytical skills and a strong physical intuition. At the same time, they were able to have their own life and they gave us the opportunity to built early our own independence. I engaged in the PhD program a few months after knowing that my father Alain would not be able attend graduation. Alain has been hard to keep out of mind, and I will never forget him. Today I want to thank him again for who he has been.

With her pride in my academic and personal success, my mother Claire Tourigny has been a major source of motivation for this work. In the young age Claire taught me how to do things in depth and how to be persistent when it becomes more involved. Without her care and dedication I would certainly not be here today.

Several other members of my family have contributed to my motivation to initiate and complete the project. On my mother's side, I will start at the root with my living grand-parents Noëlla and Georges Tourigny. They have been a constant source of inspiration and courage since my young age. Their appreciation of perseverance and hardworking and their supportive nature always remind me of their happiness. Their son Laurent has also been a strong source of inspiration in the development of my personal life and my career. Laurent is the uncle you need beside you when you have the impression that everything is falling apart, and that there is not much that can be done about it. I also want to share a special appreciation to my aunt Doris and to her husband André Bélisle for their interest and support. I wish to make a special word also to my nice Léa for her friendship, curiosity and joy.

On my father's side, I want to acknowledge my living grand-parents Simone and Jean-Paul Bellemare for their continuous interest in the projects of all their children and grand-children. I would also like to thank my sister Julie and her partner Philippe Campbell for their understanding and support. A special thank to my younger brother and sister Nicolas and Béatrice Forand for understanding the situation and for their continuous joy in life. Their mother Monique Forand and her boyfriend Clément Bernier have also been very supportive and helpful. Clément brought a new family perspective at a needing time. I would also make a special mark of appreciation to my closest cousin Christian for his friendship and positive attitude.

I would like to greatly acknowledge my father-in-law Claude Vigneault and his wife Cécile Bilodeau. They have been very supportive and their pride has been a source of motivation. Cécile and Claude are always welcoming and visiting them always leaves behind a positive attitude. I also enjoyed learning welding and assembling with Claude, putting the thesis work at rest for a couple of days.

Last but not least, it is well time for me to acknowledge my wife Dr. Julie Vigneault for supporting me throughout this adventure. Julie has the most complete and elegant personality in my eyes and she has made tremendous sacrifices to help me go through the ups and downs of the thesis work. She has been my best source of motivation and my best support to maintain an organized life. Her strong character and her faith were her best tools against the MIT students trying to do too much. However, we still missed-out numerous weekends to give me time to work and finish on time, and I hope to make it up to her in the upcoming months. She will always be the one for me, and I am sure that we have bright days coming ahead.

Table of content

List of Figures and Captions

List of Tables and Captions

Introduction

In their everyday use, many devices and components are subjected to surface contact, frictional sliding, damage and wear. The damage can be especially severe when the contact generates permanent or plastic deformation beneath the surface, leaving residual grooves or scars on the surface. The series of tribological events leading to material removal and the loss of functionality can be highly complex to analyze. However, simple experiments where a single hard indenter penetrates an initially flat surface can serve as an intermediate step for idealized analysis of contact conditions in this series of processes. These simple experiments can help in determining palliatives, critical mechanisms, and the effect of material properties in the study of contact damage.

Indentation hardness has been by far the most simple and commonly used technique for characterizing the resistance of surfaces to plastic deformation. The hardness can be measured through a variety of different techniques, but the result is always an estimate of the average contact pressure between the indenter and the surface. This hardness or contact pressure resistance has been correlated with tribological resistance in numerous situations. For example, based on the general Archard equation for sliding wear [1], the material removal rate is inversely proportional to the hardness. Such type of empirical expression has been developed for a variety of contact conditions. With these empirical relationships and the fact that indentation hardness test procedures are cost-effective and easy to implement, hardness measurements have been widely used over the past several decades.

The hardness measured through these conventional tests provides a quantity that depends on contact conditions, elastic properties and plastic properties. Significant progress has been made over the past decade to improve the testing technique and to apply instrumented indentation to a wide range of practical applications. Whereas the conventional indentation tests were based on an estimate of the residual area of contact or the remnant penetration depth, the development and commercialization of depth-sensing instrumented indentation systems have enabled continuous measurement of the force and displacement during loading and unloading. This measured force–displacement (P–h) hysteresis response has been studied in detail analytically and computationally. For different geometries of indenter tips, methodologies have been formulated to predict the P–h indentation response from material properties and vice-versa [2-7]. How the contact response quantitatively dependent on individual elasto-plastic properties is now fairly well established for homogeneous materials subjected to sharp normal indentation.

Frictional sliding is a second contact mode that could be used for the prediction of tribological resistance and as a characterization technique for material properties. Its advantages over normal indentation include the generation of a plastic strain of greater magnitude, a closer similarity to the contact conditions in many real applications, and the possibility to make use of the ratcheting effect and to study cyclic plastic deformation through repeated sliding experiments.

Despite these advantages, the mechanics of frictional sliding has not been investigated in detail. The absence of research in the area could well be due to the difficulty of addressing the full three-dimensional nature of the material flow process. There are also potential difficulties in determining the influence and the magnitude of the friction coefficient between the material and the indenter.

The objective of this thesis was to develop quantitative relationships between the frictional sliding response and material properties. The initial focus was to understand the mechanics of steady-state frictional sliding and to develop a comprehensive understanding of how the sliding process is influenced by the plastic properties of the material. In addition, it was the objective to establish a comprehensive framework to assess scratch hardness vis-à-vis the widely used normal indentation hardness. It was also aimed to use frictional sliding to characterize nanocrystalline nickel and nickel-tungsten alloys. These materials have a largely higher hardness than their microcrystalline counterparts and they are expected to have improved frictional sliding resistance.

This thesis is divided in four chapters. The first three chapters address the mechanics for the frictional sliding contact between a hard conical tip and the flat surface of a material. In Chapter 1, a finite element methodology is developed and validated using different solution schemes. Procedures are developed to characterize the frictional sliding response using three contact parameters. Dimensional analysis was used in junction with the numerical data to establish a set of dimensionless functions that predict all three contact parameters from material properties. These predictions are found in good agreement with a limited set of experimental data obtained on the pure nickel system. With the validation of the finite element method through experimental comparison, the results are presented as best estimates of the solution. The results for the strain field are then analyzed to show that representative strain is more than four times higher in frictional sliding than in normal indentation.

Chapter 2 presents additional experimental validation with copper as material system. Composition and grain-size are the two microstructural parameters controlled with the objective of maximizing the range of plastic flow characteristics covered. The two plastic properties considered in the material model are the initial yield strength and the plastic strain hardening exponent. Although the effect of strain hardening invariably couples to variations in initial yield strength, the experimental results were interpreted in conjunction with the finite element predictions to isolate the relative contribution of each plastic property on the frictional sliding response. The experimental results clearly indicate that an increase in the strain hardening exponent can significantly decrease the pile-up height. The experimental values were also compared with predictions and a good quantitative agreement was observed for the hardness, normalized pile-up height and overall friction coefficient. Finally, the effects of friction on the sliding response were investigated, both computationally and numerically. The dimensionless functions developed in Chapter 1 were modified to include the effect of the adhesive friction coefficient on the predictions. Experimentally, the friction was decreased through the use of a liquid lubricant to generate boundary lubrication. Consistently with the predictions, the most significant effect of a lubricant was a decrease in the pile-up height.

In Chapter 3, the emphasis is on engineering techniques where the dimensionless functions, developed in chapters 1 and 2, are employed for the development and validation of a reverse analysis technique. This reverse technique uses the frictional sliding response to determine the plastic properties of materials. The inputs required are the elastic properties, the scratch hardness and the normalized pile-up height. The results from the algorithm are the initial yield strength and the plastic strain hardening exponent of the material. This reverse method for frictional sliding could increase significantly the usefulness of carrying out the experiment. A major advantage over normal indentation is on the capability to predict the plastic strain hardening exponent with reasonable accuracy. The solution is shown to be unique and the sensitivity to variations in the input parameters is found to be moderate. As a complement to this reverse analysis, Chapter 3 presents an experimental study where an aluminum alloy of a single composition is aged under different conditions. The aging conditions where controlled carefully to obtain an under-aged and an over-aged sample having the indentation hardness but different microstructures and plastic strain hardening exponents. These two materials were found to have a different scratch hardness and a significantly different pile-up behavior in frictional sliding. It is proposed that the pile-up information could provide an estimate of the tribological resistance.

In the fourth chapter, the results from a comprehensive experimental study are presented for the frictional sliding response of nanocrystalline nickel and nickel-tungsten alloys. The response was characterized at two different length-scales. For the low load experiments, the penetration depth of typically 10-40 nm and the response was affected by the presence of natural oxide films, by surface tension, or by other size effects. No intrinsic effect of the grains was observed and the effect of alloying was found to be limited. At higher load, the effect of alloying remained limited in the single-pass experiment. The results approximately scale with the effect of grain-size variation on the indentation hardness. Based on the computational study from the earlier work in this thesis, the hardness is approximately proportional to the yield strength in the absence of plastic strain hardening. Therefore, the most probable cause for this correlation is a very limited strain hardening exponent in all the cases.

The new technique developed in this thesis for frictional sliding contact was tested on different material systems and a good correlation was observed between the finite element predictions and the experimental results. The effect of friction was also included in the model and, based on sensitivity analysis, the plastic flow properties of materials can be determined with a reasonable accuracy by using the frictional sliding response and elastic properties. This new reverse analysis technique has a unique solution and it could be useful for the characterization of small or graded structures.

Cited references:

[1] I. M. Hutchings, *Tribology: Friction and Wear of Engineering Materials*. Kent: CRC Press, 1992.

[2] A. E. Giannakopoulos and S. Suresh, "Determination of elastoplastic properties by instrumented sharp indentation," *Scripta Materialia*, vol. 40, pp. 1191-1198, 1999.

[3] Y.-T. Cheng and C.-M. Cheng, "Scaling approach to conical indentation in elastic-plastic solids with work hardening," *Journal of Applied Physics*, vol. 84, pp. 1284, 1998.

[4] M. Dao, N. Chollacoop, K. J. Van Vliet, T. A. Venkatesh, and S. Suresh, "Computational modeling of the forward and reverse problems in instrumented sharp indentation," *Acta Materialia*, vol. 49, pp. 3899-3918, 2001.

[5] Y.-T. Cheng, Z. Li, and C.-M. Cheng, "Scaling relationships for indentation measurements," *Philosophical Magazine A: Physics of Condensed Matter, Structure, Defects and Mechanical Properties*, vol. 82, pp. 1821-1829, 2002.

[6] N. Ogasawara, N. Chiba, and X. Chen, "On the Representative Strain of Indentation Analysis," *Journal of Materials Research*, vol. In press, 2005.

[7] L. Wang, M. Ganor, and S. I. Rokhlin, "Inverse scaling functions in nanoindentation with sharp indenters: Determination of material properties," *Journal of Materials Research*, vol. 20, pp. 987-1001, 2005.

Chapter 1: The frictional sliding response of elasto-plastic materials in contact with a conical indenter

This first chapter presents the dimensional analysis and the finite element models used to investigate the relationships between the frictional sliding response of material and their elasto-plastic properties. Dimensionless functions are defined and evaluated numerically for the different response parameters selected. The results are compared with the response in normal indentation.

1.1 Introduction

The single asperity contact of a hard indenter on a softer material can generate a permanent impression. The dependence of geometry and material properties, on the size and morphology of this impression and on the extent of deformation surrounding it, has been the subject of technological and scientific interest over the past century. Although mechanics of deformation and material penetration and/or loss in a variety of localized contact conditions [1] including frictional sliding or scratching [2] have been topics of scientific studies for many decades, normal indentation is by far the most commonly used technique to characterize the hardness of materials [3, 4]. The different scales for hardness are all estimates for the average pressure of contact, but the reference contact area used to normalize the normal force varies significantly depending on the experimental methods employed and the details of the analysis. Although the hardness value depends on the definition of contact area and indenter geometry, conventional hardness test procedures are cost-effective and easy to implement. Consequently, indentation hardness measurements have been used very extensively not only for quality control [5], but also as prime predictors of tribological resistance [6].

Over the past two decades, the development and commercialization of depth-sensing indentation instruments has facilitated the simultaneous measurement of the applied force and the induced displacement, providing for each test a force versus displacement hysteresis curve from loading and unloading. Significant theoretical and computational research have also been devoted to the establishment of relationships between the quantitative details of these force–displacement curves and the underlying elastic and plastic properties of the material being indented. For instance, the initial part of the unloading slope provides a measure of the elastic compliance that could be used to estimate the elastic modulus of indented materials [7]. Other parameters such as the curvature of the loading curve and the residual depth upon complete unloading could be used to estimate the hardness and the yield strength without measuring the contact area [8].

For instrumented sharp indentation, finite element simulations and dimensional analyses have been used in several studies to establish relationships between the hysteresis curves and the elasto-plastic properties of materials [9-14]. To determine with a reasonable precision the initial yield

strength and the strain hardening exponent, recent studies have examined the potential advantage of using two different indenter geometries to characterize the plastic properties [15-17]. Changing the tip angle changes the magnitude of the average plastic strain, therefore providing more information about the evolution of the flow stress with the plastic strain [18, 19]. As an alternative technique to determine the plastic flow properties accurately, one can use a single indenter and measure directly characteristic parameters of the residual indent profile [20-23]. After the experiment such a technique requires to determine the surface profile , but it could also exploit the known effects of strain hardening exponent on pile-up morphology [24-27]. How pile-up and hardness each quantitatively dependent on individual elasto-plastic properties is now fairly well established for homogeneous materials subjected to sharp normal indentation.

As compared to normal indentation where the stress field is axisymmetric (for a spherical or a conical indenter), it requires more computational resources to study frictional sliding using finite element methods. The scratch loading mode was used for the establishment of the first hardness scale in the pioneering work of Mohs (1824), but the technique is mostly being used nowadays in specialized areas including the visual damage and wear of polymers [28-32] and the tribological resistance of metallic-base composites [33-38]. The limited usage to characterize the plastic flow behavior is mostly due to the lack of an appropriate analytical framework to interpret frictional sliding experiments. During a frictional sliding test carried out under appropriate plasticity conditions and under a constant normal force, steady state conditions are obtained for the penetration depth, the friction force and the pile-up after an initial transient regime. For this steady state contact problem, analytical models have been developed based on the upper bound theorem, but the solution scheme requires specification of the material flow velocity field [2]. Using the finite element method, a number of recent studies have examined the effect of flow stress and tip geometry on the scratch response [39-43]. However, we found only one study for which plastic strain hardening was included [44]. In all cases, the number of material property sets studied was too limited to gain a broad fundamental understanding.

In this paper, we report results from a comprehensive computational study of frictional sliding in elasto-plastic materials. The effects of plastic strain hardening and yield strength are specifically quantified for steady state frictional sliding conditions. Following an approach similar to that used in finite element studies of instrumented indentation, dimensional functions are derived for the steady state regime of frictional sliding and the predictions are compared with experimental results in a model material system. The concept of a scratch hardness, extracted from instrumented frictional sliding experiments, is developed, and its relationship to indentation hardness is explored both experimentally and computationally.

1.2 Framework for the analysis

1.2.1 Problem formulation

The analysis focuses on the response of elasto-plastic materials in frictional sliding contact with a hard conical tip. It is possible in frictional sliding to reach a condition of constant penetration depth, normal force and tangential force. Both computationally and experimentally, this steady state regime can be obtained through different paths for the imposed normal force and/or displacement in the initial and/or stable regimes. At least theoretically, the response in steady state should be path independent.

Throughout the simulation or experiment, it is possible to continuously monitor the normal contact force P, the normal indenter displacement h and the tangential or friction force F_t. Under steady state conditions, these parameters and the geometry of the pile-up become fixed. Figure 1 presents a cross-sectional view of the process and illustrates the definition of the apex angle θ, the residual depth h_r and the residual pile-up height h_p. In addition to the known external variables, the friction coefficient μ_a and the elastic properties of the tip can also influence the steady state geometry.

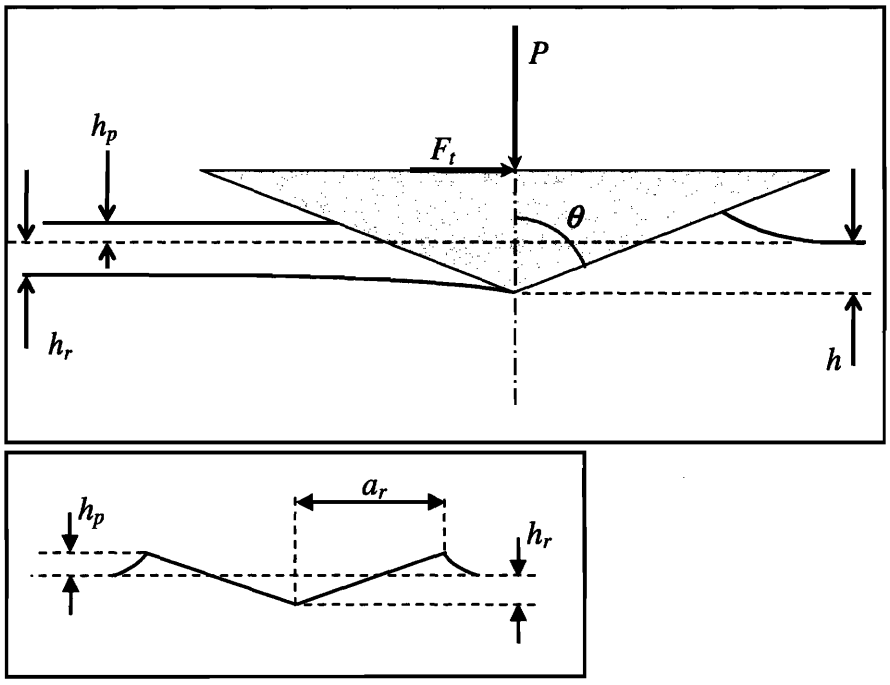

Figure 1.1: Contact geometry and nomenclature for the steady state frictional sliding process: (a) A view of the symmetry plane where the indenter moves from left to right, and (b) A cross-sectional view of the residual scratch profile.

Knowing P, h_r, θ, F_t and the material properties for the indenter and the surface can fully specify this frictional sliding process. However, as for the indentation response, the normalized pile-up height h_p/h_r can vary significantly with material properties. The analysis here will specifically quantify this dependence for materials where the elastic and plastic response can be approximated, respectively, by Hooke's law and the von Mises yield criterion with isotropic power law hardening. Under those general conditions, the dependence of the true stress σ on the true strain ε is commonly expressed as (e.g., [10])

$$\sigma = \begin{cases} E\varepsilon & for\ \sigma \le \sigma_y \\ R\varepsilon^n & for\ \sigma > \sigma_y \end{cases}, \qquad \textbf{1.1}$$

where E is the Young's modulus, R a strength coefficient, n the strain hardening exponent and σ_y the initial yield stress at zero offset strain. In this representation, the true strain ε is a uniaxial strain. The multiaxial stress state for frictional sliding will be introduced after a rearrangement of Equation 1.1. The total true strain ε can be decomposed in elastic and plastic components to obtain

$$\varepsilon = \varepsilon_y + \varepsilon_p . \qquad \textbf{1.2}$$

For continuity when $\sigma = \sigma_y$, equation 1.1 requires that

$$\sigma_y = E\varepsilon_y = R\varepsilon_y^n . \qquad \textbf{1.3}$$

When $\sigma > \sigma_y$, the substitution of equations 1.2 and 1.3 in 1.1 leads to the replacement of the coefficient R by elastic properties and to express the flow stress constitutive relation as

$$\sigma = \sigma_y \left(1 + \frac{E}{\sigma_y} \varepsilon_p \right)^n . \qquad \textbf{1.4}$$

The implementation of this relationship for the multiaxial stress of state followed the concept of equivalent plastic strain and the incremental theory of plasticity. With a constitutive model at hand, the subsequent step consists in defining the physical quantities to describe the frictional sliding response. In contrast with normal indentation, the steady state nature of the frictional sliding process does not allow us to probe the elastic recovery of the material using the normal force–normal displacement (P–h) hysteresis curve. Without knowledge of the unloading compliance in this elastic recovery, it is not possible to estimate the Young's modulus through techniques such as those originally proposed for normal indentation [7, 45, 46]. A second and related limitation for frictional sliding involves the calculation of actual area of contact that is also typically obtained through an analysis of the (P–h) hysteresis curve. Alternative ways to estimate the actual area of contact include *in-situ* imaging, but this solution would require advanced instrumentation, especially at low loads and is not always feasible under all test conditions.

The solution proposed here for measuring the contact area consists of probing directly the residual scratch width $2a_r$ through surface imaging or profilometry. Using profilometry, additional

parameters such as h_p and h_r can be readily quantified and used in the analysis. Practical aspects associated with the measurement of these quantities are discussed in sections 1.4.3 and 1.4.3. Using this residual profile approach, the scratch hardness of the material can be directly calculated using the traditional definition of hardness [1-4]

$$H_S = \frac{P}{A_r}, \tag{1.5}$$

where A_r is an estimate of the residual projected area of contact. Following the same definition as in previous models for frictional sliding contact with hard indenters [2], A_r is defined as half the area of a circle of radius a_r,

$$A_r = (\pi/2)a_r^2. \tag{1.6}$$

1.2.2 Dimensional analysis

Dimensional analysis has proven to be useful to the study of the contact mechanics for instrumented normal indentation [8]. Using a similar approach for the steady state frictional sliding process allows us to present the results in a general form and to clearly state the dependence of each physical quantity on the material and geometrical parameters. Our independent physical quantities can be expressed as

$$P = P(a_r, E, \upsilon, \sigma_y, n, E_i, \upsilon_i, \theta, \mu_a), \tag{1.7}$$

$$h_p = h_p(h_r, E, \upsilon, \sigma_y, n, E_i, \upsilon_i, \theta, \mu_a), \tag{1.8}$$

and

$$F_t = F_t(P, E, \upsilon, \sigma_y, n, E_i, \upsilon_i, \theta, \mu_a) \tag{1.9}$$

where E_i and ν_i are the Young's modulus and the Poisson's ratio, respectively, of the indenter. For the functional of the force P, the use of a_r instead of h_r was found to be more appropriate because experimental determination of h_r requires estimation of the position of original surface through an interpolation procedure which decreases the level of accuracy. Accuracy on a_r or h_r is important as the error is doubled in calculating the contact area.

The above functional relationships are often simplified [1] by introducing the effective Young's modulus for the combined indenter-substrate system as

$$E^* = \left[\frac{(1-\upsilon^2)}{E} \frac{(1-\upsilon_i^2)}{E_i} \right]^{-1}. \tag{1.10}$$

Using this effective modulus and applying the Π theorem of dimensional analysis, expressions 1.7, 1.8 and 1.9, respectively, become

$$\frac{P}{\sigma_y a_r^{\,2}(\pi/2)} = \Pi_\alpha\left(\frac{\sigma_y}{E^*}, n, \upsilon, \theta, \mu_a\right) = \frac{H_S}{\sigma_y}, \qquad \textbf{1.11}$$

$$\frac{h_p}{h_r} = \Pi_\beta\left(\frac{\sigma_y}{E^*}, n, \upsilon, \theta, \mu_a\right), \qquad \textbf{1.12}$$

and

$$\frac{F_t}{P} = \mu_{tot} = \Pi_\gamma\left(\frac{\sigma_y}{E^*}, n, \upsilon, \theta, \mu_a\right) \qquad \textbf{1.13}$$

where Π_α, Π_β and Π_γ are general dimensionless functions. Several alternative expressions could be proposed but the one presented here allows for the dimensionless functions to directly correspond to simple and important ratios of measurable quantities, namely the normalized scratch hardness H_S/σ_y, the ratio of pile-up heights h_p/h_r and the total friction coefficient μ_{tot}.

1.2.3 Computational models

For the analysis presented here, the material Poisson's ratio ν was maintained at 0.3 while all the other material parameters were varied over a wide range (see Section 1.4.2). For the conical indenter, the model assumed elastic rigidity, and the apex angle θ was fixed at 70.3°. The contact of this indenter with the surface was assumed to follow Amontons's law of friction (1699),

$$q = \mu_a\, p, \qquad \textbf{1.14}$$

where q is the tangential traction and p is the local pressure or the normal traction. As in previous contact mechanics studies that included friction [14, 47, 48] and based on experimental results reported elsewhere [49, 50], a value of 0.15 was used for μ_a. This value is believed to represent a typical contact condition between a diamond tip and the polished surface of a metal covered with a thin layer of natural oxides.

Full three-dimensional models were constructed because the stress and strain fields generated by frictional sliding cannot be approximated using two-dimensional or axisymmetric mesh domains. However, the plane defined by the normal to the surface and the sliding direction is a symmetry plane, which allows for solving only half of the full space. To further minimize the size of the problem, the meshing procedure involved the radial propagation of the seeds from the region of refined mesh. Figure 1.2 presents the indenter, the mesh and the overall simulation domain. The domain consists in two main parts: a spherical section for the mesh located upstream with respect to the indenter position and a conical section for the material located downstream. The upstream configuration is significantly more efficient, but the meshing downstream needed to remain fully refined to capture with accuracy an unloaded profile. The complete mesh domain contains 170,000 reduced integration 8-noded elements.

The finite-element computations were performed using the general purpose software package ABAQUS [51]. Three different solution schemes were used and compared for their time efficiency and accuracy. An explicit formulation with Eulerian boundary conditions was found to provide the most consistent results and enabled use of the smallest simulation domain. In this formulation, the material enters at a constant velocity through the upstream spherical surface, flows through the stationary mesh and exits downstream. The mesh adapts to geometrical changes induced by the frictional contact of the tip with the free surface.

The results from this explicit formulation were compared with elastic solutions and well-tested for convergence. For an elastic frictional contact, the contact pressure distribution and the Von Mises stress distribution agreed within 5% error with known analytical and numerical solutions from previous studies [3, 52, 53]. With plasticity, the solution was determined to be independent of the far-field boundary conditions and insensitive to mesh size. In the range where 13 to 20 elements were within the contact radius created by the indenter, the main advantage of the finer mesh was for the determination of the pile-up height and the area of contact from the coordinates of the surface nodes. For all the simulation results presented here, 13 elements were in contact with the indenter in the initial non-deformed configuration. During the simulation, the number of elements increased further as the pile-up formed. In fact, the mesh was optimized with a greater refinement near the pile-up region than near the center of contact.

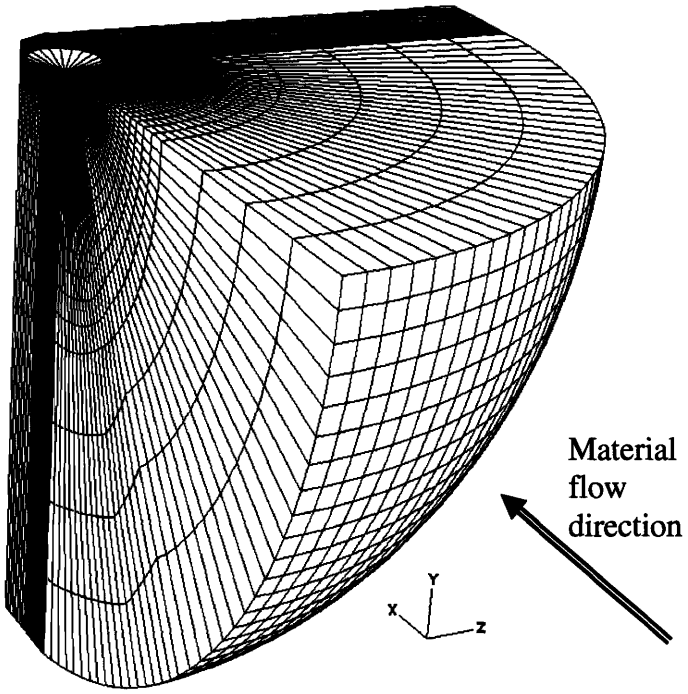

(a)

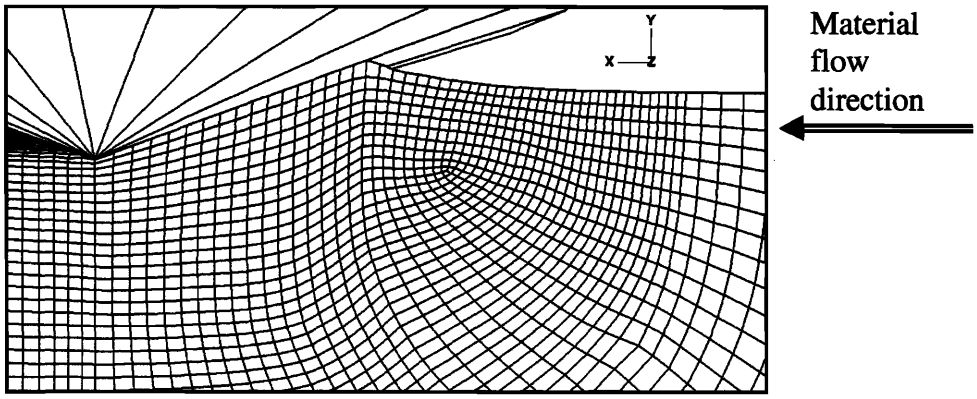

(b)

Figure 1.2: (a) Overview of mesh and the complete simulation domain with the fixed conical indenter in the top left, the material flow direction along positive X direction and the symmetry plane at Z = 0. (b) Detailed view on the symmetry plane Z = 0 of the region near the indenter with the upstream direction to the right.

To further verify both the trends and the absolute value of the predictions from the explicit/Eulerian formulation, two additional sets of finite element models were constructed and simulation results were obtained to cover a wide range of material properties. The hardness and pile-up results matched within 2% error with those obtained using an explicit scheme with Lagrangian boundary conditions. Such a good correspondence provided conclusive evidence that using Eulerian boundaries allows for a reduction in the domain size without affecting the results obtained using explicit dynamic formulation. The second set of comparative results was based on a standard implicit solution scheme with Lagrangian boundary conditions. To limit the increase in the computational time associated with the use of an implicit algorithm and with the increased domain size, only 50,000 elements were used for these simulations. As reported in Table 1.1, the results show slightly greater differences with a maximum error of 10% for the normalized hardness. To minimize the time steps required to reach a steady state regime, a small linear decrease in penetration depth was introduced for the first third of the scratching distance. For the remaining of the scratching distance, the depth was maintained constant and the steady state over a distance sufficient enough to extract an accurate residual profile. Without an initial regime with a decreasing the depth, an apparent steady state response was also reached but the residual pile-up height was found to be significantly lower as shown for two cases in Table 1.1. Part of this dependence on the trajectory could originate from the level of mesh refinement. However, even with the coarsest mesh cases, none of the explicit formulations exhibited a significant dependence on the initial scratching regime.

Table 1.1: Comparison between the simulation results obtained using standard implicit and explicit schemes.

		H_y/σ_y			h_p/h_r			μ_{tot}		
σ_y/E	n	Implicit	Explicit	Diff (%)	Implicit	Explicit	Diff (%)	Implicit	Explicit	Diff (%)
0.001	0.1	4.6	4.3	7	0.70	0.75	-7	0.394	0.399	-1
0.001	0.2	8.3	7.8	6	0.56	0.60	-7	0.392	0.396	-1
0.001*	0.2	8.5	7.8	9	0.52	0.60	-13	0.392	0.396	-1
0.001	0.35	18.4	19.3	-5	0.39	0.38	3	0.400	0.385	4
0.001	0.5	40.8	41.2	-1	0.21	0.18	17	0.382	0.361	6
0.001*	0.5	41.1	41.2	0	0.17	0.18	-6	0.375	0.361	4
0.02	0.02	2.8	2.7	4	0.72	0.69	4	0.354	0.366	-3
0.02	0.1	3.6	3.4	6	0.54	0.49	10	0.351	0.361	-3
0.02	0.2	4.5	5.0	-10	0.43	0.39	10	0.343	0.348	-1
* Constant depth for the implicit scheme										

1.3 Experimental comparison

Frictional sliding experiments were carried out on three specimens of pure nickel with different grain sizes. These nickel specimens were already well characterized for grain size distribution and tensile properties in previous studies where, based on recent classification for grain size regimes [54], they were appropriately labeled as microcrystalline (mc), ultra-fine crystalline (ufc) and nanocrystalline (nc) metals. All three specimens were mechanically polished down to a surface roughness of less than ± 5 nm and tested on a commercial nanoindentation test system (Nanotest ™, Micro Materials Ltd, Wrexham, United Kingdom). The scratch experiments were carried out under constant normal load. This load was applied through the interaction of a permanent magnet with the solenoid coil attached to the upper end of the pendulum. This pendulum is held in the center through a frictionless pivot and it holds the tip at the opposite end. Therefore, the force is applied in the upper part and transferred to the tip through the frictionless pivot. On the other hand, the tangential displacement sample was imposed by a stage micro-motor, and the tangential force was calculated from the strain in the elastic cantilever beam holding the tip. The conical diamond probe had an apex angle of 70.3° and a tip radius of 2 μm. For the purpose of the experimental comparison, the scale of experimentation sufficiently large to consider the tip as perfectly conical. After the experiment, a series of at least 30 cross-sectional profiles of the residual steady-state scratch were obtained using a Tencor P10 profilometer (KLA-Tencor, San Jose, California) equipped with a conical diamond probe which had an apex angle of 45° and a tip radius of 2 μm.

1.4 Computational results

With the fine mesh and the explicit/Eulerian solution scheme, a comprehensive parametric study was conducted to quantify the effect of material properties on the frictional sliding response in steady state. The penetration depth of the indenter was kept constant during these simulations.

1.4.1 Forces and residual profiles

For a given set of material properties, Figure 1.3 shows the force evolution and the total internal energy as a function of the magnitude of relative displacement between the indenter and the meshed domain of the substrate. The force results obtained from using an implicit scheme simulation are also included for comparison. In all cases, the normal and frictional forces are both normalized by the A_r obtained using the steady state residual profile and Eq. 1.6. Hence, the final magnitude of the non-dimensional (normalized) normal force corresponds to the scratch hardness H_s. The relative displacement must exceed 5 times the radius of contact a_r before reaching steady state conditions. With the Eulerian scheme, it takes a longer frictional traveling distance to reach steady state, but this increase is not at the expense of an increase in the size of the simulation domain. Once steady state conditions are reached at the position of contact between the indenter and surface, the simulation needs to be pursued further over at least 3 times the radius of contact in order to obtain an accurate steady state surface profile in the unloaded state. For the results obtained using the Eulerian scheme, the condition of steady state are obtained throughout the domain when the total internal energy becomes constant.

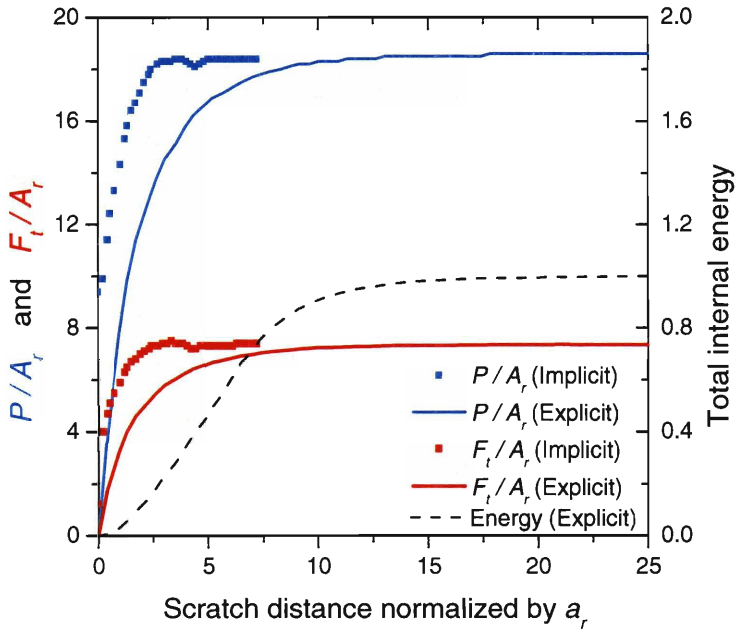

Figure 1.3: Evolution of total normal and tangential interaction forces between the indenter and the surface for material parameters σ_y/E^* = 0.001 and n = 0.35. The lines are for the explicit/Eulerian solution scheme whereas the symbols are for independent calculations using the implicit scheme (included for comparison).

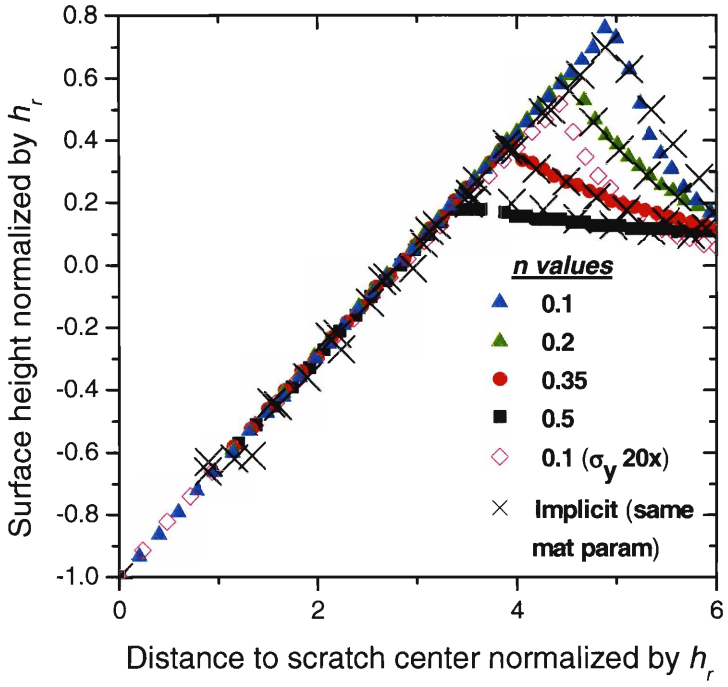

Figure 1.4: Residual surface profile as a function of strain hardening exponent for $\sigma_y/E^* = 0.001$. The profile for a material with $n = 0.1$ and $\sigma_y/E^* = 0.02$ is also included to describe the effect of initial yield strength. Also shown with cross-hairs are the simulation results from the implicit method for $\sigma_y/E^* = 0.001$ and the different values of n.

A series of residual scratch profiles is shown in Figure 1.4 to illustrate the strong influence of the strain hardening exponent n. The sliding direction is normal to this plot and the vertical axis corresponds to the symmetry plane. For a fixed ratio of $\sigma_y/E^* = 0.001$, the normalized pile-up height h_p/h_r increases gradually from approximately 0.20 to 0.75 as n decreases from 0.5 to 0.1. Also shown in Figure 1.4 is a profile for an initial yield strength σ_y yield strength that is 20 times as large. Although both σ_y/E^* and n can influence h_p/h_r, the contribution from the strain hardening exponent n to the frictional sliding response clearly appears as a dominant factor for such ductile materials. The relative influence of each parameter will be further quantified using results from the complete parametric study (c.f. Section 1.5.2).

Before presenting these parameterized results, two additional remarks are appropriate here. Instead of using h_p/h_r to characterize the pile-up behavior, alternative formulations could have been based on pile-up volume. However, calculations showed that this volume varies only slightly with respect to material properties. Such limited dependence can be easily understood from the law of volume conservation that would apply in steady state if there were no residual volume variations due to the presence of residual stresses. Finally, details need to be given regarding the calculation of h_p and a_r from the position of individual nodes in the finite element discretization. The measure of h_p is taken as the height at which the width of the pile-up peak reached the horizontal distance between adjacent nodes. Such procedure is believed to be the best possible way to eliminate fluctuations associated with different sharpness and symmetry characteristics of the node profiles.

For any set of simulation results, the peak of the profile can be sharp with a single node at the tip, blunted with two nodes at nearly the same maximum height, or anywhere in-between those two opposite cases. For the same reason, a_r was corrected for symmetry by measurements made from the mid-position of the horizontal segment drawn to determine h_p. These corrections did not change individual measurements by more than 5%, but they significantly reduced random fluctuations in H_s and h_p/h_r.

1.4.2 Dependence of the dimensionless functions on material parameters

The effect of plastic strain hardening exponent on the frictional sliding response was studied for 7 different values of n: 0, 0.02, 0.06, 0.1, 0.2, 0.35 and 0.5. For each n value, the initial normalized yield strength σ_y/E was varied by at least an order of magnitude. Following the general trend observed in most material systems, the softest materials were studied up to the highest hardening rates whereas very hard materials were studied predominantly in the regime of low hardening rates. A set of 70 material property combinations was constructed to cover homogeneously the range of material property space indicated in Table 1.2. To obtain this range and to verify the scaling assumption for the use of the ratio σ_y/E, the properties were independently varied in the range of 20 to 7000 MPa for σ_y and from 4 to 600 GPa for E.

Table 1.2: Range of elasto-plastic properties covered by the parametric finite element study.

	σ_y/E	
n	***Min***	***Max***
0	0.01	0.1
0.02	0.005	0.07
0.06	0.002	0.04
0.1	0.001	0.032
0.2	0.0004	0.02
0.35	0.0002	0.01
0.5	0.0001	0.005

The dependence on these material parameters of the dimensionless functions defined in Section 1.2.2 (Eqns 1.10 to 1.12) was determined from the FEM results obtained with this set of properties. For the function Π_β describing the pile-up behavior and the function Π_γ describing the friction behavior, logistic functions were employed to describe the dependence on n and σ_y/E^*. Although there could be fundamental justifications for employing these functions, the practical advantage and improved accuracy obtained by using them was considered here as a major advantage. In addition, these functions allow use of only a small number of fitting parameters and they have asymptotes.

For the determination of any of the three dimensionless functions, the numerical solutions were obtained by error minimization at two distinct steps. The first step was for the fitting with

respect to σ_y/E^* that was done independently for each value of n, whereas the second step consisted in fitting with respect to n the different coefficients obtained in the first step. Small adjustments were introduced through a series of iterations aimed at enduring the most monotonic dependence on n for the sub-functions established in step 2 while maintaining fidelity to the FEM data.

In the following figures, these functions are plotted as continuous lines for 5 different values of strain hardening exponent. Also plotted are the individual data points obtained from finite element results and the analysis procedures described in Section 1.2.3. Figure 1.5 is for the function Π_α, the normalized scratch hardness H_s/σ_y as a function of the normalized yield strength σ_y/E^*,

$$\Pi_\alpha(n,\frac{\sigma_y}{E^*})=\left(\frac{H_S}{\sigma_y}\right)=\alpha 1(n)\left(\frac{\sigma_y}{E^*}\right)^{\alpha 2(n)} \qquad \textbf{1.15}$$

with

$\alpha 1(n)=3.32-5.79n+2.8n^2$

and

$\alpha 2(n)=0.07-1.283n+0.248n^2$.

This simple exponential function fits the data with high accuracy throughout the material space covered. A certain amount of scatter is observed for the FEM data set. With the relative error doubling when the hardness is calculated from the contact radius, even a small fluctuation in the contact radius, inherent to space discretization, can explain this scatter. Assuming the absence of bias on the fluctuations, they should not affect significantly the determination of the dimensionless function Π_α, the normalized hardness H_s/σ_y dimensionless function. For low hardening materials with n below 0.1, Π_α presents a relatively limited dependence on the normalized yield strength as the absolute value ranges from 2.5 to 4. Interestingly, this range of hardness to yield strength ratio is similar to the range from 2.6 to 3 typical found in normal indentation tests on hard materials. For larger values of the strain hardening exponent n, the ratio of H_s/σ_y increases significantly as does its dependence on σ_y/E^*. The predictions for the property dependence reported for indentation hardness follow a similar trend [9]. However, the magnitude of the dependence reported here for frictional sliding is several times larger. Such a difference can be explained by a difference in the magnitude of the plastic strain under the indenter. A more detailed discussion about the relationships between normal indentation and frictional sliding will be presented in Section 1.5.1 after the discussion of the effect of plastic flow properties on the pile-up and frictional response.

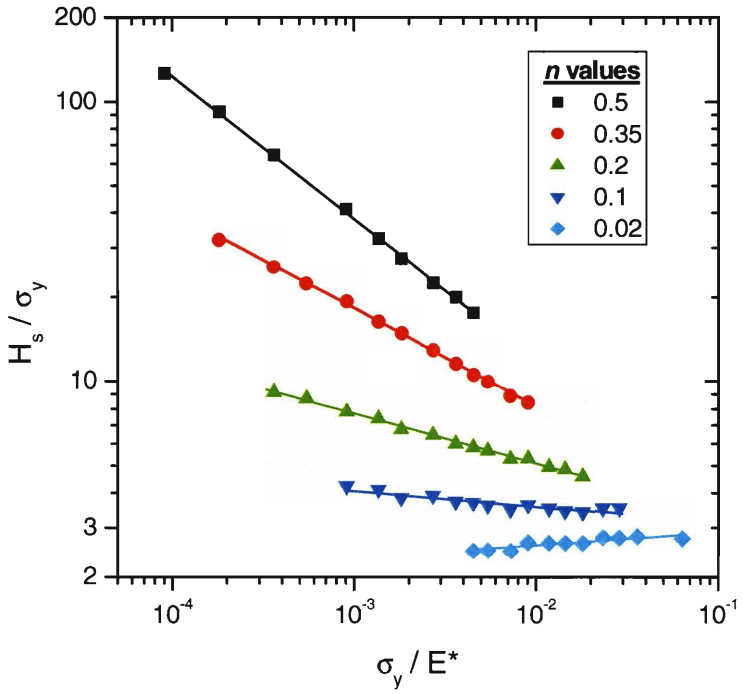

Figure 1.5: Normalized scratch hardness as a function of normalized yield strength for five different values of the strain hardening exponent n. The curves represent the output from using the predicting equation 1.14.

The second function, Π_β, is for the dependence of the normalized pile-up height on the elasto-plastic properties:

$$\Pi_\beta\left(n, \frac{\sigma_y}{E^*}\right) = \frac{h_p}{h_r} = \Pi_{\beta,RP}(n) \Big/ \left[1 + \left(\frac{\sigma_y}{X_\beta(n)\, E^*}\right) p_\beta(n)\right] \qquad \textbf{1.16}$$

with

$$\Pi_{\beta,RP}(n) = 0.904 - 1.684n + 1.987n^2 - 2.722n^3,$$

$$X_\beta(n) = 0.0378 - 0.2129n + 1.145n^2 - 3.34n^3 + 3.54n^4$$

and

$$p_\beta(n) = -0.68 \ln(n + .02).$$

This numerical function is plotted as five different continuous lines in Figure 1.6, each line representing a specific value of the strain hardening exponent *n*. Such representation illustrates the fit with the original *FEM* data points and how the he pile-up height decreases with an increase in yield strength. For the range of σ_y/E^* covered, it also indicate a pronounced influence of the strain hardening exponent for all values of σ_y/E^*. An important effect of the strain hardening exponent was already depicted in Figure 1.4, but only for a specific value of σ_y/E^*.

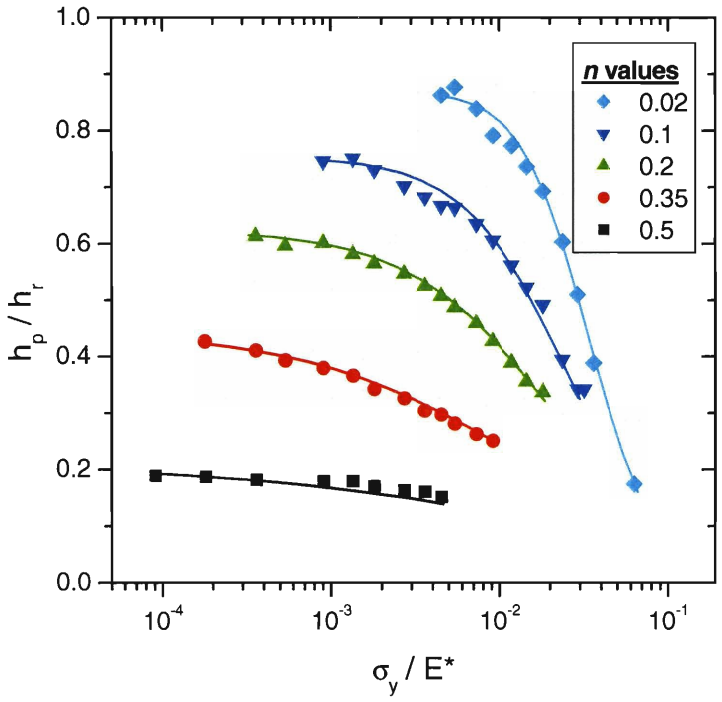

Figure 1.6: Normalized pile-up height as a function of normalized yield strength for five different values of the strain hardening exponent *n*. The curves represent the output from using the predictions of equation 1.15.

For low values of σ_y/E^*, the rigid-plastic asymptote was nearly achieved at most values of the strain hardening exponent n. For large values of σ_y/E^*, the curves and the data were truncated for $n \geq 0.35$. Such procedure limits the analysis to the cases where there is pile-up formation during scratching. The phenomenon of sink-in still leaves a residual pile-up, but the radius of residual contact does not correspond with the position of maximum height on the residual profile, requiring a more sophisticated analysis than the one presented here. This necessary truncation can explain why the elastic-limit of no residual pile-up was not approached except for the low hardening case. For $n = 0.02$, the curve clearly indicated a change from a negative to a positive inflection.

To exemplify the relative contribution of n and σ_y/E^*, we consider a typical soft metallic alloy with $n = 0.1$ and $\sigma_y/E^* = 0.001$. A decrease in the characteristic h_p/h_r of that alloy from approximately 0.75 to 0.6 can occur either if n increases by two fold or if σ_y is increased by an order of magnitude, indicating a significantly more pronounced effect of increasing hardening exponent on h_p/h_r. However, although h_p/h_r is a complementary measurement that characterizes the frictional sliding response, the normalized pile-up height does not provide the pressure bearing capability of the material. In fact, the scratch hardness of the alternative material with $n = 0.2$ would be about 4 times smaller than the one for which σ_y would be increased by an order of magnitude.

In view of the lack of any prior experimental data or computational predictions for the effect of plastic hardening on H_s/σ_y and h_p/h_r, the results presented in this paper can only be compared with the predictions of Bucaille *et al.* [39, 40] for perfectly plastic materials. For the same indenter geometry, quantitative agreement is found for the hardness values. For the normalized pile-up height, the predictions are similar for materials with low hardening but the height predictions for large σ_y/E^* were significantly lower in the previous study [39, 40]. Since the friction increases the pile-up height in frictional sliding because of the directionality of plastic flow, part of this difference could be accounted for by the assumption of frictionless contact in refs. [39, 40]. However, the former study used an implicit scheme with a constant depth. Therefore, it is possible that a change in the trajectory used to reach steady state, as described here in Section 1.2.3, would also lead to increased h_p/h_r to corroborate with the results presented here.

As a third parameter to characterize the frictional sliding response, the overall friction coefficient and the materials property dependence of its respective dimensionless function Π_γ were also determined. Figure 1.7 presents the FEM data and this function

$$\Pi_\gamma(n,\frac{\sigma_y}{E^*})=\left(\frac{F_t}{P}\right)=\mu_s=\Pi_{\gamma,RP}\Big/\left[1+\left(\frac{\sigma_y}{X_\gamma(n)\,E^*}\right)p_\gamma(n)\right] \qquad \textbf{1.17}$$

with

$\Pi_{\gamma,RP}=0.416,$

$X_\gamma(n)=0.1149-0.2378n+0.0954n^2$

and

$p_\gamma(n)=0.8-n^2/2.$

This overall ratio of tangential to normal force contains information about the friction for the normal contact between surfaces and also about the contact geometry. The contribution from the friction between normal surfaces should be approximately equal to the coefficient μ_a, which is 0.15 for all the cases presented here. The contribution for the tangential pressure applied towards upstream would depend on the actual contact geometry and the plastic flow field.

With respect to material properties, μ_{tot} varies just the same way as h_p/h_r except that the magnitude of the variation is significantly less. Such a smaller dependence can be explained by a concurrent increase in tangential and normal pressure as the area of contact increases due to a higher pile-up. Within a limited range of yield strength and for n below 0.2, the predictions presented here suggest that any intrinsic effect of material plastic flow properties would fall within the scatter associated with surface preparation, material homogeneity and friction. This prediction might appear inconsistent with several previous studies that showed changes in friction coefficient between distinct but similar materials [36, 50, 55]. However, these studies are generally carried out with a spherical tip in which case the geometry and the contact angle changes with penetration depth and pile-up height, therefore making the isolation of material properties more difficult.

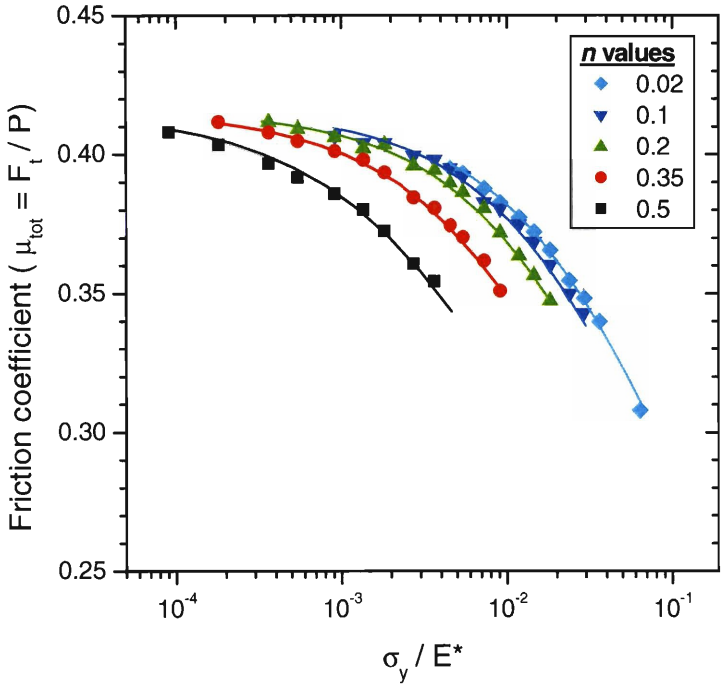

Figure 1.7: Effect of normalized yield strength and strain hardening exponent on the friction coefficients. The curves represent the output from using the predicting equation 1.16.

An additional remark is in order here regarding the process of pile-up formation. It is well known from previous literature on machining [56-59] that there is a critical apex angle θ below which the plastic deformation process transitions from ductile ploughing to chipping or machining. Although quantitative information is unavailable, it is very likely that this transition would occur at a larger angle θ for materials that have a strong tendency to form large and steep pile-up. Using the finite element models developed in this study, attempts were made to cover softer materials that would be nearly perfectly plastic while maintaining μ_a and θ to their fixed values. However, with n below 0.02 and σ_y/E^* below approximately 0.005, the normalized pile-up height h_p/h_r exceeded 0.9 and convergence required the imposition of special mesh gradients and control. It is believed that such material conditions were near this transition point for the geometry and friction conditions studied. If one were to characterize computationally or experimentally the behavior of softer perfectly plastic materials to ductile ploughing, μ_a and/or θ would probably need to be changed.

1.4.3 Experimental comparison

To compare the frictional sliding response of pure mc, ufc and nc nickel with the predictions from the parametric study, experiments were carried out under the same geometrical conditions. Using only pure nickel as a model, the effects of different phases and different friction coefficients were ruled out. In addition, carrying out the experiment at large loads eliminated the risk for surface and size effects. Because of the difference in hardness of the different nickel samples and the fact

that a constant load of 2 N was imposed in each case, the absolute dimensions of the width of the residual scratch $2a_r$ ranged from 60 μm for the mc nickel to 34 μm for the nc nickel. Additional tests carried out at different loads indicated that the response was not significantly dependent on the size of the indenter impression.

After the experiment, the pile-up height h_p and the residual depth h_r were determined from the maximum height and maximum depth obtained after linearly interpolating for the position of the original surface obtained from profilometry. The points used for this interpolation were away from the scratch center at a distance of four times the residual radius of contact ($4a_r$). With a very limited curvature and a slope below 2° for the original surface, this correction procedure was considered the most simple and reproducible alternative.

Using this procedure, individual values of a_r, h_p and h_r were obtained for each of cross-sectional profiles obtained from scanning at least 5 independent scratches. Typically, the difference in the average value obtained from independent experiments did not exceed 5%. However, for a given set of data associated with a single experiment, the standard deviation could reach up to 20% for the normalized pile-up height h_p/h_r. Such level of fluctuation corroborates well the oscillations in the process of pile-up formation and clearly emphasizes the need for a sample size of at least 25 data points.

Table 1.3: Comparison between experimental results and predictions based on elasto-plastic properties. The elasto-plastic properties were obtained from tensile tests reported elsewhere [60-62].

	Properties		H_s/σ_y			h_p/h_r			μ_{tot}		
	σ_y (MPa)	n	*Exp.*	*FEM*	Δ (%)	*Exp.*	*FEM*	Δ (%)	*Exp.*	*FEM*	Δ (%)
nc	1600	.02	2.76	2.58	7	.82	.84	-2	0.37	.39	-5
ufc	850	.06	2.92	3.09	-6	.74	.78	-4	0.38	.40	-5
mc	170	.19	7.92	7.39	7	.64	.62	3	0.38	.41	-7

For all three dimensionless parameters associated with the functions Π_α, Π_β and Π_γ, Table 1.3 presents a detailed comparison between the finite element predictions and the average values from the experimental results. With a difference of at most 7% between the predictions and the results, the finite element predictions appear to capture very well the trends as well as the absolute values of the scratch parameters H_S, h_p/h_r and μ_{tot}. Figure 1.8 compares individual experimental scratch profiles obtained for the mc and nc pure nickel samples. In agreement with the predictions shown for these materials based on their plastic flow properties (*c.f.* Table 1.3), the pile-up for the nanocrystalline nickel has a higher ratio of h_p/h_r and presents a higher slope in the region of $r > a_r$. However, although the predictions for the height of the pile-up match with the experimental results, the experimental profiles appear more blunted. Such blunting could be due to surface stiffness effects that were not taken into account by the finite element models.

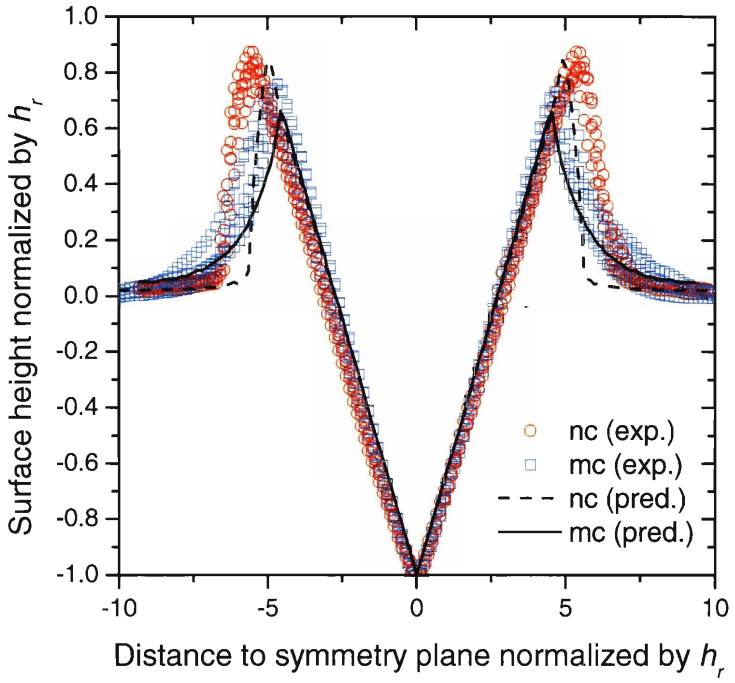

Figure 1.8: Experimental profiles for pure nc and mc nickel. The lines represent predictions for these materials based on the plastic flow properties listed in Table 1.3.

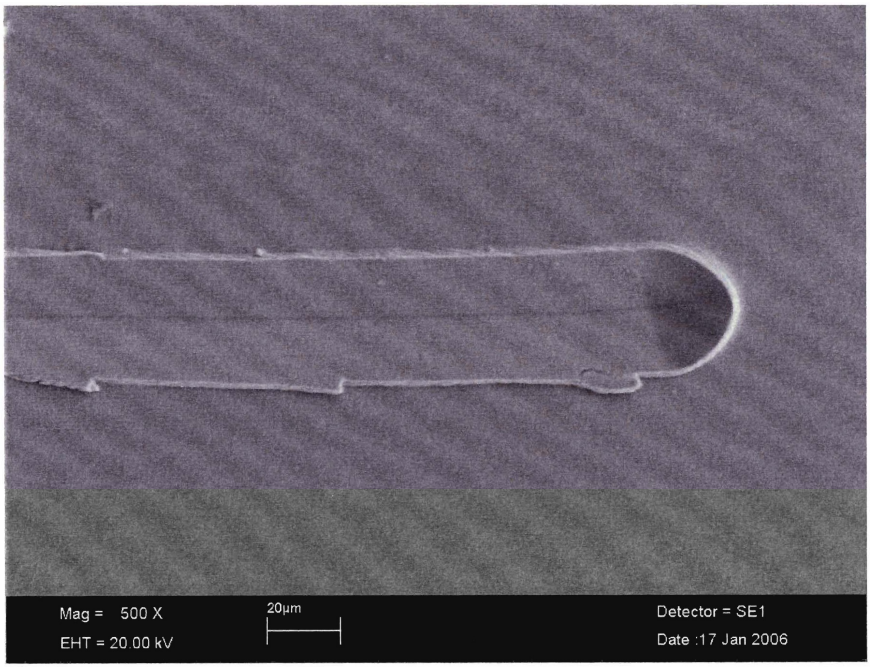

Figure 1.9: SEM image of a typical scratch on pure nc. The tip was moving from left to right. The low plastic strain hardening of this material results in localized events of instability in the process of pile-up formation as seen at three locations on the bottom side of the scar.

To provide a more detailed representation of the frictional sliding process in pure nc nickel, Figure 1.9 presents an image obtained from a scanning electron microscope (SEM). The low plastic strain hardening of this material is likely to be the origin for the localized events of instability in the formation of the pile-up as seen at three locations on the bottom side of the scar. These observations suggest that the geometrical and material conditions tested here were very near the point of physical instability discussed in the previous section. They also point to the need for a relatively large set of residual scratch profiles in order to extract accurate average values.

1.5 Discussion

In this study, we developed a new framework to analyze the material behavior in frictional sliding. For the contact between a hard conical indenter and a fixed apex angle, it is proposed to use the scratch hardness and the normalized pile-up height to relate the response with elasto-plastic properties.

1.5.1 Predicting the scratch behavior using the dimensionless functions

A special attention was given to ensure numerical accuracy. From a computational standpoint, the explicit/Eulerian scheme used in the analysis was well tested for its elastic limit and by comparing the results with those obtained with explicit/Lagrangian and implicit/Lagrangian schemes. From an experimental standpoint, all the measurements were carried out after a direct calibration of the instrument through the use of standard weights for the force measurements and of standardized surface patterns for the residual profile data. Under these conditions, the set of dimensionless functions presented in this study is expected to be relatively accurate and to correspond well with what would be the theoretical solution for this complex contact mechanics problem.

The comparison between the FEM results and the experimental results on the pure nickel model material system showed a strong agreement, both in terms of trends and absolute values. In fact, the relative difference was well below the computational variability associated with space discretization and the experimental variability inherent to the processes associated with microscale elasto-plastic contacts. And in other independent studies, a good correspondence was also observed between the predictions and the experimental results with pure copper over a wide range of different grain sizes (c.f. Chapter 2) and with aluminum alloys having different dispersion hardening precipitates (c.f. Chapter 3).

Now assuming a good accuracy for the results from FEM, the accuracy of the dimensionless functions would depend on the ability of the fitting functions to correctly interpolate between the data points. For the interpolation with respect to σ_y/E^*, a careful inspection of Figure 1.5 to Figure 1.7 should provide a convincing argument. For the interpolation with respect to n, it should be noted that all the sub-functions are very smooth with a limited curvature. The functions $\alpha 1(n)$,

$\alpha 2(n)$, $\Pi_{\beta,rp}(n)$ and $X_\gamma(n)$ are all nearly linear whereas the functions $p_\beta(n)$ and $p_\gamma(n)$ steadily decrease with n (c.f. Figure 1.10, thesis only). $X_\beta(n)$ is the only function with a decreasing slope up to a minimum point for $n = 0.4$. Following this minimum point, $X_\beta(n)$ slightly increases to capture the important change in the curvature of Π_β versus σ_y/E^* observed in the range between $n = 0.35$ and $n = 0.5$. Through the use of these sub-functions, accuracy should be obtained in the range covered by the FEM data. This range of properties can be approximated by

$$\left(4.8\times10^{-5}\right)n^{-1.22} < \left(\frac{\sigma_y}{E^*}\right) < \left(5.5\times10^{-2}\right)e^{-5.11n}, \quad where \quad 0 \le n \le 0.5, \qquad \textbf{1.18}$$

or determined by inspection of Table 1.2. This range encompasses a great variety of the elasto-plastic properties found in practice. However, the numerical functions may not be accurate outside the specified range or when the plastic flow behavior greatly differs from power law strain hardening.

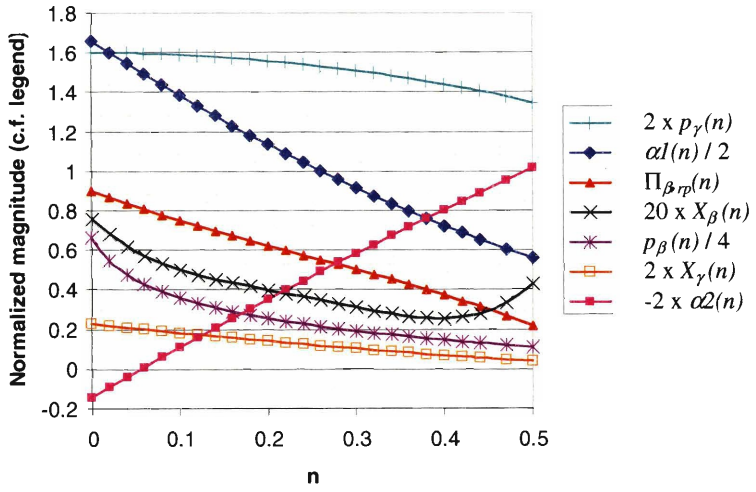

Figure 1.10: Evolution of all the sub-functions used in Π_α, Π_β and Π_γ for the effect of the plastic strain hardening exponent n.

Π_α and Π_β were both found to simultaneously depend on σ_y/E^* and n. Using equations 1.15 and 1.16, a complete sensitivity analysis was carried out for this effect of material properties. Table 1.4 presents the maximum percent variation that can result from independently varying σ_y/E^* or n by +/-5 %. In most cases, these variations are less than twice those applied to the input parameters and they were found to be rather independent of the absolute value of σ_y/E^*, but their dependence on the absolute value of the strain hardening exponent was significant. For $n \le 0.2$, the maximum variation in the predictions is similar or smaller than the variation in the material properties specified, but for higher n values the dependence intensifies for the effect of variations in n whereas it decreases for the effect of variations in σ_y/E^*. As n increases, its contribution to the magnitude of the flow stress also increases and so does the sensitivity of the predictions for H_s/σ_y and h_p/h_r. However, this increased sensitively still falls within the range of 4 times the error on the input

parameters. For all the material property cases covered in this study, frictional sliding response can be predicted with an accuracy of the same order of magnitude as the accuracy on the input data for the material properties.

Table 1.4: Sensitivity analysis for the effect of variations in material properties on the predictions from the dimensionless functions.

	Effect of σ_y				Effect of n			
	On H_s/σ_y		on h_p/h_r		on H_s/σ_y		on h_p/h_r	
	+ 5%	- 5%	+ 5%	- 5%	+ 5%	- 5%	+ 5%	- 5%
$n \leq 0.1$	5.3	-5.3	-4.7	4.8	3.4	-3.3	-1.8	1.9
$n = 0.2$	4.1	-4.1	-2.4	2.5	7.6	-7.1	-3.3	3.4
$n = 0.35$	3.2	-3.3	-1.4	1.5	13.3	-11.9	-7.0	7.4
$n = 0.5$	2.4	-2.5	-0.7	0.8	18.8	-16.2	-21.0	20.1

1.5.2 Representative plastic strain and comparison with normal indentation

The concept of representative strain has been used in recent studies on indentation [10, 12, 14, 15, 63, 64] for the amount of a characteristic plastic strain and the associated flow stress. The value is defined as the strain at which you can best establish a direct relationship between the hardness and the representative flow stress. Through this process, the variables σ_y/E^* and n are grouped into a single one that relates to the representative stress. As previously stated [10], the discrepancy in the values reported in the different studies can be explained by the differences in the definition used. For instance, the values determined using the loading curvature of the (P-h) response are significantly lower than the 8-10% found both numerically [10] and experimentally [4] for the traditional definition of hardness based on the residual area of contact.

In this study, we used the traditional definition of the scratch hardness and tried to merge the variables. It appeared impossible to achieve a maximum error of less than 5% while trying to cover the full range of n values with a single value of ε_{rep}. Therefore, the material properties space covered was split into two. For the first domain, which includes all the data for $n \leq 0.2$ along with data for $\sigma_{rep}/E^* < 0.018$ and $n = 0.35$, the evolution of the scratch hardness with respect σ_{rep}/E^* becomes approximately n independent when normalized by the flow stress at 33.6% plastic strain. This fitting is shown in Figure 1.11 along with a second plot made with a lower ε_{rep} of 15.5%. To ensure that all the possible combinations of material properties are covered within the range $0.2 < n < 0.35$, for this second domain data for $n = 0.2$ and $\sigma_{rep}/E^* > 0.016$ were added to the set of data for ≥ 0.35. By separating the material space, the maximum error felt below 4.2% and 3.2% for the plots with ε_{rep} of 33.6% and 15.5%, respectively.

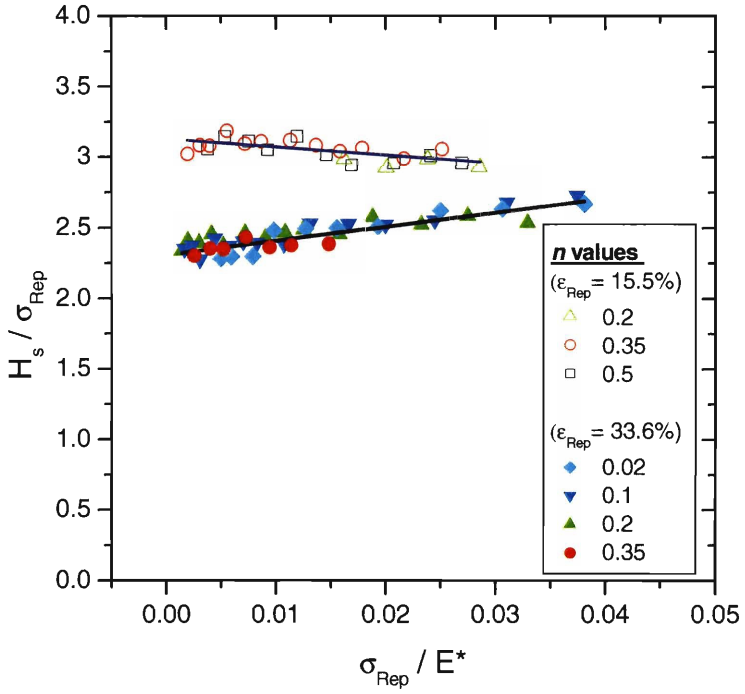

Figure 1.11: Scratch hardness normalized by the flow stress at two distinct representative strains. The lower curve is for the first material property domain for which ε_{rep} = 33.6% fits best the data, whereas the upper curve is for the second property domain and ε_{rep} = 15.5%.

Especially when a significantly different value of ε_{rep} is needed to cover the full material property space, this representative strain determined by error minimization may well be more of a mathematical convenience than a characteristic physical quantify. Ogasawara *et al.* [14] have shown that ε_{rep} would be more appropriately defined by approximating the strain field in normal indentation is biaxial. This alternative procedure was also employed in the current study, but Table 1.5 shows no reduction in the fitting error. Also, the biaxial strain assumption did not allow carrying out a fit with a single ε_{rep} for all the sets of material properties. One possible explanation for this result is the predominant shear mode of deformation that prevails during frictional sliding with the geometry studied here and a low hardening exponent n. But independently of whether ε_{rep} is associated with a true characteristic plastic strain or eigenvalue, its usage does provide simplified expressions for the scratch hardness

$$\left(\frac{H_S}{\sigma_{33.6\%}}\right) = 9.88\left(\frac{\sigma_{33.6\%}}{E^*}\right) + 2.31 \quad \Leftrightarrow \quad n \le 0.2 \quad or \quad n \le 0.35 \; and \; \left(\frac{\sigma_{33.6\%}}{E^*}\right) < 0.018 \qquad \textbf{1.19}$$

or

$$\left(\frac{H_S}{\sigma_{15.5\%}}\right) = -5.64\left(\frac{\sigma_{15.5\%}}{E^*}\right) + 3.13 \quad \Leftrightarrow \quad n \geq 0.35 \quad or \quad n \geq 0.2 \; and \; \left(\frac{\sigma_{15.5\%}}{E^*}\right) > 0.016 \qquad \textbf{1.20}$$

and also provides a basis for comparison with normal indentation under the same geometrical conditions. Such a comparison is included in Table 1.5 with literature data based on the loading curvature of the P-h response as well as based on the traditional definition of hardness.

Table 1.5: Summary of the different values obtained for ε_{rep} by using the uniaxial and/or bixial strain assumption. Also shown are literature data for instrumented indentation.

		Based on ε_p (uniaxial/shear)		Based on $2\varepsilon_p$ (biaxial)	
		ε_{rep} (%)	Max Error (%)	ε_{rep} (%)	Max Error (%)
Current study	Property domain #1	33.6	4.2	16.9	4.3
	Property domain #2	15.5	3.2	7.7	3.2
Literature on indentation (Dao *et al.*, Ogasawara *et al.*, 2005)	Functional for loading curvature	3.3	2.9	1.15	NA
	Functional for residual area of contact	8.2	6.0	---	---

1.5.3 Practical use and limitations of instrumented single scratch tests

A four fold increase in the amount of plastic strain obtained by using frictional sliding offers a greater capability to study effects of microstructure on the plastic flow process than with indentation. These effects could include strain-induced grain growth, partial crystallization or localized damage induced by the high residual tensile stress components. The residual tensile stresses are particularly high on the surface of the residual scar, especially near the point of contact with the indenter.

From a perspective of measuring plastic properties, the frictional sliding technique amplifies the effect of the strain hardening exponent on the normalized pile-up height. Whereas the maximum ratio of h_p/h_r is of the order of 0.3 for normal indentation (Cheng and Cheng 1998), this ratio can vary from 0.2 to 0.9 for the range of material properties covered in the current study. Also, the surface curvature in frictional sliding is always positive, leading to the formation of a pile of material in front of the indenter. It is much easier to measure an impression accurately with pile-up than with sink-in. Based on these considerations, it could be more suitable to use frictional sliding in conditions where the information from the residual profile would be used to establish relationships with properties.

Repeated measurements of h_p/h_r in frictional sliding can be more easily obtained by taking adjacent 2D profiles from the unloaded scratch instead of studying a full 3D pyramidal imprint. Procedures could be developed to measure the a_r and h_p by scanning the surface with the indenter tip itself, but such technique may not provide an accurate direct measurement of h_r. Preliminary experimental trials suggested that the indenter can hardly reenter fully the residual scar without the application of a relatively high load. Therefore, measuring directly the residual profile appears as the most reliable approach to establish a relationship with mechanical properties.

A parameter that was not been varied in the experiment or computationally is the Coulomb friction coefficient μ_c. Although a reasonable estimate is provided wherein, the effect of this parameter on the frictional sliding response. Early calculations indicated a limited dependence for the normalized hardness H_s/σ_y, but a significant dependence for h_p/h_r. A comprehensive study is underway for the effect of μ_c on the frictional sliding response.

1.6 Conclusions

From this study of the frictional sliding response of elasto-plastic materials, the following conclusions are drawn.

1. The frictional sliding response of elasto-plastic materials in contact with a hard conical tip can be predicted with an accuracy of the same order as the accuracy of the input data for the material properties. The material properties needed are the Young's modulus, the Poisson's ratio, the initial yield strength and the plastic strain hardening exponent.

2. As for the indentation hardness, the hardness in frictional sliding of elastic-perfectly plastic materials is between 2.5 and 3 times the yield strength. However, non-linear effects become progressively more significant as the plastic strain hardening exponent increases and the magnitude of the change in hardness becomes several times larger than the one reported for normal indentation. Also, the pile-up height in frictional sliding can be as much as 3 times as high as the one obtained through normal indentation and a transition from pile-up to sink-in occurs only at much greater values of the hardening exponent.

3. The overall friction coefficient decreases slightly with an increase in yield strength or strain hardening exponent, but for most cases the magnitude of the change would fall within the experimental scatter. This finding is specific to the contact with a conical tip where the assumption of size-independent material properties allows for the use of geometrical scaling. It does not apply to the contact with a spherical tip where the geometrical contribution of the penetration depth on the friction coefficient can lead to a misinterpretation of experimental results.

4. In frictional sliding, the pile-up height and the hardness are the response parameters that are the most sensitive to the plastic flow properties. Further research is underway to develop an engineering method for estimating experimentally these properties.

A simple scratch test induces a localized plastic flow process that can be modeled, reproduced experimentally and used for material characterization. It can also bring the contact conditions closer to those generated in actual tribological events.

1.7 References

[1] K. L. Johnson, *Contact mechanics*. London: Cambridge University Press, 1985.

[2] J. A. Williams, "Analytical models of scratch hardness," *Tribology International*, vol. 29, pp. 675-584, 1996.

[3] A. C. Fischer-Cripps, *Introduction to Contact Mechanics*. New York: Springer-Verlag, 2000.

[4] D. Tabor, *The hardness of metals*. Oxford: Clarendon press, 1951.

[5] G. Revankar, "Introduction to Hardness Testing," in *ASM Handbook: Mechanical Testing and Evaluation*, vol. 8. Materials Park: ASM International, 1990.

[6] I. M. Hutchings, *Tribology: Friction and Wear of Engineering Materials*. Kent: CRC Press, 1992.

[7] W. C. Oliver and G. M. Pharr, "An Improved Technique for Determining Hardness and Elastic-Modulus Using Load and Displacement Sensing Indentation Experiments," *Journal of Materials Research*, vol. 7, pp. 1564-1583, 1992.

[8] Y. T. Cheng and C. M. Cheng, "Scaling, dimensional analysis, and indentation measurements," *Materials Science & Engineering R-Reports*, vol. 44, pp. 91-149, 2004.

[9] Y.-T. Cheng and C.-M. Cheng, "Scaling approach to conical indentation in elastic-plastic solids with work hardening," *Journal of Applied Physics*, vol. 84, pp. 1284, 1998.

[10] M. Dao, N. Chollacoop, K. J. Van Vliet, T. A. Venkatesh, and S. Suresh, "Computational modeling of the forward and reverse problems in instrumented sharp indentation," *Acta Materialia*, vol. 49, pp. 3899-3918, 2001.

[11] Y.-T. Cheng, Z. Li, and C.-M. Cheng, "Scaling relationships for indentation measurements," *Philosophical Magazine A: Physics of Condensed Matter, Structure, Defects and Mechanical Properties*, vol. 82, pp. 1821-1829, 2002.

[12] L. Wang, M. Ganor, and S. I. Rokhlin, "Inverse scaling functions in nanoindentation with sharp indenters: Determination of material properties," *Journal of Materials Research*, vol. 20, pp. 987-1001, 2005.

[13] L. Wang and S. I. Rokhlin, "Dimensionless scaling functions for continuous stiffness nanoindentation with sharp indenters," *International Journal of Solids and Structures*, vol. 42, pp. 3807-3832, 2005.

[14] N. Ogasawara, N. Chiba, and X. Chen, "On the Representative Strain of Indentation Analysis," *Journal of Materials Research*, vol. In press, 2005.

[15] N. Chollacoop, M. Dao, and S. Suresh, "Depth-sensing instrumented indentation with dual sharp indenters," *Acta Materialia*, vol. 51, pp. 3713-3729, 2003.

[16] J.-L. Bucaille, S. Stauss, P. Schwaller, and J. Michler, "A new technique to determine the elastoplastic properties of thin metallic films using sharp indenters," presented at Proceedings of the 30th International Conference on Metallurgie, Apr 28-May 2 2002, San Diego, CA, United States, 2004.

[17] Y. P. Cao and J. Lu, "A new method to extract the plastic properties of metal materials from an instrumented spherical indentation loading curve," *Acta Materialia*, vol. 52, pp. 4023-4032, 2004.

[18] A. G. Atkins and D. Tabor, "Plastic indentation in metals with cones," *Journal of Mechanics and Physics of Solids*, vol. 13, pp. 149-164, 1965.

[19] Y. V. Milman, B. A. Galanov, and S. I. Chugunova, "Plasticity characteristic obtained through hardness measurement," *Acta Metallurgica et Materialia*, vol. 41, pp. 2532, 1993.

[20] K. Tunvisut, N. P. O'Dowd, and E. P. Busso, "Use of scaling functions to determine mechanical properties of thin coatings from microindentation tests," *International Journal of Solids and Structures*, vol. 38, pp. 335-351, 2001.

[21] K. Tunvisut, E. P. Busso, N. P. O'Dowd, and H. P. Brantner, "Determination of the mechanical properties of metallic thin films and substrates from indentation tests," *Philosophical Magazine A: Physics of Condensed Matter, Structure, Defects and Mechanical Properties*, vol. 82, pp. 2013-2029, 2002.

[22] K. Matsuda, "Prediction of stress-strain curves of elastic-plastic materials based on the Vickers indentation," *Philosophical Magazine A: Physics of Condensed Matter, Structure, Defects and Mechanical Properties*, vol. 82, pp. 1941-1951, 2002.

[23] M. Sakai, T. Akatsu, S. Numata, and K. Matsuda, "Linear strain hardening in elastoplastic indentation contact," *Journal of Materials Research*, vol. 18, pp. 2087-2096, 2003.

[24] V. Marx and H. Balke, "Critical investigation of the unloading behavior of sharp indentation," *Acta Materialia*, vol. 45, pp. 3791-3800, 1997.

[25] Y.-T. Cheng and C.-M. Cheng, "Effects of `sinking in' and `piling up' on estimating the contact area under load in indentation," *Philosophical Magazine Letters*, vol. 78, pp. 115-120, 1998.

[26] M. Mata and J. Alcala, "Mechanical property evaluation through sharp indentations in elastoplastic and fully plastic contact regimes," *Journal of Materials Research*, vol. 18, pp. 1705-1709, 2003.

[27] J. Alcala, A. C. Barone, and M. Anglada, "Influence of plastic hardening on surface deformation modes around Vickers and spherical indents," *Acta Materialia*, vol. 48, pp. 3451-3464, 2000.

[28] B. J. Briscoe, S. K. Biswas, S. K. Sinha, and S. S. Panesar, "Scratch hardness and friction of a soft rigid-plastic solid," *Tribology International*, vol. 26, pp. 183-193, 1993.

[29] K. Maeda, A. Bismarck, and B. J. Briscoe, "Mechanisms of scratching frictions and damage maps for rubber compounds," *Wear*, vol. 259, pp. 651-660, 2005.

[30] R. D. K. Misra, R. Hadal, and S. J. Duncan, "Surface damage behavior during scratch deformation of mineral reinforced polymer composites," *Acta Materialia*, vol. 52, pp. 4363-4376, 2004.

[31] R. B. Mohamed Sani, S. K. Sinha, J. P. Ying Tan, and K. Y. Zeng, "Wear debris generation mechanism for polymers studied by nanoscratching," *Philosophical Magazine*, vol. 85, pp. 2101-2122, 2005.

[32] A. Dasari, J. Rohrmann, and R. D. K. Misra, "On the scratch deformation of micrometric wollastonite reinforced polypropylene composites," *Materials Science and Engineering A*, vol. 364, pp. 357-369, 2004.

[33] Z. F. Zhang, L. C. Zhang, and Y.-W. Mai, "Particle effects on friction and wear of aluminium matrix composites," *Journal of Materials Science*, vol. 30, pp. 5999-6004, 1995.

[34] Y. N. Liang, Z. Y. Ma, S. Z. Li, S. Li, and J. Bi, "Effect of particle size on wear behaviour of SiC particulate-reinforced aluminum alloy composites," *Journal of Materials Science Letters*, vol. 14, pp. 114-116, 1995.

[35] Z. Zhang, L. Zhang, and Y.-W. Mai, "Modelling friction and wear of scratching ceramic particle-reinforced metal composites," *Wear*, vol. 176, pp. 231-237, 1994.

[36] M. Bolduc, B. Terreault, A. Reguer, E. Shaffer, and R. G. St-Jacques, "Optimum tribological improvement of aluminum using oxygen plasma source ion implantation," *Journal of Materials Research*, vol. 18, pp. 1761-1764, 2003.

[37] S. Wilson, H. M. Hawthorne, Q. Yang, and T. Troczynski, "Sliding and abrasive wear of composite sol-gel alumina coated Al alloys," *Surface and Coatings Technology*, vol. 133-134, pp. 389-396, 2000.

[38] R. L. Deuis, C. Subramanian, and J. M. Yellup, "Abrasive wear of aluminium composites - a review," *Wear*, vol. 201, pp. 132-144, 1996.

[39] J. L. Bucaille, E. Felder, and G. Hochstetter, "Mechanical analysis of the scratch test on elastic perfectly plastic materials with the three-dimensional finite element modeling," *Wear*, vol. 249, pp. 422-432, 2001.

[40] J. L. Bucaille and E. Felder, "Finite-element analysis of deformation during indentation and scratch tests on elastic-perfectly plastic materials," *Philosophical Magazine a-Physics of Condensed Matter Structure Defects and Mechanical Properties*, vol. 82, pp. 2003-2012, 2002.

[41] G. Subhash and W. Zhang, "Investigation of the overall friction coefficient in single-pass scratch test," *Wear*, vol. 252, pp. 123-134, 2002.

[42] S. W. Youn and C. G. Kang, "A study of nanoscratch experiments of the silicon and borosilicate in air," *Materials Science and Engineering A*, vol. 384, pp. 275-283, 2004.

[43] S. W. Youn and C. G. Kang, "Erratum: "A study of nanoscratch experiments of the silicon and borosilicate in air" (Materials Science and Enginering A (2004) vol. 384 (1-2) (275-283) 10.1016/j.msea.2004.06.044)," *Materials Science and Engineering A*, vol. 393, pp. 398, 2005.

[44] L. Fang, Q. Cen, K. Sun, W. Liu, X. Zhang, and Z. Huang, "FEM computation of groove ridge and Monte Carlo simulation in two-body abrasive wear," *Wear*, vol. 258, pp. 265-274, 2005.

[45] G. M. Pharr, W. C. Oliver, and F. R. Brotzen, "On the Generality of the Relationship among Contact Stiffness, Contact Area, and Elastic-Modulus During Indentation," *Journal of Materials Research*, vol. 7, pp. 613-617, 1992.

[46] W. C. Oliver and G. M. Pharr, "Measurement of hardness and elastic modulus by instrumented indentation: Advances in understanding and refinements to methodology," *Journal of Materials Research*, vol. 19, pp. 3-20, 2004.

[47] S. D. Mesarovic and N. A. Fleck, "Spherical indentation of elastic-plastic solids," *Proceedings of the Royal Society of London Series a-Mathematical Physical and Engineering Sciences*, vol. 455, pp. 2707-2728, 1999.

[48] J. L. Bucaille, S. Stauss, E. Felder, and J. Michler, "Determination of plastic properties of metals by instrumented indentation using different sharp indenters," *Acta Materialia*, vol. 51, pp. 1663-1678, 2003.

[49] F. P. Bowden and D. Tabor, *The friction and lubrification of solids*. Oxford: Oxford University Press, 1950.

[50] T. Hanlon, A. H. Chokshi, M. Manoharan, and S. Suresh, "Effects of grain refinement and strength on friction and damage evolution under repeated sliding contact in nanostructured metals," *International Journal of Fatigue*, vol. 27, pp. 1159-1163, 2005.

[51] ABAQUS Theory Manual Version 6.5, Hibbitt, Karlsson and Sorensen Inc, Pawtucket, 2005

[52] C. E. Truman, A. Sackfield, and D. A. Hills, "Contact Mechanics of Wedge and Cone Indenters," *International Journal of Mechanical Sciences*, vol. 37, pp. 261-275, 1995.

[53] B. Storakers and D. Elaguine, "Hertz contact at finite friction and arbitrary profiles," *Journal of the Mechanics and Physics of Solids*, vol. 53, pp. 1422-1447, 2005.

[54] K. S. Kumar, H. Van Swygenhoven, and S. Suresh, "Mechanical behavior of nanocrystalline metals and alloys," *Acta Materialia*, vol. 51, pp. 5743-5774, 2003.

[55] L. Guzman, G. Bonini, M. Adami, P. M. Ossi, A. Miotello, M. Vittori-Antisari, A. M. Serventi, and E. Voltolini, "Mechanical behaviour of nitrogen-implanted aluminum alloys," *Surface & Coatings Technology*
Proceedings of the 1995 9th International Conference on Surface Modification of Metals by Ion Beams. Part 1, Sep 4-8 1995, vol. 83, pp. 284-289, 1996.

[56] A. J. Black, E. M. Kopalinsky, and P. L. B. Oxley, "Investigation of the different regimes of deformation which can occur when a hard wedge slides over a soft surface: the influence of wedge angle, lubrication and prior plastic working of the surface.," *Wear*, vol. 123, pp. 97-114, 1988.

[57] T. Tsukizoe and T. Sakamoto, "Friction in scratching without metal transfer.," vol. 18, pp. 65-72, 1975.

[58] N. Gane and J. Skinner, "Friction and scratch deformation of metals on a micro scale.," vol. 24, pp. 207-217, 1973.

[59] A. J. Black, E. M. Kopalinsky, and P. L. B. Oxley, "Sliding metallic friction with boundary lubrication. An investigation of a simplified friction theory and of the nature of boundary lubrication," *Wear*, vol. 137, pp. 161-174, 1990.

[60] R. Schwaiger, B. Moser, M. Dao, N. Chollacoop, and S. Suresh, "Some critical experiments on the strain-rate sensitivity of nanocrystalline nickel," *Acta Materialia*, vol. 51, pp. 5159-5172, 2003.

[61] T. Hanlon, E. D. Tabachnikova, and S. Suresh, "Fatigue behavior of nanocrystalline metals and alloys," *International Journal of Fatigue*, vol. 27, pp. 1147-1158, 2005.

[62] T. Hanlon, "Grain size effects on the fatigue response of nanocrystalline materials," in *Dept. of Materials Science and Engineering*. Cambridge: MIT, 2004.

[63] Y. P. Cao and J. Lu, "Depth-sensing instrumented indentation with dual sharp indenters: Stability analysis and corresponding regularization schemes," *Acta Materialia*, vol. 52, pp. 1143-1153, 2004.

[64] E. Giannakopoulos and S. Suresh, "A three-dimensional analysis of fretting fatigue," *Acta Materialia*, vol. 46, pp. 177-192, 1997.

Chapter 2: Effects of plastic properties and friction on the response of metals in sliding contact

From the analysis in the previous chapter, we have a set of dimensionless functions to predict the frictional sliding response from material properties. In this Chapter, we make a more detailed comparison with experimental results on materials with largely different plastic hardening behaviors. The effects of friction on the frictional sliding response is also investigated in details, both computationally and experimentally.

2.1 Introduction

Indentation hardness tests have been used extensively for material characterization and also as a basis for predicting the tribological response [1, 2]. The indentation tests were traditionally based on an estimate of the residual area of contact or the remnant penetration depth, but the development and commercialization of depth-sensing instrumented indentation systems have enabled continuous measurement of the force and displacement during loading and unloading. Following these advances, many studies have examined the contact mechanics of instrumented indentation. Dimensional analysis and finite element methods (FEM) were employed to quantify relationships between the measured force–displacement (P–h) response and material properties [3-13]. Numerous other studies have also investigated the effects of various material properties on instrumented indentation response [14-16].

As compared to instrumented normal indentation, very few studies have investigated the mechanics for frictional sliding [17-21]. In the steady state regime of frictional sliding, the normal force is maintained constant and the tangential displacement induces the flow of material and the formation of a ridge or a pile-up on each side of the scar. Under appropriate contact conditions, our related earlier work involving finite element simulations showed a strong connection between this response and material plastic flow properties [22]. In fact, the effects of initial yield strength and plastic strain hardening exponent were computationally quantified and isolated for their contribution to the normalized hardness and normalized pile-up height. This quantitative approach to study frictional sliding could serve as an experimental tool for material characterization, but also as a simple predictor for the tribological response of materials. Several previous experimental studies have used frictional sliding experiments [23-28], but the underlying interpretation provided only partial information about the relative contribution to overall frictional sliding response from the material and contact parameters.

Friction is a contact parameter that could certainly influence significantly the response to sliding contact. For a sliding contact where significant plastic deformation develops on the indented surface, we envision at least two contributions to the overall friction coefficient defined as ratio of tangential over normal force. The first contribution is from the local interaction between surfaces in

normal contact. This friction can be accounted for using Amontons's law with an appropriate friction coefficient and it can be directly affected by lubrication. The second contribution to the overall friction is from the work of plastic deformation and it should be primarily determined by the contact geometry and material properties.

For normal indentation, finite element predictions suggest a significant influence of the friction coefficient on the pile-up behavior [29-31]. Experimentally, a lubricant was reported to decrease the indentation hardness [32, 33] and to increase the hardness in frictional sliding [34, 35]. From the viewpoint of the evolution of contact geometry, the friction force pushes the material downward during normal indentation while it pushes the material upward and to the front in frictional sliding. This fundamental difference on the influence of friction on the flow can explain the different effects on hardness. However, detailed analysis is needed for a quantitative prediction of the effect of friction in sliding contact.

In this work, we first present experimental results obtained on a model material system to demonstrate the strong influence of plastic flow properties on the pile-up behavior. The results are compared with predictions from our numerical study [22]. Based on a comparison of experiments with computational results, the effect of plastic strain hardening on the deformation field is discussed. With the absence of significant previous information, we then explore the effect of friction experimentally, using a lubricant, and numerically, using finite element methods.

2.2 Experimental and computational methods

2.2.1 Material system

Copper was selected as a model material system because large variations in the strain hardening exponent can be introduced by controlling the grain size and composition. Commercially pure copper (99.9%) and a single phase copper- 30 wt% zinc alloy were obtained from Noranda Inc (Pointe-Claire, Canada) in the form of cold worked sheets that were 0.6 mm thick. Standard dog-bone specimens were machined out of the sheets. After machining, the specimens were divided into three groups that were then heat-treated for recrystallization at the temperature of 450, 600 or 700°C for 3 h. The microstructure of each alloy was then characterized in detail, including a quantification of the average grain size $\overline{d}$ as listed in Table 2.1. With pure Cu and the brass alloy, a total of 6 material conditions were investigated. In the absence of other significant changes to the microstructure, the conditions with the different heat-treatments allowed for a specific effect of the grain size on the frictional sliding response.

Tensile tests were carried out on all materials to quantify the plastic deformation response. Prior to testing, the specimens were marked with ink a specified distance intervals to independently measure the plastic strain at maximum tensile strength. The stress-strain curves were corrected for machine/specimen compliance, and consistency was obtained between the critical engineering strain, i.e. strain at tensile strength, and the permanent elongation of the specimens that was

determined by the marking technique. A true stress vs true strain deformation representation was used to fit the data with the flow stress relationship:

$$\sigma = \sigma_y \left(1 + \frac{E}{\sigma_y} \varepsilon_p \right)^n \qquad 2.1$$

where ε_p is the equivalent plastic strain, σ_y is the initial yield strength, E is the Young's modulus of the material and n is the strain hardening exponent. The results from this fit are summarized in Table 2.1 and three example curves are shown in Figure 2.1. In the fitting procedure, more weight was given to the later part of the experimental curve where the plastic strain is most significant.

Table 2.1: Material conditions tested with average grain size, initial yield strength and strain hardening exponent based on tensile test results.

Material	*T*	$\bar{d}$	σ_y	*n*
	°C	μm	MPa	-
Cu	450	20 ± 8	145	.13
Cu	600	150 ± 30	44	.27
Cu	700	380 ± 50	28	.29
Cu-Zn	450	27 ± 6	45	.35
Cu-Zn	600	76 ± 10	15.5	.41
Cu-Zn	700	180 ± 20	7	.45

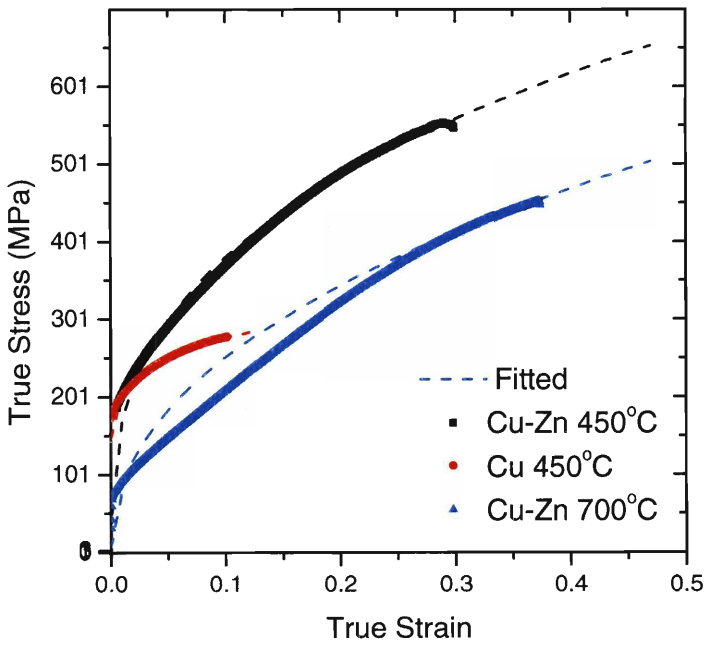

Figure 2.1: True stress versus true strain curves for three different materials and the associated fitted function using power-law strain hardening.

2.2.2 The frictional sliding experiments

All specimens were mechanically polished to a surface roughness of less than ± 5 nm and tested on a commercial nanoindentation test system (Nanotest ™, Micro Materials Ltd, Wrexham, United Kingdom). The indenter was a conical diamond with an apex angle θ of 70.3° and a tip radius of 2 μm. For the conditions of penetration depth investigated, the scale of experimentation was sufficiently large to consider this indenter as perfectly conical. The experiments were carried out under constant normal load P, at a velocity of 10 μm/s and over a total distance of 1500 μm, which was sufficient to attain steady state conditions after approximately 300 μm and continue to generate a region of valid steady-state profile. After the experiment, a series of at least 30 cross-sectional residual profiles were obtained over the steady state regime by using a Tencor P10 profilometer (KLA-Tencor, San Jose, California). The profilometer was equipped with a conical diamond probe which had an apex angle of 45° and a tip radius of 2 μm. The steady state regime was also observed with a Leo VP438 scanning electron microscope (Leo Electron Microscopy Inc, Thornwood, New York).

A schematic section of a residual scratch profile is presented in Figure 2.2 where a graphical representation for the pile-up height h_p, the residual penetration depth h_r and the contact radius a_r is presented. The contact radius a_r can be used directly to calculate the overall resistance to penetration using the traditional definition of hardness [1, 36-38]

$$H_S = \frac{2P}{\pi a_r^2} \qquad \textbf{2.2}$$

where P is the applied normal load. Assuming the absence of significant size effects, the main advantage of the conical geometry is the size-independence due to self similarity. With this assumption, the simple ratio of h_p/h_r provides an indication on the tendency of the material to form a high pile-up.

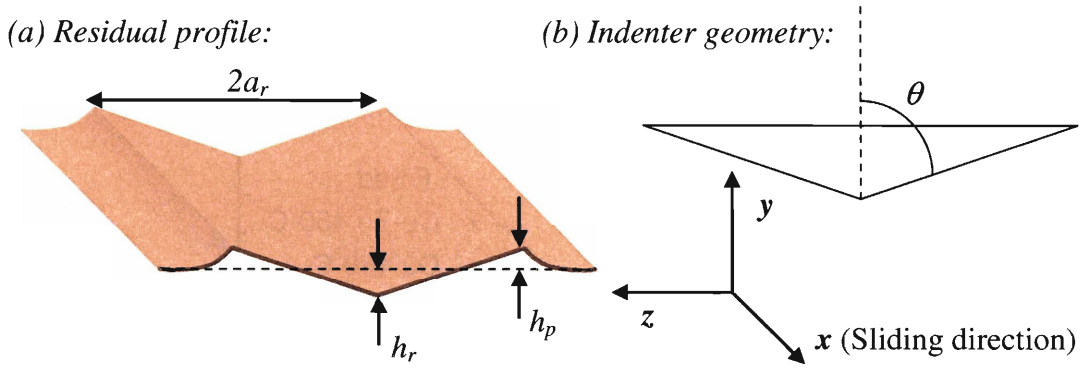

Figure 2.2: (a) A section of a residual scratch profile where the pile-up height (h_p), the residual penetration depth (h_r) and the contact radius (a_r) are indicated, and (b) a schematic view of a conical indenter with an apex angle θ. Also shown is the coordinate system for the analysis.

Friction is the third parameter of relevance to the current problem that can be analyzed experimentally and computationally. Because friction occurs at two different levels, we will separate their contribution by expressing the overall friction coefficient as

$$\mu_{tot} = \frac{F_t}{P} = f(\mu_a, \mu_w) \qquad \textbf{2.3}$$

where F_t is the total tangential force, μ_a is the coefficient of friction for the normal contact local and μ_w is friction contribution from the work of plastic deformation. μ_a is governed by Amontons's law of friction with specifies the ratio between the normal pressure and the local tangential traction tensor. The parameter μ_a will be varied experimentally using an isostearic acid (Century 1105, Arizona Chemical, Jacksonville, Florida) as a liquid lubricant. The lubricant had a viscosity of 70 cps at 25°C and it contained mainly C_{18} branched chains (59%) and C_{18} cyclic chains (11%).

2.2.3 Dimensional and numerical analysis

For steady state frictional sliding of elasto-plastic materials, the contact conditions can now be analyzed and predicted in detail. To simplify the elastic contributions from the material and the indenter, we used the reduced modulus [38]

$$E^* = \left[\frac{(1-\upsilon^2)}{E} + \frac{(1-\upsilon_i^2)}{E_i} \right]^{-1}, \qquad \textbf{2.4}$$

where E_i and ν_i are the Young's modulus and Poisson's ratio of the indenter, respectively. For the diamond used in the experiments, E_i = 1100 GPa and ν_i = 0.07 [39]. The elastic constants specified for polycrystalline Cu were taken to be: E =110 GPa and ν = 0.35 [39]. These properties were assumed to be isotropic for the conditions tested.

For a fixed cone angle θ = 70.3° and friction coefficient μ_a = 0.15, three new dimensionless functions have been defined using dimensional analysis and evaluated numerically through a comprehensive parametric study [22]. Under the assumptions for θ and μ_a, these functions predict the frictional sliding response based on material properties and the following closed-form solutions:

$$\Pi_\alpha\left(n, \frac{\sigma_y}{E^*}\right) = \left(\frac{H_S}{\sigma_y}\right) = \alpha 1(n)\left(\frac{\sigma_y}{E^*}\right)^{\alpha 2(n)}, \qquad \textbf{2.5}$$

$$\Pi_\beta\left(n, \frac{\sigma_y}{E^*}\right) = \frac{h_p}{h_r} = \Pi_{\beta,RP}(n) \Big/ \left[1 + \left(\frac{\sigma_y}{X_\beta(n)\,E^*}\right) p_\beta(n)\right] \text{ and} \qquad \textbf{2.6}$$

$$\Pi_\gamma(n,\frac{\sigma_y}{E^*})=\left(\frac{F_t}{P}\right)=\mu_{tot}=\mu_a+\left(\Pi_{\gamma,RP}-\mu_a\right)\Big/\left[1+\left(\frac{\sigma_y}{X_\gamma(n)\,E^*}\right)^{p_\gamma(n)}\right], \qquad \textbf{2.7}$$

where the subscript $_{RP}$ indicate the value of the function at the limit of rigid plastic properties, the variable F_t is for the overall lateral force and the variable μ_{tot} is for the overall friction coefficient. Simple numerical expressions were provided [22] for the other numerical terms for the sub-functions of n ($\alpha 1(n)$, $\alpha 2(n)$, $\Pi_{\beta,RP}(n)$, $X_\beta(n)$, $p_\beta(n)$, $X_\gamma(n)$ and $p_\gamma(n)$) and the constant $\Pi_{\gamma RP}$. With these functions and their underlining assumptions, one can specify the elasto-plastic properties of a material and predict the frictional sliding response in terms of normalized scratch hardness H_s/σ_y (Π_α), ratio of pile-up height (Π_β) and overall friction coefficient μ_{tot} (Π_γ).

In their most general form, these dimensionless functions are expressed as:

$$\Pi_\alpha=f(n,\frac{\sigma_y}{E^*},\mu_a,\theta), \qquad \textbf{2.8}$$

$$\Pi_\beta=f(n,\frac{\sigma_y}{E^*},\mu_a,\theta) \text{ and} \qquad \textbf{2.9}$$

$$\Pi_\gamma=f(n,\frac{\sigma_y}{E^*},\mu_a,\theta). \qquad \textbf{2.10}$$

For the current study, we specifically investigate the effect of the friction coefficient μ_a, which will add a dimension to the dimensionless functions Π_α, Π_β and Π_γ presented in Equations 2.5 to 2.7. On the other hand, the parameter θ remains fixed at 70.3° in this study. Full three-dimensional models were used because the stress and strain fields generated by frictional sliding cannot be approximated using two-dimensional or axisymmetric mesh domains. The complete mesh domain contained 170,000 reduced integration 8-noded elements. The finite element computations were performed using the general purpose software package ABAQUS [40]. The solution method was explicit and based on Eulerian boundaries where the mesh remains stationary. Additional details on the meshing procedure and validation are provided elsewhere [22]. The approach was well tested for mesh refinement and convergence, and for the independence of the solution method adapted.

Finite element solutions were obtained for fixed values of the friction coefficient $\mu_a = 0$, 0.08, 0.2 or 0.3 for. For the materials with a plastic strain hardening exponent $n \leq 0.2$, μ_a was limited to a maximum value of 0.2 because higher μ_a could generate physical and numerical instability due to excessive pile-up [22]. In the complete parametric study a minimum of 6 cases of σ_y/E were explored for any combination of n and μ_a covered, adding a total of 90 cases to the former study [22] that focused on $\mu_a = 0.15$. The same procedure as in the former study was used to extract h_p, h_r and a_r from the nodal position of the residual profile. The finite element results from both studies were all incorporated into the new dimensionless functions so as to develop a comprehensive understanding of the effects of E, σ_y, n and μ_a on frictional sliding.

2.3 Results and Discussion

2.3.1 Effects of material properties

Frictional sliding experiments were performed on pure Cu and Cu-Zn with the conical tip and at a normal load P = 2 N. For each material condition, the experiment was repeated five times and profilometry observation was carried out on all individual profiles. From these profiles the relevant scratch parameters were calculated and compared with predictions using the dimensionless functions. For each of the three parameters, Table 2.2 indicates a maximum difference between the experiment and the predictions of at most 10, 15 and 5 percents for the hardness, pile-up and friction, respectively. In addition, the differences between experiments and predictions indicate the absence of a definite trend, suggesting that the overall dependence of sliding behavior on material properties is correctly predicted over the range of material properties studied.

Table 2.2: Experimental results compared with the predictions made using the dimensionless functions from the former study. The materials are listed in order of increasing n.

Material (treatment T in °C)	Properties		H_s (GPa)			h_p/h_r			μ_{tot}		
	σ_y MPa	n	*Exp.*	*FEM*	Δ (%)	*Exp.*	*FEM*	Δ (%)	*Exp.*	*FEM*	Δ (%)
Cu(450)	145	.13	0.66	0.70	-7	.7	.70	0	.42	.406	3
Cu(600)	44	.27	0.62	0.66	-6	.57	.52	10	.43	.409	5
Cu(700)	28	.29	0.60	0.54	10	.51	.50	2	.42	.410	2
Cu-Zn(450)	45	.35	1.13	1.13	0	.44	.41	7	.41	.407	1
Cu-Zn(600)	15.5	.41	0.95	0.88	8	.3	.34	-12	.40	.410	-2
Cu-Zn(700)	7	.45	0.81	0.75	8	.28	.28	0	.41	.411	0

As listed in Table 2.2, for a heat treatment at a given temperature, pure Cu has a higher initial yield strength σ_y and a lower plastic strain hardening exponent n than Cu–Zn. It is also interesting to note that, for the condition of same heat-treatment, the pile-up height is always lower in Cu–Zn than in pure Cu. From the dimensionless function in Equation 2.6, a decrease in yield strength, as seen with Cu–Zn, is predicted to always increase the pile-up height. Therefore, any significant decrease in pile-up height observed with Cu–Zn is necessarily dues to the increase in the strain hardening exponent. Also, Equation 2.6 predicts a limited sensitivity of pile-up height to the initial yield strength σ_y for the entire range of material properties covered in this study. Therefore, we primarily focus on the variation of n to interpret the results from these experiments. These interpretations are also guided by our systematic and parametric studies of the effects of n on the sliding response.

A strong correlation was observed between the strain hardening exponent n and the normalized pile-up height. Figure 2.3(a) presents five individual residual profiles for each of the two materials recrystallized at the lowest temperature of 450°C, a condition for which n is 0.13 for pure Cu and 0.35 for Cu–Zn. On this figure, the direction of motion of the indenter is normal to the plane of the image. Although the profiles of the two materials are similar in general shape, the average value of h_p/h_r decreases from 0.70 to 0.44 as n increases from 0.13 to 0.35. Similarly, Figure 2.3(b) presents profiles for recrystallization at the highest temperature where n is 0.29 for pure Cu and 0.45 for Cu–Zn. With the decrease in n between pure Cu and Cu–Zn, the average h_p/h_r decreases by nearly two-fold, from 0.51 to 0.28. With an experimental scatter in height of the order of ± 0.05 and an excellent reproducibility between the different scratches, the variations are significant and well beyond the level of fluctuations observed during profilometry. For these two specific examples, the initial yield strength of the material was lower for the high hardening case, which would have increased the pile-up height based on Equation 2.6. Therefore, the decrease in h_p/h_r can only be due to the increase in n. In fact, the decrease and variation between the conditions shown Figure 2.3 would have been even more significant without the difference in initial yield strength between the materials. Thus, the observed effects of n alone would be seen to serve as a minimum variation.

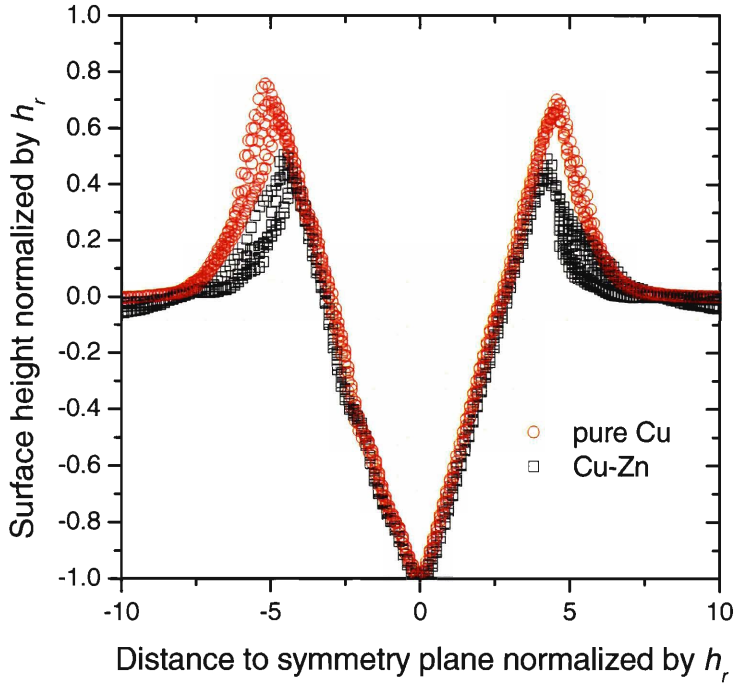

(a)

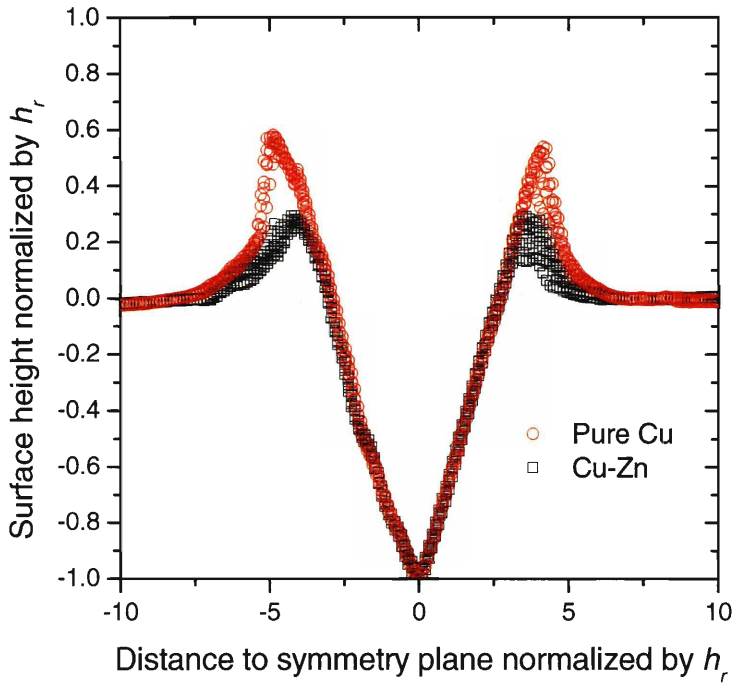

(b)

Figure 2.3: Cross-section profiles for the experiments on the materials recrystallized at (a) the lowest temperature of 450°C and (b) the highest temperature of 700°C. There are five data sets for each of the two materials.

Figure 2.4 presents secondary electron images obtained in a scanning electron microscope. For each of the four material conditions, the images present the steady state regime and the final termination of the experiment. In the steady state regime, the pile-up is more regular for the samples recrystallized at 450°C than for those recrystallized at 700°C. At least in Cu–Zn, the preferential orientation of the deformation bands illustrates an effect of individual grains. For pure Cu recrystallized at 700°C, there are also changes in the orientation of the bands on the free surface that are consistent with the intrinsic effect of grains. Since the grains are larger for the highest recrystallization temperature of 700°C, the intrinsic effect of grains with different orientations could well explain the variability in scar width and on the surface features.

The intrinsic effects from the microstructure have caused local fluctuations in the scratch pattern such as the scar width and the pile-up height. However, it is interesting to note that the average values remained consistent with the finite element predictions that are based on a continuum formulation. Due to the lateral displacement, frictional sliding offers the specific advantage to probe a larger volume of material and to generate relatively more accurate averages of properties from a single experiment than a normal indentation test. However, further research is still needed to fully characterize the effect of material and contact conditions on the response. In particular, it is of interest to determine the extent to which the overall friction coefficient is influenced by material parameters.

The overall coefficient of friction μ_{tot} is a quantity that can be measured readily using an instrumented nanoindenter wherein the frictional sliding experiment is performed. For all six ductile materials investigated, Table 2.2 shows a maximum difference of less than 7% in the value of μ_{tot}. A reasonable agreement was obtained between the experiments and the predictions. However, at least for the range of conditions studied, it would be difficult to use only the friction information to differentiate between the materials. A similar observation was also made from a previous study on nickel where the effect grain-size refinement and large variations in yield strength did not significantly change the overall friction coefficient [22]. Although the friction coefficient μ_{tot} can be readily monitored during an experiment, the two scratch parameters that are most sensitive to material properties are definitely the hardness and the normalized pile-up height. In other words, for the conditions explored in this work, relatively little variation in overall friction coefficient was found.

Our finite element simulations also provide useful information on the distribution of the equivalent plastic strain underneath the indenter during frictional sliding. For this purpose, results were extracted from the elements located in the unloaded region and at a distance ar./2 from the symmetry plane. The results are reported as a function of the distance beneath the scratch surface. Figure 2.5(a) presents a series of equivalent plastic strain contour plots for a relatively soft material where $\sigma y/E^* = 0.001$. As the strain hardening exponent decreases, the equivalent plastic strain near the surface increases significantly. For the strain distribution beneath the surface, it is clear that the plastic strain deceases less rapidly for the materials with a higher hardening exponent. A more distributed plastic strain with increasing n is consistent with the decrease in the pile-up height as the flow of material is further from the material indenter interface.

The initial yield strength also influences the plastic strain distribution. Figure 2.5(b) presents a similar series of results for a harder material where $\sigma_y/E^* = 0.01$. Although the general shape of these curves remains the same as those for the softer material, there is a general and significant decrease in the magnitude of the plastic strain. When used together, Figure 2.5 (a) and (b) provide a description of the evolution of equivalent plastic strain for different strain hardening exponent and initial yield strength values. The hardening exponent significantly affects the distribution while the initial yield strength clearly influences the average magnitude of the equivalent plastic strain.

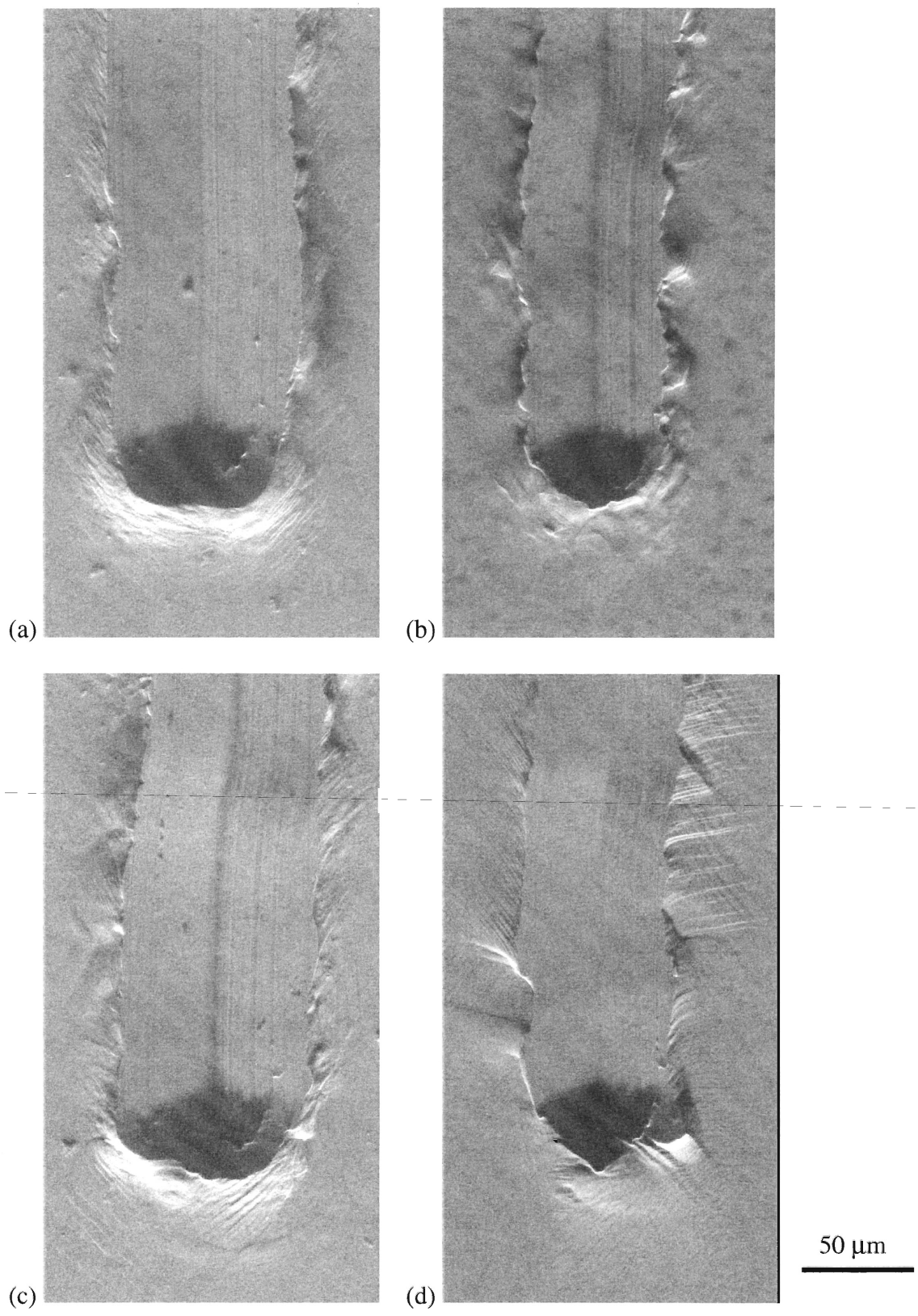

Figure 2.4: Top surface image over the steady regime and the termination of a scratch for: (a) pure Cu recrystallized at 450°C, (b) Cu-Zn also at 450°C, (c) pure Cu at 700°C, and (d) Cu-Zn also at 700°C. The indenter was traveling from top to bottom.

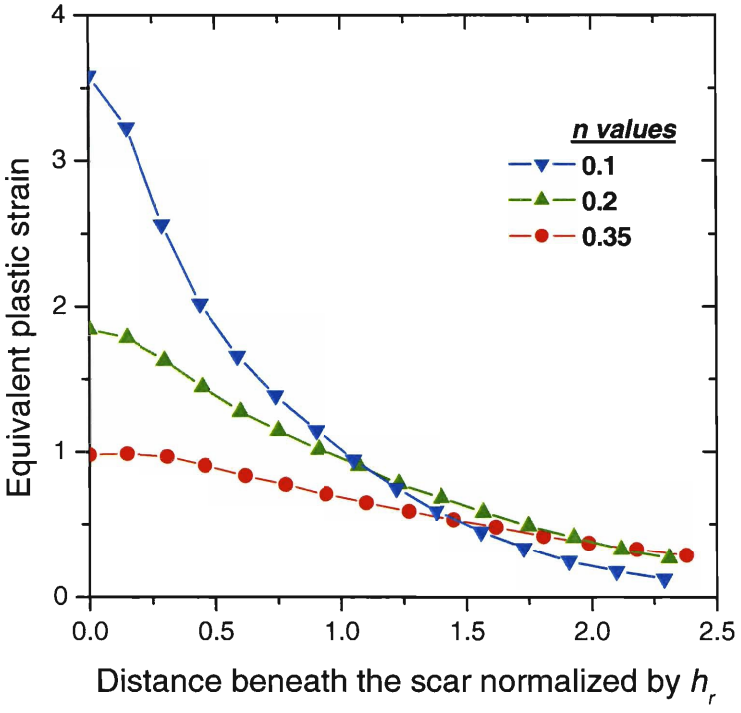

(a)

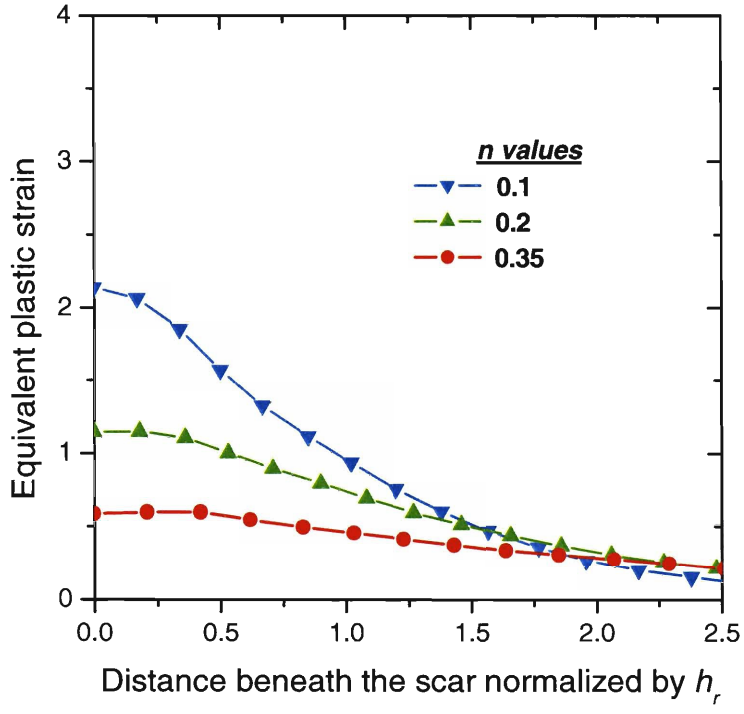

(b)

Figure 2.5: Magnitude of the equivalent plastic strain beneath the indenter for (a) $\sigma_y/E^* = 0.001$ and (b) $\sigma_y/E^* = 0.01$.

2.3.2 Quantitative descriptions of sliding with friction

In the second part of this study, we consider the effect of the friction coefficient μ_a on the sliding contact response. Computationally, three parameters were varied independently: the friction coefficient μ_a, the normalized initial yield strength σ_y/E^* and the strain hardening exponent n. We studied the effect of each of these parameters on the general dimensionless functions Π_α, Π_β and Π_γ in Equations 2.8 to 2.10. Although different functions could have been used to represent the new data, the general dependency on n and σ_y/E^* was very similar to that of the earlier analysis which led to the functional form in Equations 2.4 to 2.7. Therefore, the effect of the friction coefficient was included in the former functional form by adding penalty terms. The new sub-functions and the related values of it coefficients were determined by minimization of the residuals.

For the normalized scratch hardness H_s/σ_y, the best fit was obtained by using the function

$$\Pi_\alpha = \left(\frac{H_S}{\sigma_y}\right) = [\alpha 1(n) + n\,\Gamma_{\alpha 1}(\mu_a)]\left(\frac{\sigma_y}{E^*}\right)[\alpha 2(n) + \Gamma_{\alpha 2}(\mu_a)] \qquad \textbf{2.11}$$

with

$$\Gamma_{\alpha 1}(\mu_a) = 0.12 - 0.64 \Big/ \left[1 + e^{30(\mu_a - 0.1)}\right],$$

$$\Gamma_{\alpha 2}(\mu_a) = 0.006 - 0.0278 \Big/ \left[1 + e^{25(\mu_a - 0.1)}\right]$$

and the subfunctions ($\alpha 1(n)$ and $\alpha 2(n)$) as evaluated previously. For hardness, the contribution from the friction coefficient μ_a is included with the terms that previously depended only on the strain hardening exponent n. The sub-functions $\Gamma_{\alpha 1}$ and $\Gamma_{\alpha 2}$ are exponential growth functions and their value monotonically varies with μ_a. They were especially chosen to minimize the error when fitting all the data throughout the range of material properties.

Figure 2.6 presents this function Π_α and the associated finite element data points on log–log plots of the normalized hardness H_s/σ_y versus the normalized yield strength σ_y/E^*. In such a representation, each series of adjacent curves represents different values of μ_a and the different series are for the different values of n. Based on this plot, the effect of friction appears most minimal at a transition point where n = 0.35. For n above 0.35, the hardness apparently increases with increasing μ_a, but the effect is relatively limited. For n below 0.35, the hardness decreases with an increase in the friction coefficient μ_a. This decrease in hardness could be due to an increase in the amount of material being pushed to the side of the indenter and the increase in the area of contact through a higher pile-up.

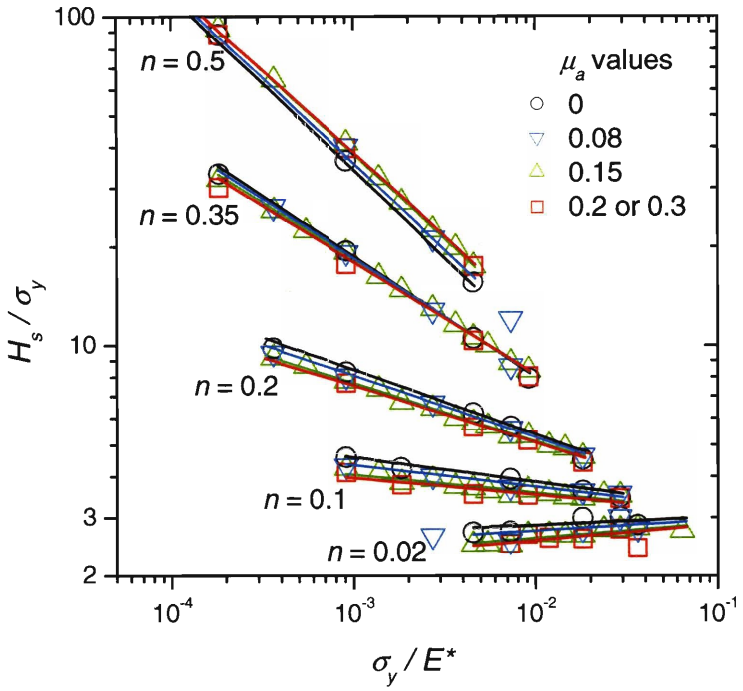

Figure 2.6: Effect of the friction coefficient μ_a on the normalized hardness versus normalized yield strength relationship.

The second function studied is Π_β for the normalized pile-up height h_p/h_r. The behavior of this function should be asymptotic on both sides with little influence of yield strength for rigid plastic materials and with a residual height of zero in the elastic limit. The logistic function selected in previous study respects both of these limits and it allows for a simple expression of the pile-up height:

$$\Pi_\beta = \frac{h_p}{h_r} = \Pi_{\beta,RP}(n)\,\Gamma_{\beta,RP}(\mu_a) \Bigg/ \left[1 + \left(\frac{\sigma_y}{X_\beta(n)\,\Gamma_{X\beta}(\mu_a)\,E^*}\right)^{p_\beta(n)}\right] \qquad \textbf{2.12}$$

with

$$\Gamma_{\beta,RP}(\mu_a) = 0.909 + 0.627\mu_a,$$
$$\Gamma_{X\beta}(\mu_a) = 0.651 + 1.21\mu_a + 7.61\mu_a^2,$$

and the sub functions of n ($\Pi_{\beta RP}(n)$, $X_\beta(n)$ and $p_\beta(n)$) as evaluated previously. Figure 2.7 presents the function evaluated at the different values of n and μ_a for which we have finite element results. The sets of curves for the specified values of n illustrate in more detail the combined influence of n and σ_y/E^* on h_p/h_r. Within each set of these curves, the normalized pile-up height h_p/h_r always

increases when the friction coefficient μ_a increases. This increase in height can be associated with an increase in the interaction forces that push the material to the front and laterally.

The absolute value of the offset in h_p/h_r caused by variations in μ_a is significant and it only weakly depends on material properties for the strain hardening exponent range: $0.02 \le n \le 0.35$. For the largest value of $n = 0.5$, the effect of friction is significantly decreased as the conditions for a transition between pile-up and sink-in are approached. The sink-in phenomenon was observed in the simulation for $n = 0.5$ and $\sigma_y / E^* > 0.005$, but the results are not presented because sink-in results in a residual position of contact that does correspond to the position of the maximum height on the residual pile-up. Including these effects would require a more detailed analysis that would probably find a limited practical interest because very few practical materials are harder than the range covered here.

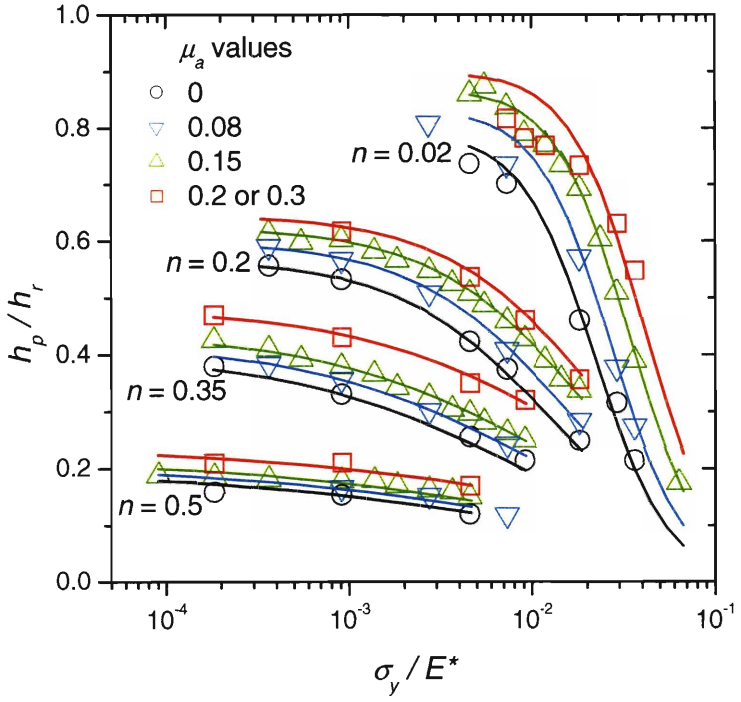

Figure 2.7: Effect of the frictional coefficient μ_a on the normalized pile-up height versus normalized yield strength relationship.

The last function Π_γ is for the overall friction coefficient μ_{tot} or the ratio of the lateral force F_t over the normal force P for the interaction between the indenter and the surface. The effect of friction was incorporated to yield

$$\Pi_\gamma = \left(\frac{F_t}{P}\right) = \mu_{tot} = \mu_a + \left(\Pi_{\gamma,RP}\ \Gamma_{\gamma,RP}(\mu_a) - \mu_a\right) \Bigg/ \left[1 + \left(\frac{\sigma_y}{X_\gamma(n)\ \Gamma_{X\gamma}(\mu_a)\ E^*}\right) p_\gamma(n)\right] \qquad \textbf{2.13}$$

with

$$\Gamma_{\gamma,RP}(\mu_a) = 0.586 + 2.6\mu_a + 0.877\mu_a^2,$$

$$\Gamma_{X\gamma}(\mu_a) = 0.8 + 1.33\mu_a + 0.235\mu_a^2$$

and the sub functions of n ($\Pi_{\gamma RP}$, $X_\gamma(n)$ and $p_\gamma(n)$) as evaluated previously. To emphasize that μ_{tot} is a sum of two contributions from the quantities μ_a and μ_w (see Equation 2.3). μ_w encompasses all the contributions to the lateral force that cannot be accounted for by Amontons's law of friction with a coefficient μ_a evaluated from the nominally elastic contact between two bodies. Therefore, μ_w account for all increases in F_t that are required to deform the material plastically and to move it under and on the side of the indenter to leave the path for the indenter. Therefore, μ_w would be the primary term to depend on material properties.

Figure 2.8 graphically represents the function Π_γ where the sets of adjacent curves are now for a given value of the friction coefficient μ_a and the different series are for the five different values of μ_a. The curves were plotted using Equation 2.9 but the finite element data points are also included to illustrate the fitting accuracy. For the different values of μ_a, the representation also indicates a limited dependence of material properties for all the cases, but that for a given set of material properties, the μ_w term consistently increases with μ_a. Another feature that persists for the different values of μ_a is the independence of friction on material properties in the limit of rigid-plastic behavior.

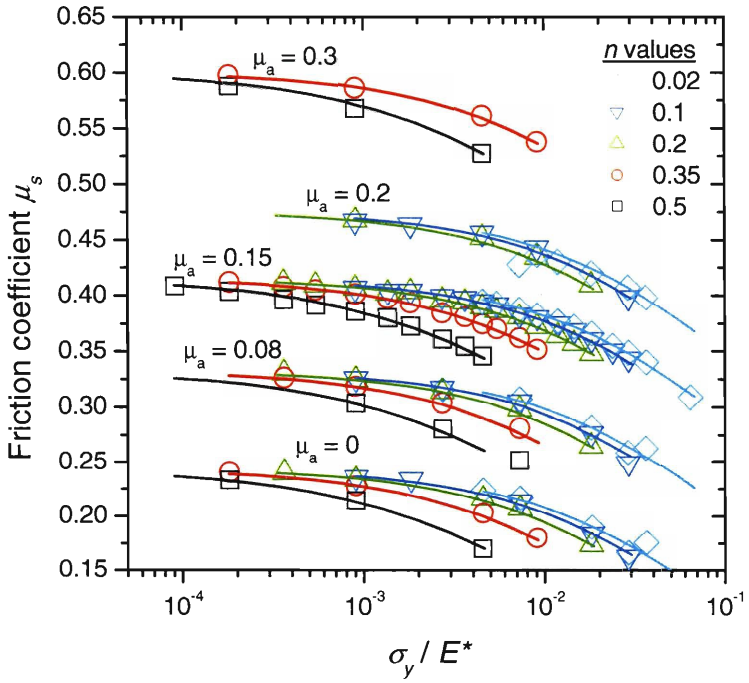

Figure 2.8: Effect of the frictional coefficient μ_a on the overall friction coefficient versus normalized yield strength relationship.

An experimental study was undertaken to measure and control the friction coefficient. μ_a was measured through a repeated frictional sliding test in which a spherical tip with a radius of 100 µm was used for repeatedly sliding over the same area 12 times. The normal load P was fixed at 1 N and the material was a high strength specimen of pure copper with an indentation hardness of 1.5 GPa. Under those conditions, the ratcheting or deepening of the impression progressively reduced and became negligible after approximately 8 passes. Figure 2.9 shows the raw friction signal obtained during such an experiment. The friction coefficient is found to decrease from an initial value of approximately 0.22 for the first pass to a steady state value of approximately 0.14. This technique of measuring μ_a may result in a small overestimation with a potential for a limited amount of plasticity in steady state, but it offers a reasonable estimate μ_a in an efficient manner.

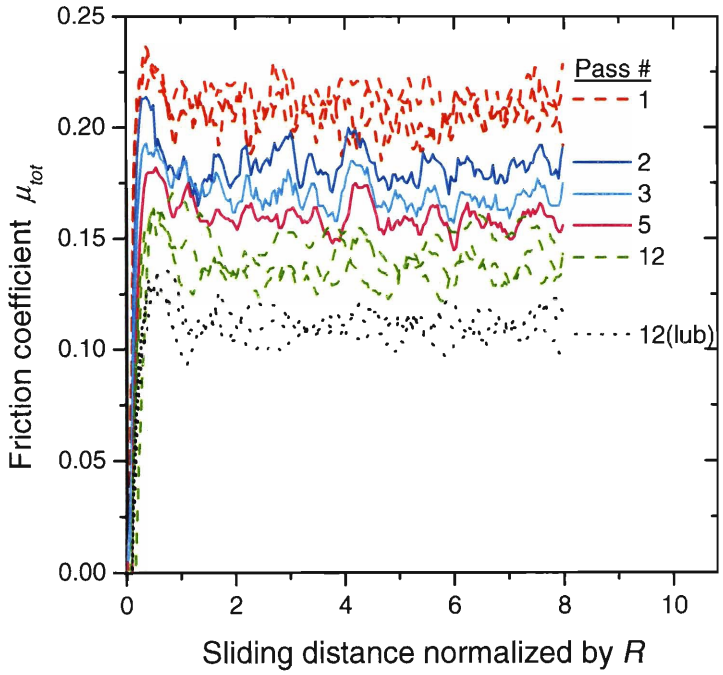

Figure 2.9: Experimental determination of the friction coefficient μ_a. From top to bottom the curves represent the coefficient of friction μ_{tot} for an increasing number of passes over the same area until a steady state is reached. In steady state regime the ratcheting effect vanishes and μ_{tot} becomes approximately the friction coefficient μ_a. The dotted lime at the bottom is for the steady state with lubrication.

To experimentally vary μ_a, we used the isostearic acid (c.f. Section 2.3.2) as a liquid lubricant. The lubricant was added to the surface and the tip after carrying out the load and displacement calibrations. With the relatively small velocity of the tip, the conditions allowed only for boundary lubrication. To verify the influence on μ_a, the experiment with a spherical tip presented in Figure 2.9 was followed by another experiment under the same conditions but with lubricant. For each pass, the friction coefficient was significantly lower with a lubricant and Figure

2.9 presents the results for the steady state regime. The use of lubrication enabled to decrease the steady state friction coefficient from 0.14 to 0.11. This 25% decrease could have several beneficial effects including a reduction in the tendency to form chips in hard materials for which the plastic strain hardening exponent is limited. The variation also allows for a more comprehensive comparison between computational predictions and experimental results.

Frictional sliding experiments were carried out with the six different Cu specimens under the same conditions described in Section 2.4.1 except for lubrication. The results for the normalized pile-up height are presented in Figure 2.10 and compared with the earlier results without lubricant. The materials on Figure 2.10 are classified by their value of the strain hardening exponent n. The values of the pile-up height is consistently lower with a lubricant, but the effect of lubrication is found to progressively decrease with increasing n and eventually vanish for $n = 0.5$. For the scratch hardness, the results presented in Table 2.3 are consistent with the predictions from the simulation for n below 0.35 where the hardness increased with decreasing μ_a. Above $n = 0.35$, a decrease in hardness was observed for all three Cu–Zn alloys to an extent slightly larger than that predicted computationally. A detailed comparison between the experimental results with lubrication and the finite element predictions is presented in Table 2.3. For hardness and pile-up height, the maximum difference between the experimental results and the predictions is within 11%. For the conditions tested, we find a reasonable agreement for the trends and absolute values.

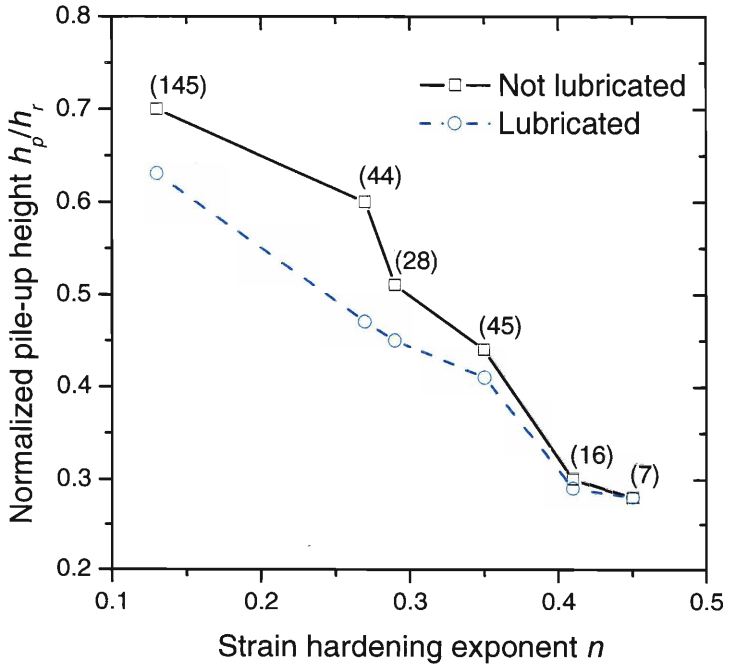

Figure 2.10: Influence of lubrication on the experimentally measured values of the pile-up height. The numbers in parenthesis are the values of the initial yield strength in units of MPa for each case.

Table 2.3: Experimental results compared with the predictions made using the new analysis that incorporates the effect of lubrification. The materials are listed in order of increasing *n*.

Material (T in °C)	Properties		H_s (GPa)			h_p/h_r		
	σ_y MPa	n	*Exp.*	*FEM*	Δ (%)	*Exp.*	*FEM*	Δ (%)
Cu (450)	145	.13	0.71	0.73	-2	0.63	0.68	-7
Cu (600)	44	.27	0.70	0.67	4	0.47	0.50	-7
Cu (700)	28	.29	0.62	0.56	11	0.45	0.49	-7
Cu-Zn (450)	45	.35	1.19	1.17	2	0.41	0.39	4
Cu-Zn (600)	15.5	.41	0.92	0.91	1	0.29	0.33	-11
Cu-Zn (700)	7	.45	0.78	0.78	0	0.28	0.28	1

2.4 Conclusions

The frictional sliding contact of elasto-plastic materials was studied experimentally and computationally. The following conclusions can be drawn.

1. A large plastic strain hardening exponent significantly decreases the normalized pile-up height for the material left on each side of the scar. A more refined grain microstructure reduces the variability in the frictional sliding process, but it also increases the normalized pile-up height.

2. A large plastic strain hardening exponent or higher yield strength decreases the magnitude of the equivalent plastic strain underneath the indenter. It also distributes the strain to a greater distance beneath the surface of contact.

3. Dimensionless functions developed in our parallel study [22] on instrumented frictional sliding were modified to include the effect of the friction coefficient. For materials for which the strain hardening exponent is below 0.35, the scratch hardness increases if the friction decreases.

4. The most significant effect of friction is to increase the normalized pile-up height. The effect decreases for very large values of the strain hardening exponent. No previous studies had reported the specific effect of friction on the frictional sliding response of a large variety of materials.

5. An isostearic acid used as a boundary lubricant can decrease by 25% the friction coefficient between the surface and the diamond tip. The experimental effect of lubrication on the hardness and pile-up was consistent with the finite element predictions.

The frictional sliding experiment can be well controlled and designed to consistently yield results in agreement with the computational predictions. It could become an alternative or a complement to a normal indentation test.

2.5 References

[1] A. C. Fischer-Cripps, *Introduction to Contact Mechanics*. New York: Springer-Verlag, 2000.

[2] I. M. Hutchings, *Tribology: Friction and Wear of Engineering Materials*. Kent: CRC Press, 1992.

[3] M. Dao, N. Chollacoop, K. J. Van Vliet, T. A. Venkatesh, and S. Suresh, "Computational modeling of the forward and reverse problems in instrumented sharp indentation," *Acta Materialia*, vol. 49, pp. 3899-3918, 2001.

[4] Y. T. Cheng and C. M. Cheng, "Scaling, dimensional analysis, and indentation measurements," *Materials Science & Engineering R-Reports*, vol. 44, pp. 91-149, 2004.

[5] M. Mata, M. Anglada, and J. Alcala, "A hardness equation for sharp indentation of elastic-power-law strain-hardening materials," *Philosophical Magazine A: Physics of Condensed Matter, Structure, Defects and Mechanical Properties*, vol. 82, pp. 1831-1839, 2002.

[6] K. Matsuda, "Prediction of stress-strain curves of elastic-plastic materials based on the Vickers indentation," *Philosophical Magazine A: Physics of Condensed Matter, Structure, Defects and Mechanical Properties*, vol. 82, pp. 1941-1951, 2002.

[7] K. Tunvisut, E. P. Busso, N. P. O'Dowd, and H. P. Brantner, "Determination of the mechanical properties of metallic thin films and substrates from indentation tests," *Philosophical Magazine A: Physics of Condensed Matter, Structure, Defects and Mechanical Properties*, vol. 82, pp. 2013-2029, 2002.

[8] J. L. Bucaille, S. Stauss, E. Felder, and J. Michler, "Determination of plastic properties of metals by instrumented indentation using different sharp indenters," *Acta Materialia*, vol. 51, pp. 1663-1678, 2003.

[9] N. Chollacoop, M. Dao, and S. Suresh, "Depth-sensing instrumented indentation with dual sharp indenters," *Acta Materialia*, vol. 51, pp. 3713-3729, 2003.

[10] Y. P. Cao and J. Lu, "Depth-sensing instrumented indentation with dual sharp indenters: Stability analysis and corresponding regularization schemes," *Acta Materialia*, vol. 52, pp. 1143-1153, 2004.

[11] N. Ogasawara, N. Chiba, and X. Chen, "On the Representative Strain of Indentation Analysis," *Journal of Materials Research*, vol. In press, 2005.

[12] L. Wang, M. Ganor, and S. I. Rokhlin, "Inverse scaling functions in nanoindentation with sharp indenters: Determination of material properties," *Journal of Materials Research*, vol. 20, pp. 987-1001, 2005.

[13] W. C. Oliver and G. M. Pharr, "Measurement of hardness and elastic modulus by instrumented indentation: Advances in understanding and refinements to methodology," *Journal of Materials Research*, vol. 19, pp. 3-20, 2004.

[14] M. R. VanLandingham, "Review of instrumented indentation," *Journal of Research of the National Institute of Standards and Technology*, vol. 108, pp. 249-265, 2003.

[15] R. Schwaiger, B. Moser, M. Dao, N. Chollacoop, and S. Suresh, "Some critical experiments on the strain-rate sensitivity of nanocrystalline nickel," *Acta Materialia*, vol. 51, pp. 5159-5172, 2003.

[16] C. A. Schuh and T. G. Nieh, "A survey of instrumented indentation studies on metallic glasses," *Journal of Materials Research*, vol. 19, pp. 46-57, 2004.

[17] L. Fang, Q. Cen, K. Sun, W. Liu, X. Zhang, and Z. Huang, "FEM computation of groove ridge and Monte Carlo simulation in two-body abrasive wear," *Wear*, vol. 258, pp. 265-274, 2005.

[18] J. L. Bucaille, E. Felder, and G. Hochstetter, "Mechanical analysis of the scratch test on elastic perfectly plastic materials with the three-dimensional finite element modeling," *Wear*, vol. 249, pp. 422-432, 2001.

[19] J. L. Bucaille and E. Felder, "Finite-element analysis of deformation during indentation and scratch tests on elastic-perfectly plastic materials," *Philosophical Magazine a-Physics of Condensed Matter Structure Defects and Mechanical Properties*, vol. 82, pp. 2003-2012, 2002.

[20] S. W. Youn and C. G. Kang, "A study of nanoscratch experiments of the silicon and borosilicate in air," *Materials Science and Engineering A*, vol. 384, pp. 275-283, 2004.

[21] G. Subhash and W. Zhang, "Investigation of the overall friction coefficient in single-pass scratch test," *Wear*, vol. 252, pp. 123-134, 2002.

[22] S. Bellemare, M. Dao, and S. Suresh, "The frictional sliding response of elasto-plastic materials in contact with a conical indenter," *International Journal of Solids and Structures*, vol. 43, 2006.

[23] Z. F. Zhang, L. C. Zhang, and Y.-W. Mai, "Particle effects on friction and wear of aluminium matrix composites," *Journal of Materials Science*, vol. 30, pp. 5999-6004, 1995.

[24] Y. N. Liang, Z. Y. Ma, S. Z. Li, S. Li, and J. Bi, "Effect of particle size on wear behaviour of SiC particulate-reinforced aluminum alloy composites," *Journal of Materials Science Letters*, vol. 14, pp. 114-116, 1995.

[25] Z. Zhang, L. Zhang, and Y.-W. Mai, "Modelling friction and wear of scratching ceramic particle-reinforced metal composites," *Wear*, vol. 176, pp. 231-237, 1994.

[26] M. Bolduc, B. Terreault, A. Reguer, E. Shaffer, and R. G. St-Jacques, "Optimum tribological improvement of aluminum using oxygen plasma source ion implantation," *Journal of Materials Research*, vol. 18, pp. 1761-1764, 2003.

[27] S. Wilson, H. M. Hawthorne, Q. Yang, and T. Troczynski, "Sliding and abrasive wear of composite sol-gel alumina coated Al alloys," *Surface and Coatings Technology*, vol. 133-134, pp. 389-396, 2000.

[28] R. L. Deuis, C. Subramanian, and J. M. Yellup, "Abrasive wear of aluminium composites - a review," *Wear*, vol. 201, pp. 132-144, 1996.

[29] M. Mata and J. Alcala, "The role of friction on sharp indentation," *Journal of the Mechanics and Physics of Solids*, vol. 52, pp. 145-165, 2004.

[30] S. Carlsson, S. Biwa, and P.-L. Larsson, "On frictional effects at inelastic contact between spherical bodies," *International Journal of Mechanical Sciences*, vol. 42, pp. 107-128, 2000.

[31] S. D. Mesarovic and N. A. Fleck, "Spherical indentation of elastic-plastic solids," *Proceedings of the Royal Society of London Series a-Mathematical Physical and Engineering Sciences*, vol. 455, pp. 2707-2728, 1999.

[32] H. Shi and M. Atkinson, "A Friction Effect in Low-Load Hardness Testing of Copper and Aluminum," *Journal of Materials Science*, vol. 25, pp. 2111-2114, 1990.

[33] M. Atkinson and H. Shi, "Friction Effect in Low Load Hardness Testing of Iron," *Materials Science and Technology*, vol. 5, pp. 613-614, 1989.

[34] C. A. Brookes and P. Green, "Anisotropy in the scratch hardness of cubic crystals.," vol. 368, pp. 37-57, 1979.

[35] C. A. Brookes, "Scratch and indentation hardness of crystals.," vol. 43, pp. 529-543, 1981.

[36] D. Tabor, *The hardness of metals*. Oxford: Clarendon press, 1951.

[37] J. A. Williams, "Analytical models of scratch hardness," *Tribology International*, vol. 29, pp. 675-584, 1996.

[38] K. L. Johnson, *Contact mechanics*. London: Cambridge University Press, 1985.

[39] MatWeb:www.matweb.com, "Material Property Data," *by Automation Creations, Inc.*, 2006.

[40] ABAQUS Theory Manual Version 6.5, Hibbitt, Karlsson and Sorensen Inc, Pawtucket, 2005

Chapter 3: Frictional sliding contact as a test technique to determine plastic properties

In the previous chapters, dimensionless functions we derived and evaluated numerically using finite element methods. This chapter illustrates the increased sensitivity to plastic flow properties by presenting results from frictional sliding on two distinct materials with the same indentation hardness. Thereafter, the sensitivity to plastic flow properties is exploited to develop algorithms to extract plastic flow properties from a frictional sliding experiment. The sensitivity of the algorithm is analyzed using the experimental results obtained in Chapters 1 and 2.

3.1 Introduction

The hardness of materials is known to depend on elastic properties, plastic properties, indenter geometry and loading conditions. Testing techniques have been recently improved to establish closer connections between the indentation response and specific material properties [1]. The development and commercialization of depth-sensing instrumented indentation systems has enabled the continuous monitoring of force and displacement during loading and unloading. Most of the new analysis techniques employ these force-displacement measurements for the extraction of material properties. The algorithms developed include those based on measurements from a single sharp indenter [2-7], from sharp indenters having different apex angles [8-10] or from a single spherical indenter [11, 12]. With these techniques, it is now possible to use the indentation response and extract estimates for the elasto-plastic properties.

Frictional sliding or scratch testing is an alternative technique to characterize the hardness and response of materials in contact with hard indenters. During frictional sliding in conditions where the tip apex angle is large enough to prevent the onset of discontinuous plasticity [13, 14], a steady state regime is reached after applying a constant normal force over a sufficient distance. The characteristics of the residual scratch profile in this steady state regime can be used to document the resistance and properties of materials. Early studies showed variations in the ratio of indentation hardness to scratch hardness between different materials [15-17], suggesting that the two quantities would not correlate. Furthermore, studies based on the finite element method indicated that the plastic strain generated beneath the surface is much greater in frictional sliding than in normal indentation [18, 19]. Therefore, frictional sliding is an alternative technique that could be used to probe material properties under conditions of larger values of plastic strain.

Recently, progress was made in determining the relationships between the frictional sliding response and material properties. Dimensionless functions were established to predict the residual scratch profile parameters by using the elasto-plastic properties of the materials as an input [19]. This work differed from the previous work on frictional sliding [18, 20-23] because the effect of plastic strain hardening was included and a large range of elasto-plastic properties was covered. In a subsequent study [Ch2], a series of experiments on the copper system demonstrated experimentally

the strong influence of plastic strain hardening on the pile-up height. The effect of the friction coefficient was also investigated, both numerically and experimentally. It was found that a major effect of friction is to increase the normalized pile-up height.

In this study, we provide experimental evidence that the frictional sliding experiment could complement indentation hardness. The plastic flow properties of an aluminum alloy were tailored to provide the same indentation hardness with different dispersions of precipitates. A significantly different behavior was observed in the frictional sliding experiment and compared with the predictions. Additionally, the methodology is used to develop a new procedure for extracting plastic flow properties from the frictional sliding test. This method is tested for sensitivity, accuracy and stability of the solution.

3.2 Experimental and computational methods

3.2.1 Choice of a model material system

A high purity 2000 series aluminum alloy was selected to generate two materials with the same indentation hardness but different microstructures. The alloy AA 2524-T3 was received from Alcoa (Alcoa Technical Center, Alcoa Center, Pennsylvania) as a sheet product 0.8 mm thick. Standard tensile specimens were machined out of these sheets according the ASTM E-8 with the axis at 45° from the rolling direction in order to probe the average properties. The machined specimens were heat-treated at 190 ± 5°C for different periods of time. After this aging treatment, microhardness and tensile tests were carried out to determine the properties of the alloy.

The tensile tests were carried out based on the ASTM E-8 test standard [24] to obtain a precise estimate of flow stress evolution. The specimens were marked prior to testing to independently measure the plastic strain at the ultimate strength. The stress-strain curves were corrected for machine/specimen compliance, and consistency was obtained between the critical engineering strain, i.e. strain at the ultimate tensile strength, and the permanent elongation of the specimens that was determined by marking. A true stress–true strain deformation representation was used to fit the data with the flow stress relationship:

$$\sigma = \sigma_y \left(1 + \frac{E}{\sigma_y} \varepsilon_p \right)^n \qquad 3.1$$

where ε_p is the equivalent plastic strain, σ_y is the initial yield strength, E is the Young's modulus of the material and n is the strain hardening exponent.

3.2.2 The frictional sliding experiments

The specimens were mechanically polished with the rolling direction normal to the plane. The final surface roughness was less than ± 5 nm as characterized using a Q-Scope 250 (Quesant Instrument Corporation, Santa Cruz, California) atomic force microscope in non contact mode. The specimens were then tested on a commercial nanoindentation test system (Nanotest ™, Micro Materials Ltd, Wrexham, United Kingdom). The indenter was a conical diamond with an apex angle θ of 70.3° and a tip radius of 2 μm. For the conditions of penetration depth investigated, the scale of experimentation was sufficiently large to consider this indenter as perfectly conical. The experiments were carried out under constant normal load P, at a velocity of 10 μm/s and over a total distance of 1500 μm, which was sufficient to attain steady state conditions after approximately 300 μm and continue to generate a region of valid steady-state profile. After the experiment, a series of at least 30 cross-sectional residual profiles were obtained over the steady state regime by using a Tencor P10 profilometer (KLA-Tencor, San Jose, California). The profilometer was equipped with a conical diamond probe which had an apex angle of 45° and a tip radius of 2 μm.

A schematic section of a residual scratch profile is presented in Figure 3.1 where a graphical representation for the pile-up height h_p, the residual penetration depth h_r and the contact radius a_r is presented. The contact radius a_r can be used directly to calculate the overall resistance to penetration using the traditional definition of hardness [25-28]

$$H_S = \frac{2P}{\pi a_r^2}. \qquad \textbf{3.2}$$

where P is the applied normal load. Assuming the absence of significant size effects, the main advantage of the conical geometry is the size independence. With this assumption, the simple ratio of h_p/h_r provides an indication on the tendency of the material to form a high pile-up.

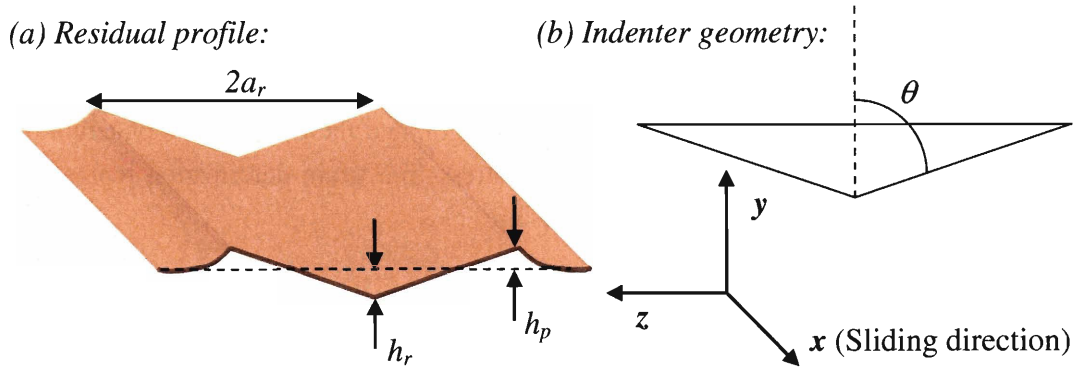

Figure 3.1: (a) A section of a residual scratch profile where the pile-up height (h_p), the residual penetration depth (h_r) and the contact radius (a_r) are indicated, and (b) a schematic view of a conical indenter with an apex angle θ. Also shown is the coordinate system for the analysis.

Friction is the third parameter of relevance to the current problem that can be analyzed experimentally and computationally. Because friction occurs at two different levels, we will separate their contribution by expressing the overall friction coefficient as

$$\mu_{tot} = \frac{F_t}{P} = f(\mu_a, \mu_w) \qquad 3.3$$

where F_t is the total tangential force, μ_a is the coefficient of friction for the normal contact local and μ_w is friction contribution from the work of plastic deformation. μ_a is governed by Amontons's law of friction with specifies the ratio between the normal pressure and the local tangential traction tensor. From a previous study [Ch2], it have been found that μ_{tot} depends only limitedly on material properties. On the other hand, the effect of μ_a on the response was significant. To determine μ_a experimentally we used the repeated pass technique described elsewhere [Ch2] and found a coefficient of *0.15*.

3.2.3 Dimensional and numerical analysis

In steady state frictional sliding of elasto-plastic materials the contact conditions can now be analyzed and predicted in details using dimensional analysis and finite element methods. The elastic contributions from the material and the indenter can be simplified using the reduced modulus [28]

$$E^* = \left[\frac{(1-\upsilon^2)}{E} + \frac{(1-\upsilon_i^{\,2})}{E_i} \right]^{-1}, \qquad 3.4$$

where E_i and ν_i are the Young's modulus and Poisson's ratio of the indenter, respectively. For the diamond used in the experiments, E_i = 1100 GPa and ν_i = 0.07 [29]. The elastic constants specified for polycrystalline Cu were taken to be: E =73.1 GPa and ν = 0.33 [29]. These properties were assumed to be isotropic for the conditions tested.

For frictional sliding contact, independent functional can be expressed for independent quantities such as the scratch hardness H_s and the pile-up height h_p. By making the quantities dimensionless and using the $\prod$ theorem, the functions can be evaluated numerically and then used for any specific material condition within the solution space. For a fixed cone angle θ of 70.3°, the finite element results from a detailed parametric study enabled to numerically determine the dimensionless functions:

$$\Pi_\alpha = \left(\frac{H_S}{\sigma_y} \right) = [\alpha 1(n) + n\,\Gamma_{\alpha 1}(\mu_a)] \left(\frac{\sigma_y}{E^*} \right) [\alpha 2(n) + \Gamma_{\alpha 2}(\mu_a)], \qquad 3.5$$

$$\Pi_\beta = \frac{h_p}{h_r} = \Pi_{\beta,RP}(n)\,\Gamma_{\beta,RP}(\mu_a) \Bigg/ \left[1+\left(\frac{\sigma_y}{X_\beta(n)\,\Gamma_{X\beta}(\mu_a)\,E^*}\right)^{p_\beta(n)}\right] \text{ and} \qquad \textbf{3.6}$$

$$\Pi_\gamma = \left(\frac{F_t}{P}\right) = \mu_{tot} = \mu_a + \left(\Pi_{\gamma,RP}\,\Gamma_{\gamma,RP}(\mu_a) - \mu_a\right) \Bigg/ \left[1+\left(\frac{\sigma_y}{X_\gamma(n)\,\Gamma_{X\gamma}(\mu_a)\,E^*}\right)^{p_\gamma(n)}\right], \qquad \textbf{3.7}$$

where the subscript $_{RP}$ indicates the value of the function at the limit of rigid plastic properties, the variable F_t is for the overall lateral force and the variable μ_{tot} is for the overall friction coefficient. Simple numerical expressions were provided [19] for the other numerical terms for the sub-functions of n ($\alpha 1(n)$, $\alpha 2(n)$, $\Pi_{\beta RP}(n)$, $X_\beta(n)$, $p_\beta(n)$, $\Pi_{\beta R}$, $X_\gamma(n)$, $p_\gamma(n)$) and the sub-functions of μ_a ($\Gamma_{\alpha 1}(\mu_a)$, $\Gamma_{\alpha 2}(\mu_a)$, $\Gamma_{\beta RT}(\mu_a)$, $\Gamma_{X\beta}(\mu_a)$, $\Gamma_{\gamma RT}(\mu_a)$, $\Gamma_{X\gamma}(\mu_a)$). With these functions and the underlining assumptions, one can specify the elasto-plastic properties of a material and predict the response in terms of the normalized scratch hardness H_s/σ_y (Π_α) , the ratio of pileup height (Π_β) and the overall friction coefficient μ_{tot} (Π_γ) . The third function Π_γ for the overall friction coefficient was omitted in the analysis because of its low sensitivity to material properties as demonstrated in previous experiments (Ch1, Ch2).

3.3 Results and Discussion

3.3.1 Indentation hardness versus scratch hardness

The evolution of hardness as a function of aging time is presented in Figure 3.2 for the aluminum alloy used in this study. The hardness initially decreases and then rapidly increases. Subsequent to a maximum which occurs between 5 and 10 hours, the hardness progressively decreases to its original value of 142 HV after 200 hours. These results on the aging behavior are consistent with literature data on similar alloys [30]. For the frictional sliding experiments, we tested the materials in the as-received condition and in the condition aged for the longest period of time of 200 hours. This condition leads to two materials with the same indentation hardness.

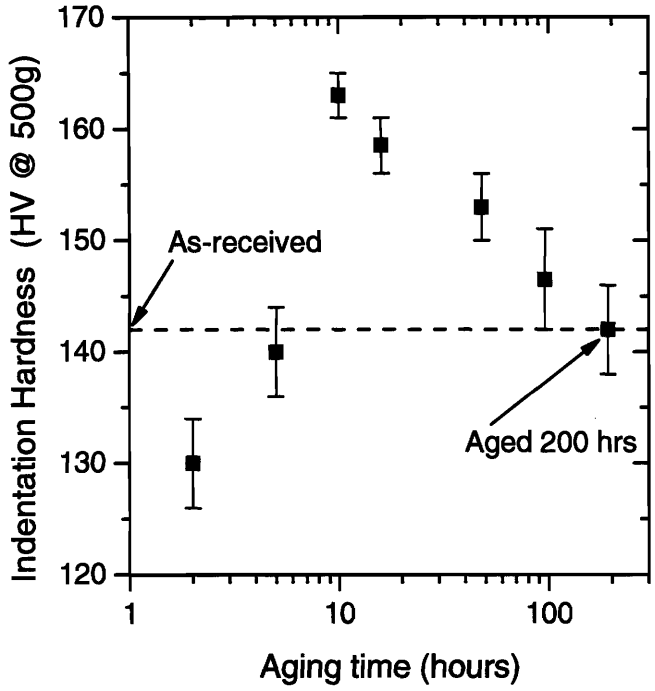

Figure 3.2: Evolution of microhardness of the aluminum alloy AA2524-T3 with aging time. The horizontal dotted line is for the hardness of the as-received material.

Figure 3.3 compares the residual cross-sectional profiles from frictional sliding experiments on the two materials. The scales are normalized by the residual penetration depth h_r, so as to develop a better relative comparison of the behavior. The profiles from the as-received specimen present a lower maximum height h_p and a smooth transition from the maximum towards the original un-deformed surface. For the aged specimens, the maximum height h_p is higher and the transition from the maximum to the original surface is significantly more abrupt. These differences in the relative shape of the profiles could well translate into a different resistance to tribological damage. A more blunted profile would reduce the amount of material removal in a subsequent tribological event.

The average normalized pile-up height and the experimental scratch hardness are presented in Table 3.1. Although the materials have the same indentation hardness, the scratch hardness of the as-received specimen is 18% higher while at the same time its pile-up height is 30% lower. These differences offer new experimental evidence that two similar materials with the same value of the indentation hardness can have a different scratch hardness as well as a different behavior in frictional sliding. With the differences observed, the results clearly indicate an influence of the testing technique on the comparative ranking of the materials. For a given application, it may prove most appropriate to use the testing technique that reproduces more closely the real contact conditions.

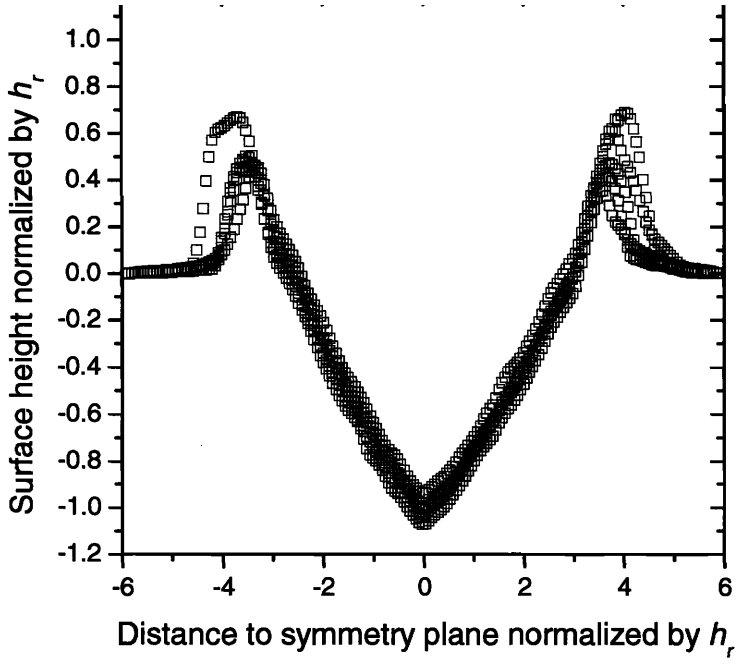

(a)

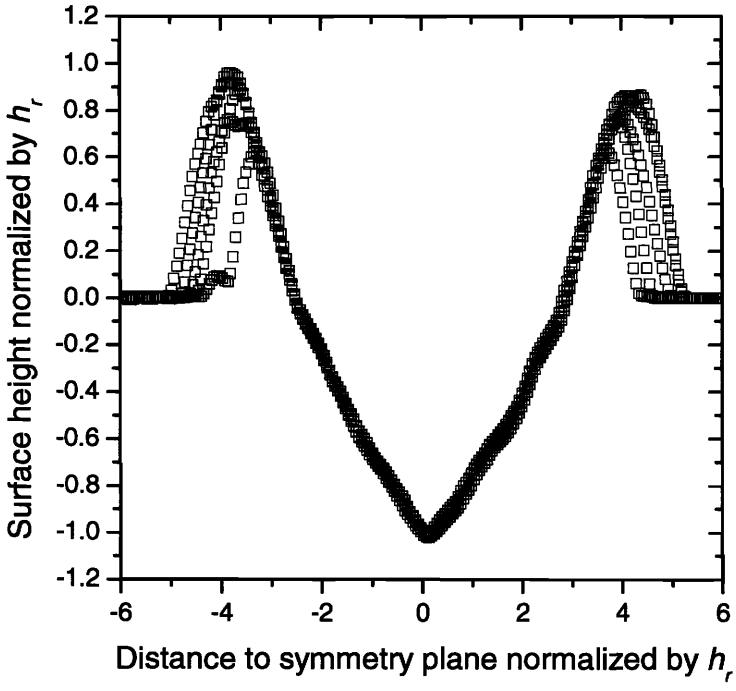

(b)

Figure 3.3: Residual cross-sectional profiles for the aluminum alloy in the (a) as-received and (b) over-aged conditions. The sliding direction is normal to the plane.

The size and distribution of the hardening precipitates was the main microstructural parameter varied through the aging treatment. This treatment changed the plastic strain hardening characteristic of the material, and these changes in the plastic flow properties of the alloy can be used to interpret the difference in the frictional sliding response. As listed in Table 3.1, the aging treatment resulted in an increase in initial yield strength σ_y, but also a significant decrease in the strain hardening exponent n. Using the dimensionless functions Π_α and Π_β from Equations 3.4 and 3.5, the increase in σ_y would increase hardness and decrease pile-up for the aged material. Therefore, the only possible explanation for the decrease in scratch hardness and the increase in normalized pile-up height is that aging reduced the plastic strain hardening exponent.

Table 3.1 also presents the predictions obtained from the elasto-plastic properties and the dimensionless functions Π_α and Π_β. A good correspondence is observed between the experimental measurements and the predictions with differences less than 8% in all cases. In addition to the aluminum alloy presented in this study, we used the dimensionless functions Π_α and Π_β to interpret results from frictional sliding response of pure nickel, pure copper and a single phase brass alloy. For each of these materials, we studied a large range of grain sizes and found an excellent correspondence between experimental results and predictions.

Table 3.1: Summary for the comparison between finite element predictions and the experimental results. The plastic properties of the materials are listed as a reference.

	Experimental		Plastic properties		FEM predictions	
	H_S (GPa)	h_p/h_r	σ_y (GPa)	n	H_S (GPa)	h_p/h_r
As-received	1.3 ± .2	0.54 ± .13	0.22	.18	1.28	.58
Aged	1.1 ± .1	0.79 ± .15	0.33	.08	1.14	.76

3.3.2 Extracting properties from the frictional sliding experiment

With a well-tested methodology for predicting the frictional sliding response from mechanical properties, attention is now directed at how the functions Π_α and Π_β could be used to extract properties from the frictional sliding experiments. As part of the analysis, we will consider the sensitivity of the technique to errors in the experimental data. Figure 3.4 presents a summary of the proposed reverse algorithm and related assumptions. The algorithm assumes that coefficient of friction μ_a is known. It is assumed that the friction coefficient μ_a is independent of the pressure applied and that the value of μ_a is determined experimentally following a methodology such as the nearly elastic contact [Ch2]. It also assumes known elastic properties for the tip and the material, indicating that the value of E^* needs to be determined. It also requires that to the real material plastic flow relationship can be approximated by a power-law and the incremental theory of plasticity. Finally, the indenter is considered as a perfect cone with an apex angle of 70.3°.

With the measured values of H_s and h_p/h_r as principal experimental inputs, the objective is to extract n and σ_y/E^*. The dimensionless functions can be rewritten as:

$$\Pi'_{\alpha}(H_S, E^*, n, \mu_a) = \left(\frac{\sigma_y}{E^*}\right) = \left[\left(\frac{H_S}{E^*}\right) \Big/ \left(\alpha 1(n) + n\,\Gamma_{\alpha 1}(\mu_a)\right)\right]^{\left[1/\left(1+\alpha 2(n)+\Gamma_{\alpha 2}(\mu_a)\right)\right]} \qquad \textbf{3.8}$$

and

$$\Pi'_{\beta}(\Pi'_{\alpha}, n, \mu_a) = \frac{h_p}{h_r} = \Pi_{\beta,RP}(n)\,\Gamma_{\beta,RP}(\mu_a) \Big/ \left[1 + \left(\frac{\Pi'_{\alpha}}{X_{\beta}(n)\,\Gamma_{X\beta}(\mu_a)}\right) p_{\beta}(n)\right]. \qquad \textbf{3.9}$$

To solve this system numerically, we need to replace the expression of Π'_{α} in Π'_{β} and to solve numerically Π'_{β} by varying n until reaching the experimental value of h_p/h_r. As it will be shown in the next figures, the value of h_p/h_r steadily decreases with increasing n, simplifying the solution procedure. Once n is determined by iteration on Π'_{β}, it can be inserted back in Π'_{α} to determine σ_y/E^*. To solve numerically this system, the set of equations can be implemented in a calculus spreadsheet by reserving columns for the outputs and for each sub-function of n or μ_a. A single iteration loop is need for solving Π'_{β} through determining n. To complete the algorithm, it is important as a final step to verify whether the numerical solution for n and σ_y/E^* is within the bounds covered by the parametric study used to establish Π'_{α} in Π'_{β}:

$$\left(4.8\times10^{-5}\right) n^{-1.22} < \left(\frac{\sigma_y}{E^*}\right) < \left(5.5\times10^{-2}\right) e^{-5.11n}, \quad \textit{where} \quad 0 \le n \le 0.5, \qquad \textbf{3.10}$$

This range of material properties covers a large variety of engineering materials, but there are exceptional cases outside the range defined above that would need a different analysis [19].

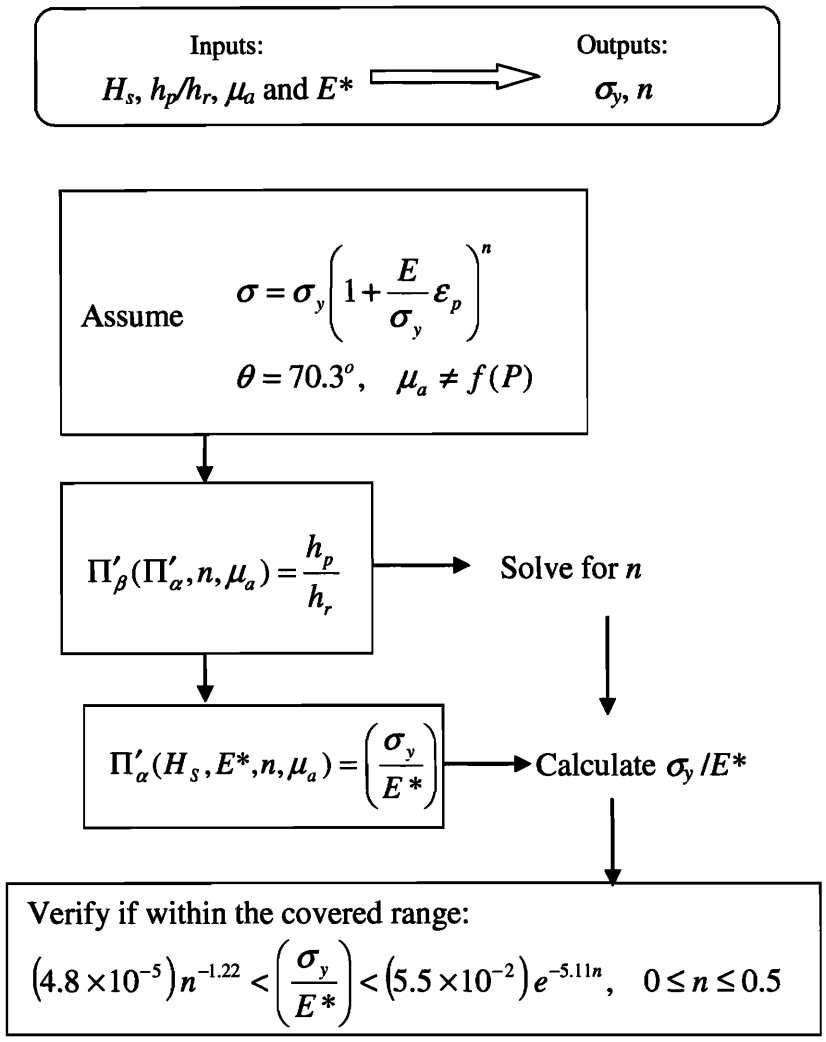

Figure 3.4: Summary of the reverse algorithm proposed to extract plastic flow properties from a frictional sliding experiment

The solution field for the reverse analysis can be represented graphically with the plastic flow properties σ_y/E^* and n as coordinate axis. For the purpose of the discussion in the remaining of this section, the friction coefficient μ_a is fixed at 0.15. The first set of curves for the solution is presented in Figure 3.5 for specific values of the normalized hardness H_s/E^*. For each curve, H_s/E^* was set at fixed value and the material parameters were varied to identify all possible combinations of solutions. The solutions for constant H_s/E^* all have a decreasing slope, indicating that a decrease in normalized initial yield strength σ_y/E^* can be counterbalanced by an increase in n in order to maintain a constant hardness.

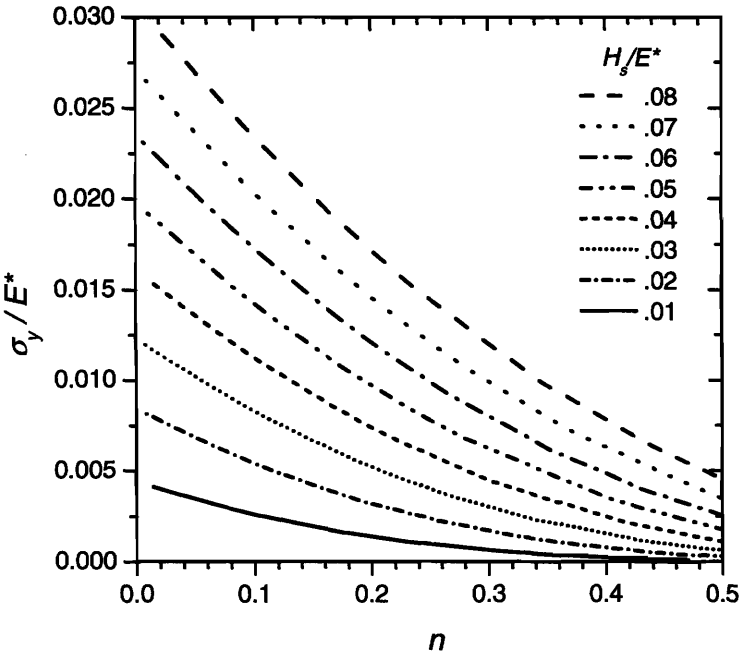

Figure 3.5: Combinations of normalized yield strength σ_y/E^* and strain hardening exponent n for which the normalized hardness H_s/E^* remains constant. The different curves are for eight different values of H_s/E^*.

To complete the representation of the solution, curves for constant values of the normalized pile-up height h_p/h_r are presented in Figure 3.6. On this plot, the vertical scale for the normalized yield strength σ_y/E^* was changed to logarithmic in order to improve the resolution for soft materials. The curves of constant h_p/h_r have a relatively high negative slope, especially at low yield strength or high strain hardening exponent. Each of these constant h_p/h_r curves intersects with the second set of curves for a constant hardness H_s/E^*. These hardness curves are reproduced from the previous Figure 3.5 and included to discuss the solution to the algorithm for extracting properties. It is clear from the two sets of curves shown that the fields are continuous and monotonically varying with properties. Also, throughout the regime, the local slope of the constant h_p/h_r curves is always higher than the slope of constant H_s/E^*. Therefore, to each set of values for H_s/E^* and h_p/h_r corresponds a single intersection point in this plane of plastic flow properties, σ_y/E^* versus n. At the same time, the stability of the solution is ensured for the algorithm of extracting plastic flow properties from H_s/E^* and h_p/h_r. Providing that the elastic and contact properties are known, the normalized hardness and the normalized pile-up height are sufficient to determine the plastic strain hardening exponent and the initial yield strength.

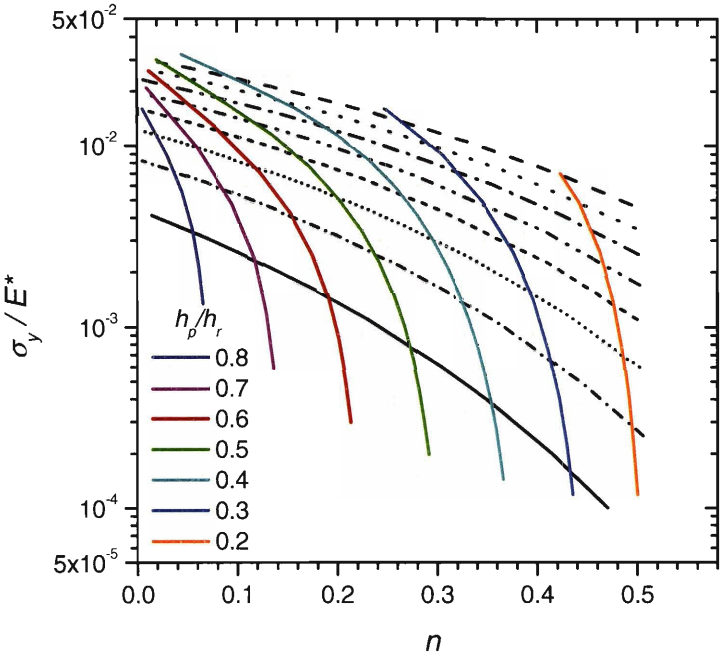

Figure 3.6: Solution field for extracting plastic flow properties from scratch hardness and normalized pile-up height h_p/h_r. The series of curve with the lowest slope is from Figure 3.5 for the different values of the normalized hardness H_s/E^*. The new series of curve is for the different values of the normalized pile-up height that decreases from left to right.

The reverse algorithm and the curves presented here can be used as a reference for comparing materials on the basis of constant hardness. We consider an example where the normalized hardness H_s/E^* is maintained fixed at 0.02 and we want to determine which sets of plastic flow properties would respect the constraint. According to Figure 3.6, there is a continuous spectrum of solutions for going along the specific curve of $H_s/E^* = 0.02$. Five different possibilities were depicted among all possible solutions and Figure 3.7 presents the constitutive stress-strain curve of each of them. Although these materials will yield the same H_s/E^*, other parameters of the frictional sliding behavior can differ significantly including the indicated variation in normalized pile-up height h_p/h_r. The material with the lowest yield strength may appear softer on the basis of its plastic flow properties up to a flow stress of approximately 30%, but this material has the same scratch hardness and a significantly lower normalized pile-up height h_p/h_r. Clearly, hardness alone is an incomplete predictor of the response in frictional sliding.

On the other hand, the practical significance of decreasing the pile-up height h_p/h_r cannot be assessed quantitatively from the framework used in the study. In principle, a more blunted pile-up with a lower maximum height would be less likely to be removed in subsequent tribological events. A lower h_p/h_r may also make the material less prone to plastic instability or chipping when the tip apex angle θ decreases. However, more research is needed in this area before quantitative relationships can be established.

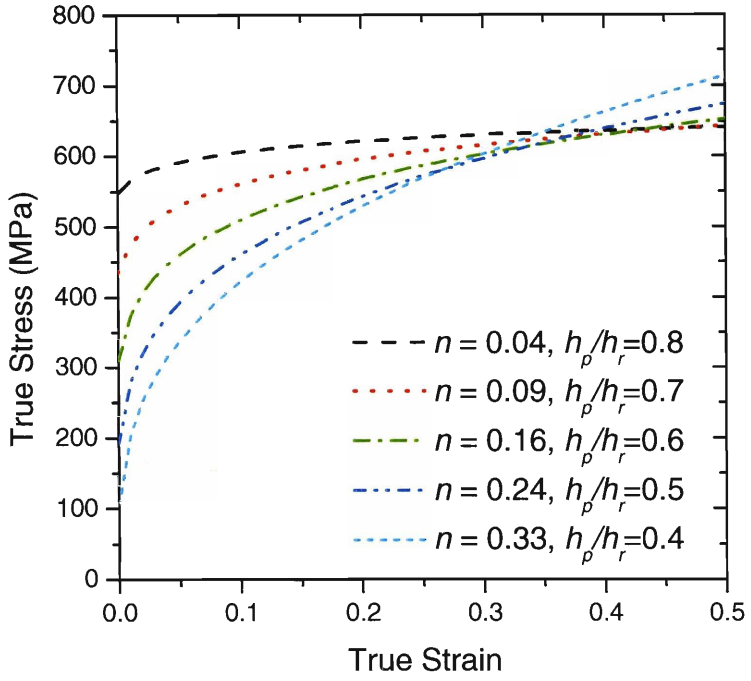

Figure 3.7: Flow stress curves of materials with the same normalized scratch hardness H_s/E^* of 0.02

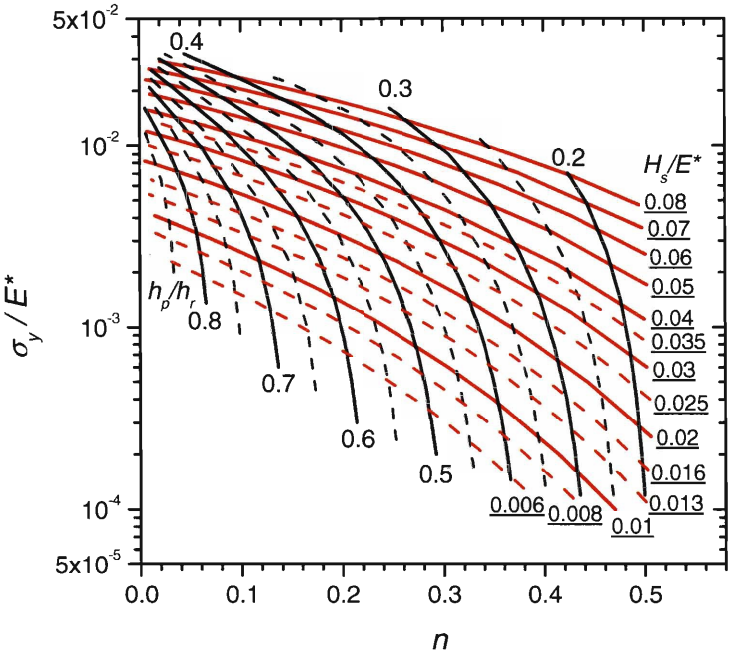

Figure 3.8: Abacus for estimating the strain hardening exponent and the normalized initial yield strength from the normalized scratch hardness and the normalized pile-up height.

To complement the above methodology on extracting properties from the dimensionless functions Π_α in Π_β, Figure 3.8 presents an abacus with several intermediate values for the curves of the constant H_s/E^* and constant h_p/h_r. On this abacus, the underlined numerical values are for the H_s/E^* curves; whereas, the dotted lines for h_p/h_r are all at a 0.05 offset from the solid lines. This abacus could be used as a tool to identify alternative combinations of properties and their characteristics in frictional sliding. The representation is subjected to the same underlying assumptions and it was drawn for a friction coefficient μ_a of 0.15. It could also serves as a first order approximation of the solution scheme presented in Figure 3.8.

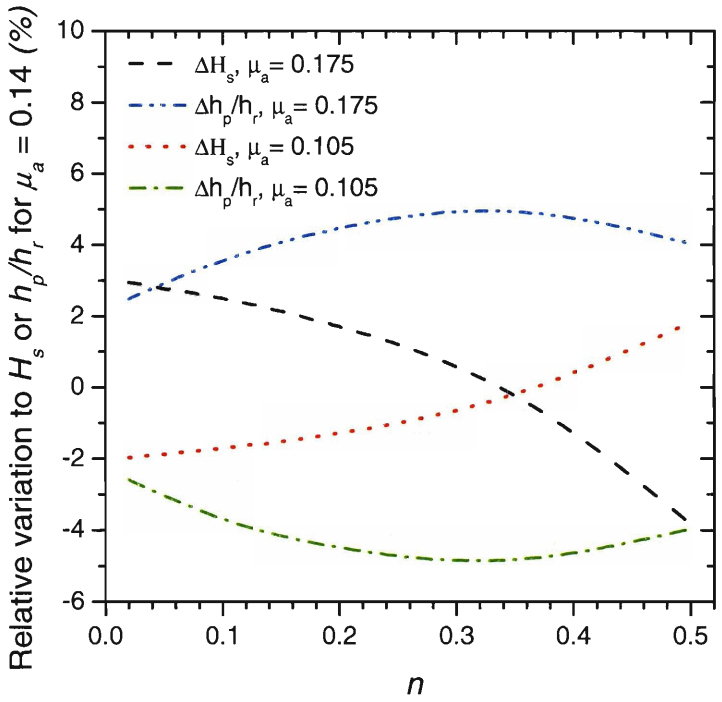

Figure 3.9: Variation in the value of hardness H_s and normalized pile-up height h_p/h_r that results from a friction coefficient μ_a different than 0.14.

3.3.3 Sensitivity analysis

Determining experimentally the friction coefficient μ_a can be subject to a certain level of uncertainty. With the objective of presenting representative values for the sensitivity of the parameters h_p/h_r and H_s/E^* to μ_a, the dimensionless functions Π_α and Π_β from Equations 3.4 and 3.5 were used to vary μ_a from a mean value of 0.14 by ± 25%. The normalized yield strength of the material was fixed at $\sigma_y/E^* = 0.0045$. Figure 3.9 presents the results for the relative variation in h_p/h_r and H_s/E^* as a function of the plastic strain hardening exponent. Throughout the range covered, all variations are within 5%. The error that can be generated varies between the material conditions and they can be easily determined for any condition using the dimensionless functions Π_α and Π_β. On the other hand, the sensitivity of the functions is relatively limited. Although the

most precise value of μ_a is more suitable, a variation within 10% would probably fall well within the experimental scatter.

The effect of experimental scatter on the extracted values of plastic flow properties is also important in determining the robustness of the reverse algorithm proposed here. We first present the results from applying the reverse algorithm to experimental results on the aluminum alloy with the different heat treatment. The frictional sliding results from previous studies on pure copper, a copper-zinc alloy and pure nickel were also utilized. For each copper-based material, the grain size was varied through a recrystallization heat-treatment [ch2]; whereas, the processing technique was changed to obtain microcrystalline, ultrafile crystallline and nanocrystalline pure nickel [19]. Table 3.2 presents a comparison between the properties extracted from the frictional sliding results and those obtained from the tensile test measurements. With three exceptions out of the 22 properties extracted, the error fall within less than 18%. Interestingly, the average and maximum error is significantly lower for the prediction the of the plastic strain hardening exponent.

The sensitivity to ± 5% variations in h_p/h_r and H_s/E^* was also studied in details using the reverse algorithm. Table 3.2 presents a summary where the results are classified by categories of values of n. The 8 values of error reported on each line were the maximum found for the different values of σ_y/E^* studied for each category of n. With 4 exceptions, the effect of a 5% variation is of at most 15%. This result can be considered as a moderate sensitivity for a reverse algorithm. With the relationship between the strain hardening exponent and tensile ductility, the reverse algorithm can allow to predict the tensile behavior with a reasonable level of certainty.

Table 3.2: Comparison between the predictions for the reverse algorithm and experimental values. The data for pure Cu, Cu-Zn and pure Ni are from previous work [Ch1, Ch2].

	Experimental		Extracted properties		Properties from tension	
	H_S (GPa)	h_p/h_r	$\sigma_{0.2\%}$ (MPa)	n	$\sigma_{0.2\%}$ (MPa)	n
Al (As-received)	1.3	0.54	180	0.21	220	0.18
Al (Aged)	1.1	0.79	370	0.05	330	0.08
Cu (450°C)	0.66	.7	135	0.13	145	0.13
Cu (600°C)	0.62	.57	58	0.23	44	0.27
Cu (700°C)	0.60	.51	35	0.28	28	0.29
Cu-Zn (450°C)	1.13	.44	59	0.32	45	0.35
Cu-Zn (600°C)	0.95	.3	12.9	0.44	15.5	0.41
Cu-Zn (700°C)	0.81	.28	7.8	0.45	7.0	0.45
Ni (nc)	4.42	0.84	1723	0.02	1600	0.02
Ni (ufc)	2.63	0.76	804	0.07	850	0.06
Ni (mc)	1.35	0.63	201	0.18	170	0.19

Table 3.3: Sensitivity analysis for the reverse algorithm.

	Δ on σ_y for H_s		Δ on n for H_s		Δ on σ_y for h_p/h_r		Δ on n for h_p/h_r	
	+5%	-5%	+5%	-5%	+5%	-5%	+5%	-5%
$n \leq 0.1$	7.9	-7.7	-11.8	12.1	14.4	-12.1	-21.9	21.1
$0.1 < n \leq 0.2$	10.8	-10.0	-15.2	15.8	13.3	-12.8	-15.5	16.9
$0.2 < n \leq 0.35$	11.3	-10.9	-11.3	10.8	12.8	-11.8	-12.6	13.3
$0.35 < n \leq 0.5$	20.3	-11.6	-11.2	3.8	12.3	-11.3	-8.1	7.9

3.4 Conclusions

Frictional sliding and normal indentation were compared experimentally and a set of dimensionless functions was used to develop a new methodology for extracting the plastic flow properties from a frictional sliding experiment. The following conclusions can be drawn.

1. Two materials with the same indentation hardness can have significantly different scratch hardness. They can also present a significantly different pile-up behavior in frictional sliding, adding to the advantages of using frictional sliding as a test technique when it reproduces more closely the contact conditions in a real application.

2. The plastic properties of a material can be extracted from the response to a frictional sliding test. Provided that the elastic moduli and contact properties are known, the normalized hardness and the normalized pile-up height are sufficient to determine the plastic strain hardening exponent and the initial yield strength.

3. The algorithm proposed to extract properties has a reasonable sensitivity to variations in the input parameters. Small variations in the friction also have a limited effect on the properties. Using averaged measurements and well calibrated equipment can endure reliability of the results.

The frictional sliding test could well serve as a predictor of the tribological response and as a testing technique to probe the plastic flow properties of materials. The technique is now proven to be highly capable to identifying small variations in the strain hardening exponent of the material, a quantity that is a prime indicator of ductility in a tensile test. An analysis framework is now available to fully predict the frictional sliding response from known material properties or extract plastic properties from the frictional sliding response.

3.5 References

[1] Y. T. Cheng and C. M. Cheng, "Scaling, dimensional analysis, and indentation measurements," *Materials Science & Engineering R-Reports*, vol. 44, pp. 91-149, 2004.

[2] A. E. Giannakopoulos and S. Suresh, "Determination of elastoplastic properties by instrumented sharp indentation," *Scripta Materialia*, vol. 40, pp. 1191-1198, 1999.

[3] Y.-T. Cheng and C.-M. Cheng, "Scaling approach to conical indentation in elastic-plastic solids with work hardening," *Journal of Applied Physics*, vol. 84, pp. 1284, 1998.

[4] M. Dao, N. Chollacoop, K. J. Van Vliet, T. A. Venkatesh, and S. Suresh, "Computational modeling of the forward and reverse problems in instrumented sharp indentation," *Acta Materialia*, vol. 49, pp. 3899-3918, 2001.

[5] Y.-T. Cheng, Z. Li, and C.-M. Cheng, "Scaling relationships for indentation measurements," *Philosophical Magazine A: Physics of Condensed Matter, Structure, Defects and Mechanical Properties*, vol. 82, pp. 1821-1829, 2002.

[6] N. Ogasawara, N. Chiba, and X. Chen, "On the Representative Strain of Indentation Analysis," *Journal of Materials Research*, vol. In press, 2005.

[7] L. Wang, M. Ganor, and S. I. Rokhlin, "Inverse scaling functions in nanoindentation with sharp indenters: Determination of material properties," *Journal of Materials Research*, vol. 20, pp. 987-1001, 2005.

[8] J. L. Bucaille, S. Stauss, E. Felder, and J. Michler, "Determination of plastic properties of metals by instrumented indentation using different sharp indenters," *Acta Materialia*, vol. 51, pp. 1663-1678, 2003.

[9] N. Chollacoop, M. Dao, and S. Suresh, "Depth-sensing instrumented indentation with dual sharp indenters," *Acta Materialia*, vol. 51, pp. 3713-3729, 2003.

[10] Y. P. Cao and J. Lu, "Depth-sensing instrumented indentation with dual sharp indenters: Stability analysis and corresponding regularization schemes," *Acta Materialia*, vol. 52, pp. 1143-1153, 2004.

[11] Y. P. Cao and J. Lu, "A new method to extract the plastic properties of metal materials from an instrumented spherical indentation loading curve," *Acta Materialia*, vol. 52, pp. 4023-4032, 2004.

[12] M. H. Zhao, N. Ogasawara, N. Chiba, and X. Chen, "A new approach to measure the elastic-plastic properties of bulk materials using spherical indentation," *Acta Materialia*, vol. 54, pp. 23-32, 2006.

[13] A. J. Black, E. M. Kopalinsky, and P. L. B. Oxley, "Investigation of the different regimes of deformation which can occur when a hard wedge slides over a soft surface: the influence of wedge angle, lubrication and prior plastic working of the surface.," *Wear*, vol. 123, pp. 97-114, 1988.

[14] A. A. Torrance, "Three-dimensional cutting criterion for abrasion.," *Wear*, vol. 123, pp. 87-96, 1988.

[15] T. C. Buttery and J. F. Archard, "Grinding and abrasive wear," *Proc. Inst. Mech. Engng.*, vol. 185, pp. 537-551, 1971.

[16] C. A. Brookes, P. Green, P. H. Harrison, and B. Moxley, "Some observations on scratch and indentation hardness measurements," *J. Phys. D: Appl. Phys.*, vol. 5, pp. 1284-1293, 1972.

[17] V. Jardret, H. Zahouani, J. L. Loubet, and T. G. Mathia, "Understanding and quantification of elastic and plastic deformation during a scratch test," *Wear*, vol. 218, pp. 8-14, 1998.

[18] J. L. Bucaille, E. Felder, and G. Hochstetter, "Mechanical analysis of the scratch test on elastic perfectly plastic materials with the three-dimensional finite element modeling," *Wear*, vol. 249, pp. 422-432, 2001.

[19] S. Bellemare, M. Dao, and S. Suresh, "The frictional sliding response of elasto-plastic materials in contact with a conical indenter," *International Journal of Solids and Structures*, vol. 43, 2006.

[20] L. Fang, Q. Cen, K. Sun, W. Liu, X. Zhang, and Z. Huang, "FEM computation of groove ridge and Monte Carlo simulation in two-body abrasive wear," *Wear*, vol. 258, pp. 265-274, 2005.

[21] J. L. Bucaille and E. Felder, "Finite-element analysis of deformation during indentation and scratch tests on elastic-perfectly plastic materials," *Philosophical Magazine a-Physics of Condensed Matter Structure Defects and Mechanical Properties*, vol. 82, pp. 2003-2012, 2002.

[22] S. W. Youn and C. G. Kang, "A study of nanoscratch experiments of the silicon and borosilicate in air," *Materials Science and Engineering A*, vol. 384, pp. 275-283, 2004.

[23] G. Subhash and W. Zhang, "Investigation of the overall friction coefficient in single-pass scratch test," *Wear*, vol. 252, pp. 123-134, 2002.

[24] C. E28, *Standard test methods for tension testing of metallic materials*, vol. E8. West Conshohocken, PA: ASTM International, 2004.

[25] D. Tabor, *The hardness of metals*. Oxford: Clarendon press, 1951.

[26] J. A. Williams, "Analytical models of scratch hardness," *Tribology International*, vol. 29, pp. 675-584, 1996.

[27] A. C. Fischer-Cripps, *Introduction to Contact Mechanics*. New York: Springer-Verlag, 2000.

[28] K. L. Johnson, *Contact mechanics*. London: Cambridge University Press, 1985.

[29] MatWeb:www.matweb.com, "Material Property Data," *by Automation Creations, Inc.*, 2006.

[30] J. R. Davis, *Aluminum and aluminum alloys*. Materials Park: ASM International, 1993.

Chapter 4: The frictional sliding response of nanocrystalline nickel and nickel-tungsten alloys

This last and forth chapter presents a summary of experimental results from a comprehensive investigation on the frictional sliding response of nanocrystalline nickel and alloys. As a major difference, a spherical tip was used for all the experiments. At low load, the use of a spherical geometry was a necessity with no other axisymmetric shapes commercially available. Also, the spherical tip was less prone to changes in geometry from wearing against hard asperities on the surface. With significant previous research on the mechanical properties and behavior of nanocrystalline metals and alloys, this study on frictional sliding was a logical subsequent step as a potential application would be for small devices or as surface engineering overlay.

4.1 Introduction

Nanocrystalline metals and alloys were recently developed and they have been studied extensively, both computationally and experimentally [1]. Their high indentation hardness and high tensile yield strength made them candidates for applications where the mechanical resistance is important. According to previous operating definitions, a material would be nanocrystalline if the size of all grains in the microstructure falls below 100 nm [1]. Among other properties, the mechanical behavior and plastic deformation characteristics of nanocrystalline materials revealed differences as compared to crystalline materials with larger grain sizes.

It is now well established that nanocrystalline materials present increased strain-rate sensitivity in the plastic deformation regime [2-6]. The higher dependence of the flow stress on strain rate was revealed through both tensile tests and instrumented indentation experiments. The increased time dependence on deformation events has also been observed in constant load and cyclic loading experiments [7]. A decrease in the activation volume with decreasing grain size was recently proposed [8] and it could explain these time dependent phenomena.

The mechanisms of deformation in nanocrystalline metals and alloys can depend on the particular system of interest and on grain size. Within the nanocrystalline grain-size regime, at grain sizes of typically less than 10-15 nm there is a breakdown in the Hall-Petch relationship which stipulates the rate of increase in hardness with decreasing grain size in conventional materials [1]. Below this critical grain size, grain boundary sliding and migration have been proposed as a possible deformation mechanism [9-15]. However, above the threshold size, in-situ transmission electron microscopy in nanocrystalline pure nickel provided experimental evidence of significant dislocation activity [16]. In spite of this dislocation activity, microscopy on deformed specimens revealed deformation-induced changes of the grain boundaries but a low remnant density of dislocations [16]. With the apparent limited multiplication do dislocations, the sources for plastic

strain hardening in nanocrystalline nickel could very well be limited. Also, the information available suggest that the grain boundaries are acting as sources and sinks for dislocations for grain sizes between 10-15 and 100 nm.

Grain refinement also changes the fracture resistance. In pure nickel, grain refinement was found to have a beneficial effect on the fatigue crack initiation resistance, but a deleterious effect on the crack fatigue propagation resistance [17, 18]. Based on these results, it was proposed to use nanocrystalline nickel as a surface coating [17]. Since surfaces was often are subjected to repeated contact and nanocrystalline materials may find applications for tribological resistance with their higher hardness, an initial study was undertaken to study the effect of grain size and microstructure on the frictional sliding response [19]. Yield strength was identified as a critical parameter in the response and the response of nanocrystalline pure nickel was found significantly superior to the resistance of pure with coarser grain sizes.

In this study, we also use frictional sliding but the extent of plastic deformation was increased by selecting a ratio of penetration depth to tip radius between 5 and 10 higher. In conditions of frictional sliding with high plasticity [20], previous finite element analysis and experimental results [ch2] indicated a large influence of plastic strain hardening on the pile-up height. Therefore, the frictional sliding test technique was selected because it reproduces a basic tribological event and it allows an investigation of the strain hardening properties. The testing technique was applied at two different length scales and on appropriate nanocrystalline materials to investigate their resistance to frictional sliding and the effect of grain size and alloying on the plastic flow behavior at large plastic strain.

4.2 Experimental techniques

4.2.1 Materials and preparation

The materials for this study were pure nickels and nickel-tungsten alloys. Based on the recent classification of grain sizes [1], the three types of pure nickel studied were appropriately labeled as microcrystalline (mc), ultra-fine crystalline (ufc) and nanocrystalline (nc). These materials were from the same processing batch as in previous studies where their structure and mechanical properties were investigated and reported in details [2, 18, 21]. Except for pure mc nickel which was cold worked and annealed, all the other materials investigated in this study were produced by electrodeposition. For the second material system, nanocrystalline nickel-tungsten alloys were studied for three different average grain sizes of 40, 17 and 9 nm. The grain sizes were measurement through x-ray diffraction and the variations in grain size were obtained by varying the tungsten composition in the electrolytic batch. Details on the processing technique, composition and mechanical properties of these alloys are available in Detor *et al.* [22].

The specimens were mechanically polished with the deposition orientation normal to the plane. The final particle size suspension polishing was 50 nm. Special care was necessary to

prevent surface adhesion of these 50 nm particles as well as of the 250 nm diamond particles. The best practice found was to use a small quantity of soap (Liquinox) with di-ionized water and ultrasonic vibration. The sample needed to be soaked right after polishing before the drying of the surface and a series of rinsing cycles was often necessary. The final surface roughness of the clean surface was less than ± 3-5 nm as characterized using a Q-Scope 250 (Quesant Instrument Corporation, Santa Cruz, California) atomic force microscope in non contact mode.

4.2.2 Experimental testing

After a detailed characterization of the surface, low load experiments were carried out using a 500 nm spherical tip. A commercial nanoindentation test system (TriboScope®, Hysitron Inc, Minneapolis, MN) was used to applied a constant normal force P and induce a tangential displacement over a sliding distance of 10 μm. During the experiment, the lateral force and normal displacement were continuously monitored. Each testing condition was repeated between 5 and 10 times to access repeatability and to generate statistics. The surface of each scar was then characterized for topography using the Q-Scope 250 atomic force microscope. Full three-dimensional images were imported and analyzed to extract information about the residual scratch profiles. Only the regions of steady state were considered for this analysis.

As a bench mark for comparison, all the materials were also tested at higher normal loads with another nanoindentation test system (Nanotest ™, Micro Materials Ltd, Wrexham, United Kingdom). In this case, the indenter was a spherical diamond with a tip radius of 25 μm and the experiments were carried out under a constant normal load P, which was varied between the experiments to cover a range of testing conditions. For all the experiments, the tip traveled at a velocity of 10 μm/s and over a total distance of 450 μm. This distance was sufficient because steady state conditions were attained after approximately 75 μm and then sliding was continued to generate a large region of valid steady-state. After the experiment, a series of cross-sectional residual profiles were obtained over the steady state regime by scanning the surface with the piezo-tube and the measurement head of the TriboScope®. The measurement head was loaded with a spherical indenter having a radius of 500 nm and the applied normal load was fixed to 10 μN during scanning at a velocity of 15 μm/s.

4.2.3 Analysis framework

The analysis of the results focuses on the steady state regime which develops after a traveling distance of the order of three or five times the contact radius. Since the experiments performed in this study included a detailed characterization of the residual surfaces, we will use specific surface measurements to quantify the response of the different materials. Figure 4.1 presents a schematic of a residual scratch profile with an illustration of the residual width ($2a_r$), residual penetration depth (h_r) and the residual pile-up height (h_p). Using this height information, the dimensionless ratio h_p/h_r

can be expressed and calculated for the different materials. On the other hand, the residual width can be used to calculate the scratch hardness

$$H_S = \frac{2P}{\pi a_r^2} \qquad \textbf{4.1}$$

where P is the magnitude of the applied load. Finally, the ratio of tangential force F_t over normal force P can be used to calculate an overall friction coefficient

$$\mu_{tot} = \frac{F_t}{P} = f(\mu_a, \mu_w) \qquad \textbf{4.2}$$

where μ_a is the coefficient of friction for the normal contact local and μ_w is friction contribution from the work of plastic deformation. μ_a is governed by Amontons's law of friction with specifies the ratio between the normal pressure and the tangential traction tensor for the local interaction between the indenter and the surface.

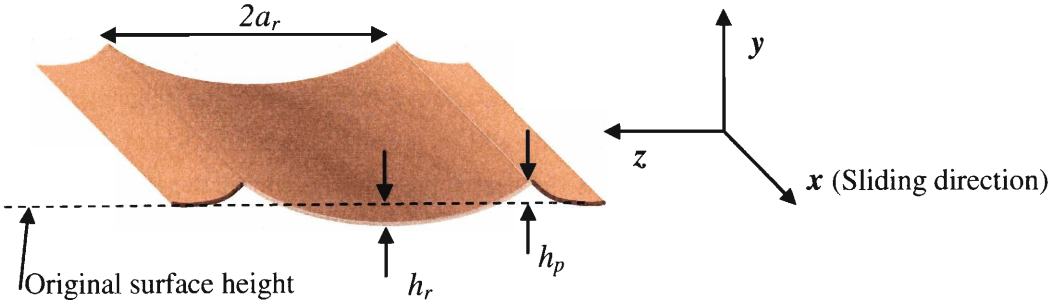

Figure 4.1: Schematic of a residual scratch profile with the sliding direction along the *x* axis and the measured quantities as indicated: residual width (a_r), residual depth (h_r) and residual pile-up height (h_p).

For the conical tip geometry, quantitative dimensionless expressions were developed in previous research for the relationships between the response parameters herein described (H_s, h_p/h_p and μ_{tot}) and the properties of the material [20] as well as the contact conditions [ch2]. For the low load experiment in the current study, the use of a spherical geometry was a necessity with no other axisymmetric shapes commercially available. Also, using an initially sharp tip would have probably resulted in a change in tip geometry with time as a result of wear when contacting hard asperities of natural oxides. Unfortunately, the methodology developed for a conical indenter is not directly applicable because the contact geometry becomes a function of the penetration depth for a spherical indenter.

4.3 Experimental results

Because of this effect of penetration depth on contact geometry, the response to frictional sliding has been investigated at different values of the contact normal load. For the experiments with a 500 nm spherical diamond tip at low loads, the normal load P was set at 200, 500 and 1000 μN for all the material conditions. Figure 4.2 (a) presents the evolution of the overall friction coefficient for these different loads and for all the materials studied. Except for the pure nc Ni and the Ni-W alloy with 40 nm grain size, all the other material conditions show a significant decrease in the frictional coefficient with decreasing grain size. Also, the friction increases with the applied normal load for all the materials.

To interpret these effects and estimate the contribution to friction originating from a change in the geometry of contact, the friction results are re-plotted in Figure 4.2 (b) as a function of the penetration depth. Although there are still differences between the material conditions, these differences have been largely reduced by changing the point of comparison from same normal load to same residual depth. Therefore, a major part of the decrease in the friction coefficient with decreasing grain size is an indirect effect of the change in hardness on the penetration depth. As the grain size decreases and the hardness increases, the penetration depth decreases and so does the coefficient μ_w for the amount of plastic work involved in the generation of the permanent groove.

In this study, the objective is primarily to investigate differences in the response of the materials to plastic deformation. Therefore, the results will be presented as a function of penetration depth. The use of residual depth as a reference is the best approach to compare the behavior of the different materials under similar contact geometries and plastic formation fields. Through the calculation of scratch hardness, this representation also allows for a comparison of the overall resistance of the material to penetration. Finally, for the loading condition with a spherical tip, the tip radius R can be considered as an important scaling variable and we will normalize the penetration depth by R in order to make a better comparison between the experimental results at low and high loads.

The scratch hardness is plotted in Figure 4.3 for the experiments at low load with the tip radius R = 500 nm. For all materials, the hardness decreases with the penetration depth. This result is contrary to the expectations from continuum-based theories for the indentation with spherical tips [23-25]. The decrease could well result from a size effect of surface effects. On pure mc nickel, the thickness of the natural oxide can easily reach 2-5 nm in air at room temperature [26, 27]. Depending on whether the natural oxide breaks in several pieces or act as a stiffening agent for the surface, different effects could be observed. We will discuss further these potential size and surface effects when presenting the results for the residual surface profiles.

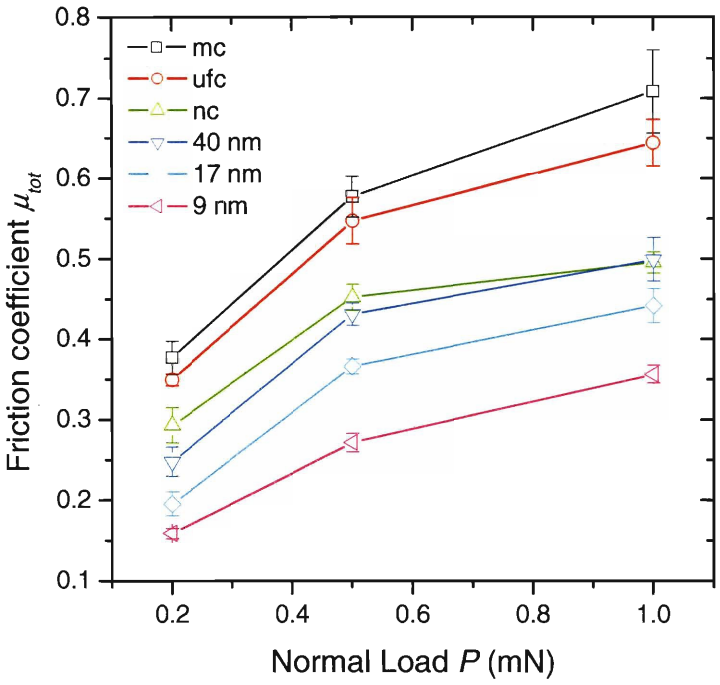

(a)

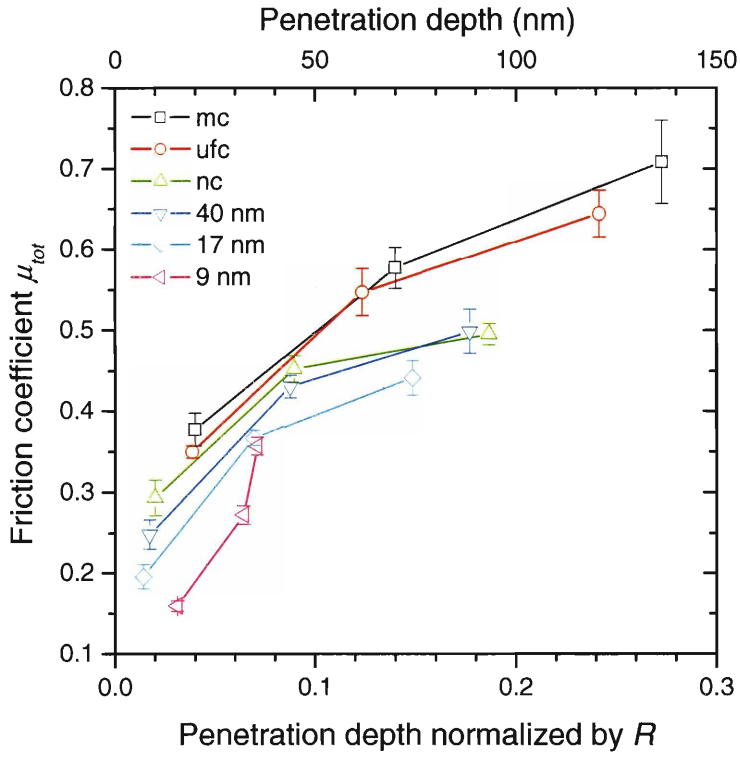

(b)

Figure 4.2: Evolution of the friction coefficient (a) with applied load *P* and (b) penetration depth for the different materials studied. The microcrystalline (mc), ultrafine crystalline (ufc) and the nanocrystalline (nc) series are for pure nickel. The 40, 17 and 9 nm grain size series are for the nickel tungsten alloys.

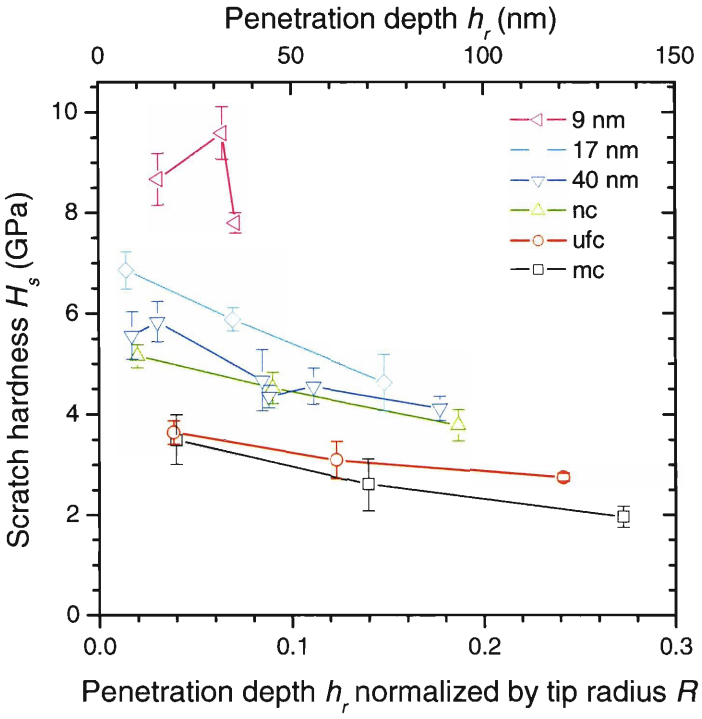

Figure 4.3: Evolution of the scratch hardness as a function of the penetration depth for the different materials in the experiments with the 500 nm spherical tip.

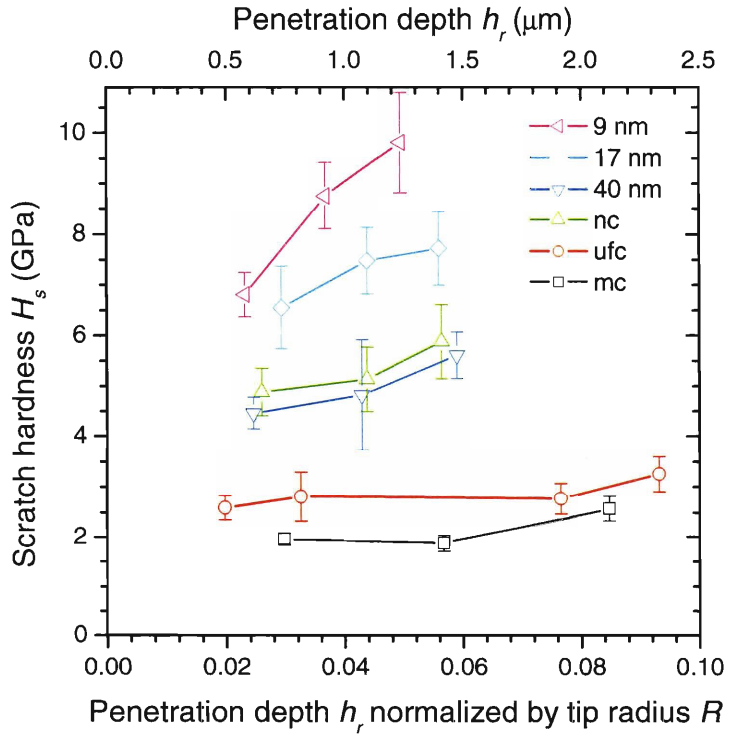

Figure 4.4: Evolution of the scratch hardness as a function of the penetration depth for the different materials in the experiments with the 25 μm spherical tip.

Experiments were also carried out at high loads with a tip radius R = 25 μm. In this case, Figure 4.4 shows an increase in scratch hardness with penetration. With the increase in the length scale of the experiment, this change is consistent with the disappearance of size and surface effects. On the other hand, the hardness values for the different materials are relatively similar to those obtained at low loads. Also, both at low and high loads, the difference between the Ni-W alloy with 40 nm grain size and the pure nc Ni appears just within the experimental scatter.

The scratch hardness results were compared with bulk indentation micro-hardness from a pyramidal Vickers indenter. Since the scratch hardness varies with penetration depth, a reference normalized penetration depth h_r/R of 5% was selected as a representative value. As shown in Figure 4.5, the scratch hardness and the indentation hardness appear correlated but with a significant non-linearity. The non-linearity is more apparent for the softer materials, both in the low and high load experiments where pure mc and ufc nickel appear comparatively harder in frictional sliding than in indentation. Also, for the nanocrystalline materials, the slope of the H_S versus H_I relationships is significantly greater than unity. Under these conditions, a unit change in indentation hardness results in a larger change on scratch hardness. Since the experiments at low and high loads let to this same observation, the high slope of the H_S versus H_I relationships should not be from size or surface effects. Whether the origin would lies simply on the use of a spherical tip is currently under experimental investigation. However, since the scratch hardness was normalized at a fixed penetration depth, the contribution from tip geometry should be minimal.

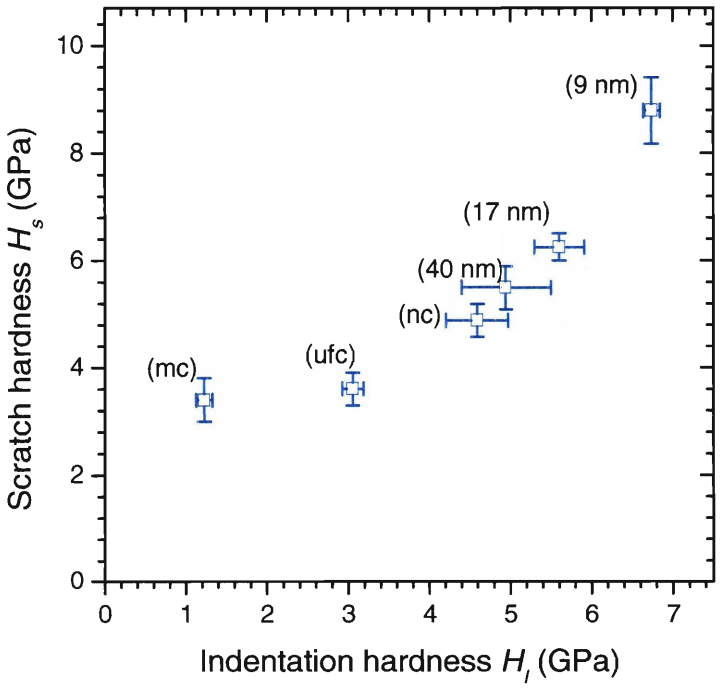

(a)

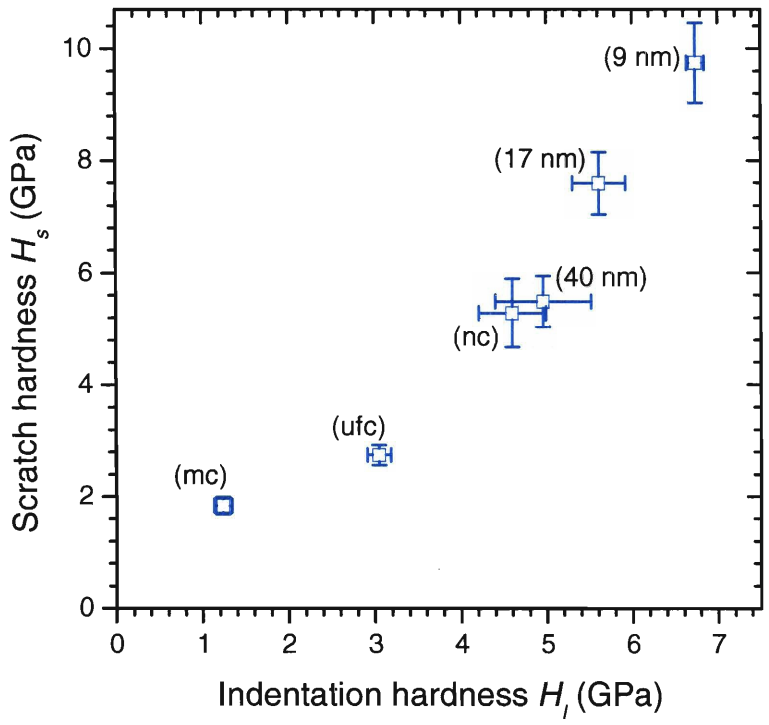

(b)

Figure 4.5: Relationship between the scratch hardness and the indentation micro hardness for the frictional sliding experiments with the (a) 500 nm and (b) the 25 μm spherical tips. The scratch hardness was taken for the normalized penetration depth h_r/R of 5%.

A second parameter of interest from the residual scratch profiles is the normalized pile-up height. For a conical geometry, previous numerical [20] and experimental studies [ch2] indicated a strong effect of the plastic work hardening exponent of the material on pile-up height. Although the concept needs to be clarified for the spherical geometry, it can be expected that a change in the hardening exponent should also translate in a different pile-up. Figure 4.6 (a) presents the evolution of the normalized pile-up height with penetration depth for the different materials. For a normalized penetration depth h_r/R of less than 10%, it appears that the ratio of normalized pile-up height decreases with penetration depth.

As seen in Figure 4.6 (b), the behavior of mc and ufc pure nickel present an opposite trend with an increase in the normalized pile-up height as the penetration depth increases. To describe the extent to which size and surface effects may have contributed to the behavior, Figure 4.6 (b) also presents the pile-up results for frictional sliding contact of a 25 μm tip on the same materials. With the increase in the length scale of the experiment, the pile-up height increased by a factor of approximately 2. With the absence of significant other changes in the test conditions than the length scale, the low pile-up height observed for pure mc and ufc nickel at low loads is most likely a size or a surface effect. Size and surface effects may complicate the analysis of the results, but quantifying their effect is an important step towards a mechanistic understanding of the

experimental frictional sliding response at low loads. These contact properties at low load may become practically important.

To describe further the response at low loads, the following figures present actual cross-sectional profiles for the steady state regime. Figure 4.7 presents a comparative view for the response of nc pure Ni and Ni-W with a 40 nm grain size. Under these conditions with a normal load P = 500 μN, the two materials present a very similar behavior. The scatter and broadness of the pile-up might be slightly higher with the Ni-W alloy, but the average measurements are rather similar. Very similar observations were made at the different loads. These observations can be supported by the very similar scratch hardness (Figure 4.3) and normalized pile-up height (Figure 4.6) for these two materials in all the conditions investigated. All the results available from the low and high load experiments suggest to absence of statistically significant difference in the frictional sliding response of nc pure Ni and Ni-W with a 40 nm grain size.

In light of the earlier discussion about the important effect of strain hardening on pile-up, the results suggest the absence of significant change in the hardening behavior of the materials. Tunsgten in nanocrystalline nickel may act as an obstacle for the nucleation or motion of dislocations. Such strengthening can explain the similar scratch hardness for a slightly coarser grain size in the Ni-W alloy. However, similarly to deformation in pure nanocrystalline nickel, the strengthening mechanism with tungsten does not appear to generate significant work hardening because the normalized pile-up height is unaffected by alloying.

Other material conditions did present significant differences in their pile-up behavior. The Ni-W alloy with a 9 nm grain size presented the highest normalized pile-up height (Figure 4.6). Figure 4.8 compares the cross-sectional profile of this 9 nm grain size with the 40 nm grain size Ni-W alloy. Although the penetration depth is slightly larger with the 40 nm grain size alloy, the 9 nm grain size alloy presents to a broader and more blunted pile-up. In the situation shown here (and also in all the other load cases with the 9 nm grain size alloy), the surface area of the pile-up region is greater than the surface area of the residual scar. The areas can be calculated using the line for surface height equal zero (interpolated initial surface) to separate the regions. With the steady state nature of the frictional sliding process and by neglecting the volume changes from the residual elastic stresses, the surface area of these two regions should be approximately equal providing that the mechanism of permanent deformation is not dilatational.

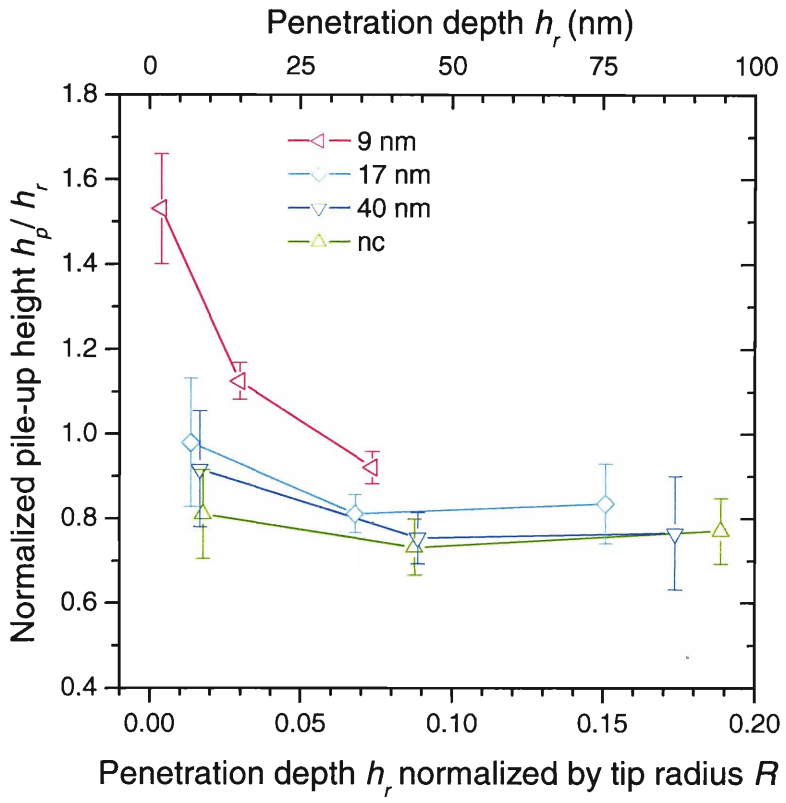

(a)

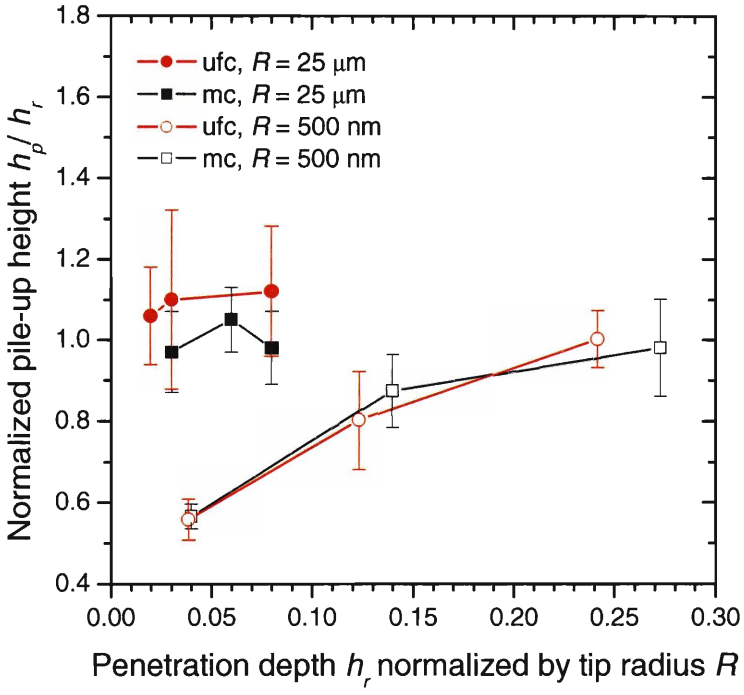

(b)

Figure 4.6: Evolution of the normalized pile-up height as a function of penetration depth for frictional sliding with a 500 nm spherical tip: (a) Nanocrystalline pure nickel and Ni-W alloys with grain sizes of 9, 17 and 40 nm; (b) ultrafine crystalline (ufc) and microcrystalline (mc) pure nickel. The results from sliding with a 25 μm spherical tip are also shown in (b).

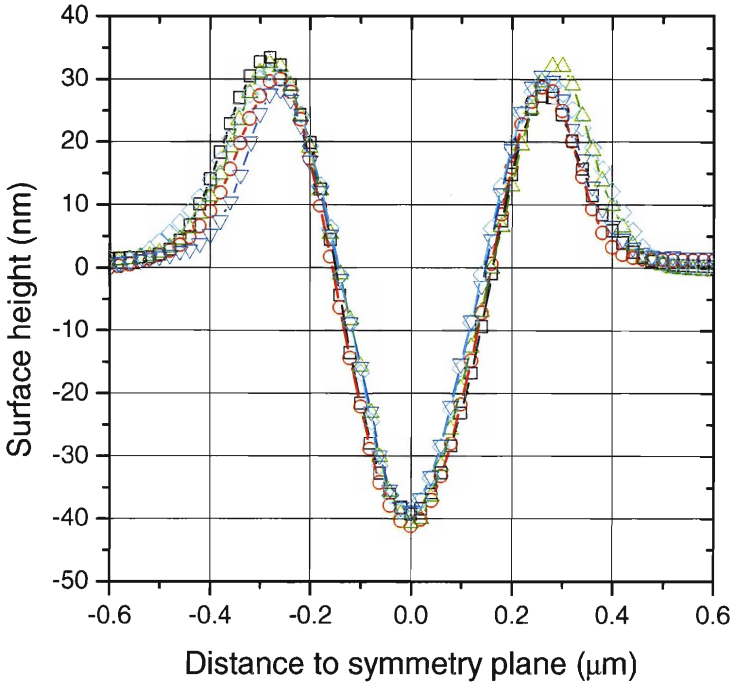

(a)

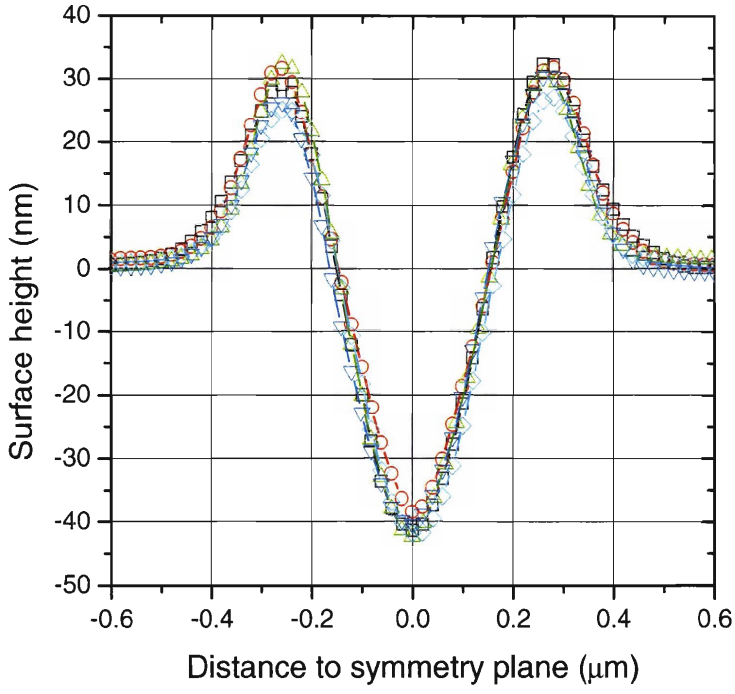

(b)

Figure 4.7: Residual scratch profile for the (a) nanocrystalline pure nickel and (b) nanocrystalline nickel tungsten alloy with a 40 nm grain size. The normal load was 500 μN.

The apparent volume dilation observed predominantly with the 9 nm grain size alloy could be explained by a number of possibilities. A first possibility would be that with a higher flow stress, the components of residual stresses are larger in the 9 nm grain size alloy. However, with the important amount of plasticity involved in these specific conditions, the residual stresses should be relatively similar for the different alloys. As a second possibility, the breaking of the natural oxide may affect the plastic flow and generate pores in the pile-up material. A third possibility would be a direct size effect of having grain size and pile-up height of same order of magnitude. The level of fluctuations in the process of pile-up formation is an additional parameter to consider in interpreting volume dilatation and we will address this question.

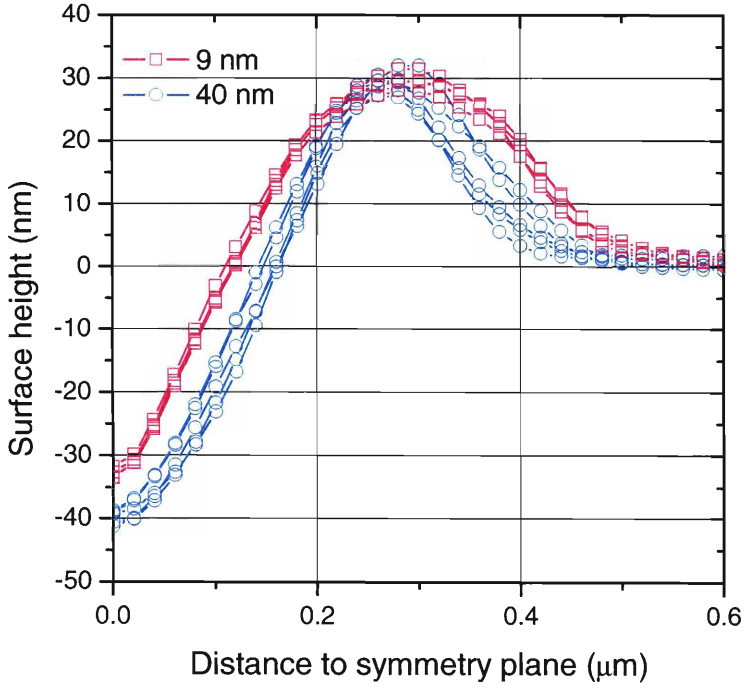

Figure 4.8: Comparison of the residual scratch profile of two nanocrystalline nickel tungsten alloys under conditions of similar penetration depth. For the alloy with a grain size of 9 nm, the normal load was 1 mN.

Detailed topographical views of the residual surface profiles are presented in Figure 4.9 for the 9 nm grain size alloy and for pure ufc nickel. The overall vertical scale is only 22 nm and, therefore, the roughness of the original surface can also be observed. The conditions selected allow for comparing the pile-up under similar contact geometry. The 9 nm grain size alloy presents a significantly greater pile-up than ufc pure nickel. In fact, the deformation process at this load resulted in more apparent dilatation than for the condition presented for a larger load in Figure 4.8. On the other hand, it is remarkable to note the regular pile-up morphology with the scratching distance. For the ufc pure nickel, similar comments can be made about the regularity of the pile-up

although a few irregularities are observed along the sliding distance. A particularity to ufc nickel is the sharpness and low elevation of the pile-up, a behavior consistent with a greater effective strain hardening at the length scale of the experiment.

The effect of small scale testing on lowering the pile-up of the ufc pure nickel has already been discussed in details. The apparent volume dilatation in the 9 nm Ni-W alloy has also been discussed. The information provided in Figure 4.9 provides a convincing argument that the deformation process of formation of these high and blunted pile-ups is rather steady and regular in nature. The origin of the dilatational is not fully understood. However, a careful examination revealed that the proportion of the dilatational decreases rapidly with an increase in the penetration depth. Therefore, the dilatation mechanism operates predominantly at low loads. The experiment here cannot isolate between possible mechanisms such as the small grain size and deformation zone or the effects from surface tension and natural oxides. On he other hand, the experiment clearly point to effects that cannot be treated from continuum mechanics.

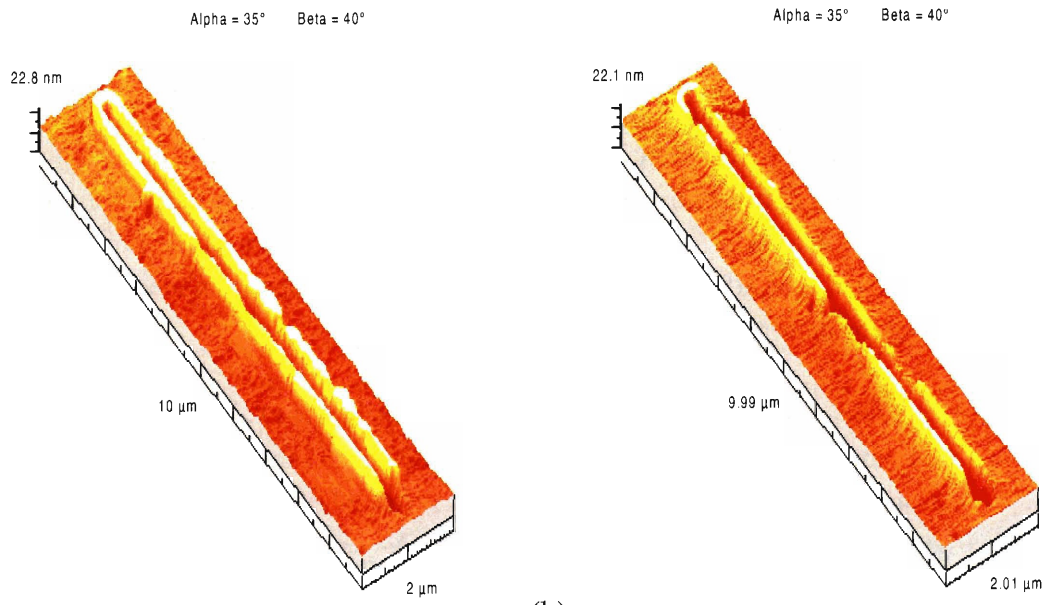

(a) (b)

Figure 4.9: Full topographical images of (a) nc Ni-W alloy with a grain size of 9 nm tested at a normal load of 500 µN for a steady state penetration depth of 14 nm and (b) pure ufc Ni tested at a normal load of 200 µN for a depth of 17 nm. These conditions of different load allow for a comparison at similar penetration depth. The tip was traveling from bottom to top.

4.4 Conclusions

The frictional sliding response of nanocrystalline materials was studied in details through low load and high load experiments with spherical tips. The following conclusions can be drawn.

1. Size and/or surface effects are observed in frictional sliding at low loads. The specifics on the length scale effect are different for nanocrystalline materials than for materials with larger grain sizes.

2. For large grain sizes, the pile-up height observed in the low load experiments was significantly lower than the values observed at higher loads where the continuum assumption applies. The lower pile-up height and its sharpness were consistent with a higher effective strain hardening of the material.

3. For the nanocrystalline materials, size or surface effects were observed from the important decrease in the scratch hardness with increasing penetration depth. This trend is contrary to experimental measurements carried out at higher loads and to expectations from continuum-based models.

4. For the hardest nickel tungsten alloy, the size effect was most noticeable by an apparent dilatational component in the process pile-up formation. The proportion of the apparent dilatational component increased significantly as the penetration depth decreased, clearly indicating that the effect is primarily due to the fine scale of the experiment. The effect could be associated with the similarity in the size of the grain and of the deformation zone or to surface effects.

5. Under the conditions investigated, one nanocrystalline nickel tungsten alloy behaved very similar to pure nanocrystalline nickel. Although tungsten in nickel strengthens the structure for plastic yielding, the results collected suggest that tungsten would not significantly affect the strain hardening behavior of nanocrystalline nickel.

This experimental study provided detailed information about the frictional sliding response of nanocrystalline materials. The influence of size scale and surface effects was partially differentiated from microstructural effects through the use of different loading conditions. The spherical tip geometry enables to collect a greater amount of information about the material, but it also limit the analysis as no quantitative framework is available to predict the effect of material and contact parameters.

4.5 References

[1] K. S. Kumar, H. Van Swygenhoven, and S. Suresh, "Mechanical behavior of nanocrystalline metals and alloys," *Acta Materialia*, vol. 51, pp. 5743-5774, 2003.

[2] R. Schwaiger, B. Moser, M. Dao, N. Chollacoop, and S. Suresh, "Some critical experiments on the strain-rate sensitivity of nanocrystalline nickel," *Acta Materialia*, vol. 51, pp. 5159-5172, 2003.

[3] L. Lu, R. Schwaiger, Z. W. Shan, M. Dao, K. Lu, and S. Suresh, "Nano-sized twins induce high rate sensitivity of flow stress in pure copper," *Acta Materialia*, vol. 53, pp. 2169-2179, 2005.

[4] Y. M. Wang and E. Ma, "Strain hardening, strain rate sensitivity, and ductility of nanostructured metals," *Materials Science and Engineering a-Structural Materials Properties Microstructure and Processing*, vol. 375-77, pp. 46-52, 2004.

[5] Q. Wei, S. Cheng, K. T. Ramesh, and E. Ma, "Effect of nanocrystalline and ultrafine grain sizes on the strain rate sensitivity and activation volume: fcc versus bcc metals," *Materials Science and Engineering a-Structural Materials Properties Microstructure and Processing*, vol. 381, pp. 71-79, 2004.

[6] J. Chen, L. Lu, and K. Lu, "Hardness and strain rate sensitivity of nanocrystalline Cu," *Scripta Materialia*, vol. 54, pp. 1913-1918, 2006.

[7] B. Moser, T. Hanlon, K. S. Kumar, and S. Suresh, "Cyclic strain hardening of nanocrystalline nickel," *Scripta Materialia*, vol. 54, pp. 1151-1155, 2006.

[8] R. J. Asaro and S. Suresh, "Mechanistic models for the activation volume and rate sensitivity in metals with nanocrystalline grains and nano-scale twins," *Acta Materialia*, vol. 53, pp. 3369-3382, 2005.

[9] A. H. Chokshi, A. Rosen, J. Karch, and H. Gleiter, "On the Validity of the Hall-Petch Relationship in Nanocrystalline Materials," *Scripta Metallurgica*, vol. 23, pp. 1679-1683, 1989.

[10] R. A. Masumura, P. M. Hazzledine, and C. S. Pande, "Yield stress of fine grained materials," *Acta Materialia*, vol. 46, pp. 4527-4534, 1998.

[11] J. Schiotz, F. D. Di Tolla, and K. W. Jacobsen, "Softening of nanocrystalline metals at very small grain sizes," *Nature*, vol. 391, pp. 561-563, 1998.

[12] H. Van Swygenhoven and P. A. Derlet, "Grain-boundary sliding in nanocrystalline fcc metals," *Physical Review B*, vol. 64, 2001.

[13] H. Van Swygenhoven, P. M. Derlet, and A. Hasnaoui, "Atomic mechanism for dislocation emission from nanosized grain boundaries," *Physical Review B*, vol. 66, 2002.

[14] D. Feichtinger, P. M. Derlet, and H. Van Swygenhoven, "Atomistic simulations of spherical indentations in nanocrystalline gold," *Physical Review B*, vol. 67, 2003.

[15] K. J. Van Vliet, S. Tsikata, and S. Suresh, "Model experiments for direct visualization of grain boundary deformation in nanocrystalline metals," *Applied Physics Letters*, vol. 83, pp. 1441-1443, 2003.

[16] K. S. Kumar, S. Suresh, M. F. Chisholm, J. A. Horton, and P. Wang, "Deformation of electrodeposited nanocrystalline nickel," *Acta Materialia*, vol. 51, pp. 387-405, 2003.

[17] T. Hanlon, Y. N. Kwon, and S. Suresh, "Grain size effects on the fatigue response of nanocrystalline metals," *Scripta Materialia*, vol. 49, pp. 675-680, 2003.

[18] T. Hanlon, E. D. Tabachnikova, and S. Suresh, "Fatigue behavior of nanocrystalline metals and alloys," *International Journal of Fatigue*, vol. 27, pp. 1147-1158, 2005.
[19] T. Hanlon, A. H. Chokshi, M. Manoharan, and S. Suresh, "Effects of grain refinement and strength on friction and damage evolution under repeated sliding contact in nanostructured metals," *International Journal of Fatigue*, vol. 27, pp. 1159-1163, 2005.
[20] S. Bellemare, M. Dao, and S. Suresh, "The frictional sliding response of elasto-plastic materials in contact with a conical indenter," *International Journal of Solids and Structures*, vol. 43, 2006.
[21] T. Hanlon, "Grain size effects on the fatigue response of nanocrystalline materials," in *Dept. of Materials Science and Engineering*. Cambridge: MIT, 2004.
[22] A. J. Detor and C. A. Schuh, "Grain boundary segregation and the equilibrium grain size in nanocrystalline Ni-W alloys," *JOM*, vol. 56, pp. 318, 2004.
[23] J. G. Swadener, E. P. George, and G. M. Pharr, "The correlation of the indentation size effect measured with indenters of various shapes," *Journal of the Mechanics and Physics of Solids*, vol. 50, pp. 681-694, 2002.
[24] Y. G. Wei and J. W. Hutchinson, "Hardness trends in micron scale indentation," *Journal of the Mechanics and Physics of Solids*, vol. 51, pp. 2037-2056, 2003.
[25] M. A. G. Maneiro and J. Rodriguez, "Pile-up effect on nanoindentation tests with spherical-conical tips," *Scripta Materialia*, vol. 52, pp. 593-598, 2005.
[26] M. Taguchi and M. Watanabe, "Mass change of nickel fresh surface at the beginning of oxidation," *Journal of the Japan Institute of Metals*, vol. 65, pp. 38-44, 2001.
[27] D. J. Siconolfi and R. P. Frankenthal, "Air Oxidation of a Ni-P Alloy," *Journal of the Electrochemical Society*, vol. 136, pp. 2475-2480, 1989.

Summary and Conclusions

In this thesis, a new framework was developed to characterize the steady state frictional sliding response of elasto-plastic materials. The framework is based on using the scratch hardness, the normalized pile-up height and the overall friction coefficient as prime parameters for the contact response. Quantitative relationships have been established to predict these prime parameters from the mechanical properties of the materials being investigated. For these relationships, the effect of the surface friction coefficient was also determined and included. Although all the predicting relationships were determined by using finite element methods, they were validated using different solution schemes and through a comprehensive comparison with experimental results on selected material systems. Also, the mechanics of steady state frictional sliding was compared with normal indentation and an algorithm was developed to extract plastic flow properties from a scratch experiment. The key contributions from this thesis can be summarized as follow:

1. The steady state frictional sliding response can now be predicted using the dimensionless form of the equations for the scratch hardness, pile-up height and overall friction coefficient. The accuracy of the predictions is of the same order as the accuracy of the input data for the material and contact properties. With these dimensionless functions, it becomes unnecessary to carry out any additional finite element calculation as the functions are smoothly covering any combination of material and contact properties within the specified range.

2. As compared to normal indentation, frictional sliding induces more plastic deformation and curvature to the free surface. Calculations based on the representative strain indicated a 4 fold increase in the magnitude of the equivalent plastic strain in frictional sliding. Frictional sliding also increases the height of the pile-up formed on each side of the indenter by a factor up to 3 and it eliminates the phenomenon of sink-in for the range of material properties studied. Sink-in would eventually occur in frictional sliding, but only for conditions of high yield strain and strain hardening that fall outside the properties range of most engineering materials. Finally, the comparison of the scratch hardness with the indentation hardness indicated the independence of the two quantities. This independence was demonstrated computationally and also experimentally, by comparing the frictional sliding response of two materials with the same initial indentation hardness.

3. The plastic strain hardening exponent affects very significantly the pile-up height. Both the computational predictions and the experimental results on a model material system showed a large decrease in the pile-up height with increasing strain hardening. The initial yield strength can also influence the pile-up morphology, but to a much lower extent. This trend and its quantification could provide a tool to relate

material properties and their tribological response. However, further work is needed to clearly establish relationships between pile-up and wear resistance.

4. The plastic properties can now be extracted from the response to a steady state frictional sliding test. Provided that the elastic moduli and contact properties are known, the normalized hardness and the normalized pile-up height are sufficient to determine the plastic strain hardening exponent and the initial yield strength. The sensitivity of this reverse algorithm to variations in the input parameters was reasonable based on calculations using the dimensionless functions. Also, in comparison with instrumented indentation, the proposed algorithm to extract plastic properties is found to have a significantly improved resolution on the estimate of the plastic strain hardening exponent.

In addition to this work on the relationships between the contact response and mechanical properties, the experimental frictional sliding response of nanocrystalline nickel and nickel-tungsten alloys were studied at low and high loads. Size and/or surface effects were observed in frictional sliding at low loads. The results and interpretation can be summarized as follow:

5. For the nanocrystalline materials, size or surface effects were observed from the important decrease in the scratch hardness with increasing penetration depth. This decrease was contrary to experimental measurements carried out at higher loads and to expectations from continuum-based models.

6. For the hardest nickel tungsten alloy, size effects were most noticeable by an apparent dilatational component in the process of pile-up formation. The proportion of the apparent dilatational component increased significantly as the penetration depth decreased, clearly indicating a size effect that could be associated with surface effects or with the similarity between grain size and the size of the deformation zone.

7. Under the conditions investigated, one nanocrystalline nickel tungsten alloy behaved very similar to pure nanocrystalline nickel. Although tungsten in nickel strengthens the structure for plastic yielding, the results collected suggest that tungsten would not significantly affect the strain hardening behavior of nanocrystalline nickel.

While scratch tests have been used as a qualitative tool in the past decades, the framework developed in this thesis may help improve the quality of the quantitative analysis of the steady state frictional sliding experiments. The technique could be a complement to instrumented indentation by providing a greater sensitivity to the strain hardening exponent. On the other hand, further research in multiscale modeling help establish direct relationships steady state frictional experiment and actual tribological processes.

Appendix

The following figure was generated using the indentation hardness expressing from Dao et al (2001) and the scratch hardness expression from Equation 3.5 in this thesis. The different curves are for the different values of n as indicated. It shows how the ratio in the two quantities depends on the strain hardening exponent n. The figure is best supporting information for Chapter 3.